6-18-2018

Experimental and Numerical Investigation of Liquid-Assisted Gas-Lift Unloading

Renato Peixoto Coutinho

Louisiana State University and Agricultural and Mechanical College, repeco@gmail.com

EXPERIMENTAL AND NUMERICAL INVESTIGATION OF LIQUID-ASSISTED GAS-LIFT UNLOADING

A Dissertation

Submitted to the Graduate Faculty of the
Louisiana State University and
Agricultural and Mechanical College
in partial fulfillment of the
requirements for the degree of
Doctor of Philosophy in Petroleum Engineering

in

The Department of Petroleum Engineering

by
Renato Peixoto Coutinho
B.S., Federal University of Ceara - Brazil, 2009
M.S., Federal University of Ceara - Brazil, 2012
August 2018

To my parents, Claudio Coutinho Jr. and Rosana P Coutinho, my wife Erika V Pagan, and my sister Gabriela, for the their love, guidance and support during the course of my life. None of my accomplishments would have been possible without them.

Acknowledgments

My sincere appreciation to my committee chair, Dr. Paulo J. Waltrich, not only for giving me the support during this period, but also for trusting that I was able to conduct this project and giving me this excellent opportunity to learn. My appreciation also goes to Dr. Wesley C. Williams, Dr. Seung Kam, Dr. Krishnaswamy Nandakumar, and Dr. Chester Wilmot for serving as committee members. I consider myself fortunate to have then involved in this work.

Special thanks go to my family for their continuous and unconditional love, guidance and support. I am forever grateful to my parents, Claudio Coutinho Jr and Rosana P Coutinho, for giving me the opportunities and experiences that have made me who I am. They generously encouraged me to explore new directions in life and seek my own destiny. My deepest gratitude goes to my wife, Erika V Pagan. Her love, patience and friendship were absolutely crucial and inspired me during this path. I am grateful to my sister, Gabriela, for always being there for me as a friend. This journey would not have been possible without them, and I dedicate this milestone to them.

I really appreciate the support of my colleagues: Pedro Cavalcanti, Khodur Altarabusi, Catalina Posada, John Whitehead, Jack Blears, Sandeep Gupta, Bruno Xavier, Matheus Capovilla and Ligia Tornisiello with whom I have shared personal and academic conversations. They made my time at LSU much more enjoyable. My gratitude is also extended to Mrs. Janette Wooden, Ms. Janet Dugas, Mrs. Andi Donmyer and Mr. Doug Hoy for the necessary administrative and technical support and friendship during this time. I am thankful to the faculty of the Petroleum Engineering department who were essential to my learning process.

I also thank the Shell oil company, for providing the necessary financial support for this research project.

Table of Contents

List of Symbols, Subscripts and Abbreviations

Symbol	Description
A	Area or Coefficient for Equation 3.14
B	Coefficient for Equation 3.14
B	Formation volume factor
C	Coefficient for Equation 3.14
c_1	Coefficient for Equation 3.10
c_2	Coefficient for Equation 3.10
c_3	Coefficient for Equation 3.10
C_D	Discharge coefficient
C_L	Specific heat of liquid
C_p	Specific heat of gas at constant pressure
C_v	Flow coefficient
C_v	Specific heat of gas at constant volume
d	Diameter
D_H	Hydraulic diameter
F_R	Froude number
F_{wo}	Water-oil ratio
g	Acceleration of gravity
g_c	Gravitational constant (32.174 lbm-ft/lbf-sec^2)
H_l	Liquid Holdup
ID	Inner diameter
k	Ratio of specifics heats (C_p/C_v)
L	Depth
n	Polytropic exponent for gas
N	Number of compression stages
ND	Nominal diameter
OD	Outer diameter
p	Pressure
q	Volumetric flow rate
R	In-situ gas-liquid ratio
S	Slip ratio
u	Velocity
V	Specific volume or Volume
w	Mass flow rate
x	In-situ gas mass fraction
y	Pressure ratio (p_2/p_1)
Z	Compressibility factor
z	Interval length
α	Void fraction
γ	Fluid specific gravity
δ	Ratio of the orifice diameter by the upstream pipe diameter
Δp	Pressure drop
ε	Efficiency
λ	Volumetric fraction

ρ	Density
$\bar{\rho}$	Average density

Subscripts	Description
1	Upstream conditions
2	Downstream conditions
an	Annulus
bean	Orifice
bh	Bottomhole conditions
bottom	Bottom section
c	Critical flow condition
ch	Choke
elec	Electricity
f	Friction
G	Gas
GLV	Gas-Lift Valve condition
inj	Injection conditions
inner	Inner pipe
L	Liquid
m	Mixture
max	Maximum
min	Minimum
outer	Outer pipe
plot	From Figure 3.4
plot	Obtained in Figure 3.4
sc	Standard condition
sg	Superficial gas
sl	Superficial liquid
tb	Tubing
top	Top section
total	Total value
w	Water
wh	Wellhead conditions

Abbreviation	Description
CAPEX	Capital Expenditures
FCV	Flow Control Valve
FE	Flow Element
GLR	Gas-Liquid-Ratio
GLV	Gas-Lift Valve
GVF	Gas-Volume-Fraction
HP	Horsepower
ID	Inner diameter
IPO	Injection Pressure Operated
LAGL	Liquid-Assisted Gas-Lift
LT	Level Transducer

ND	Nominal diameter
OD	Outer diameter
OPEX	Operating Expenses
PERTT	Petroleum Engineering Research & Technology Transfer
PT	Pressure Transducer
PVC	Polyvinyl Chloride
PVT	Pressure, Volume and Temperature
RTD	Resistance Temperature Detectors
TT	Temperature transducer

Abstract

The case for a unique form of gas-lift unloading, termed "Liquid-Assisted Gas-Lift (LAGL)," is presented. This work demonstrates that the injection of a gas-liquid mixture allows transport of gas to a deep injection point utilizing injection pressure considerably lower than single-phase gas injection. The LAGL is demonstrated in a 2,880 *ft* deep test well. The test well is kicked-off using an injection pressure that would normally be lower than the pressure for single-point single-phase gas injection at this depth. Experimental results indicate that the LAGL can lower the injection pressure by up to 75%.

This work breaks the LAGL system in three sub-systems: two-phase downward flow in annulus, two-phase flow through orifice Gas-Lift Valves (GLVs), and upward two-phase flow in pipes. The last sub-system is well described in the literature and will not be investigated in this work. However, there is a lack of studies on two-phase downward flow in annulus and through GLVs. Therefore, these two topics are investigated in this work.

An experimental and numerical study on two-phase flow through orifice GLVs is presented. The experimental results are compared to numerical models published in the literature for two-phase flow through restrictions. It was observed that some models can successfully characterize two-phase flow thorough gas-lift valves with errors lower than 10%.

Experimental characterization is performed for downward two-phase flow in the annulus and the result is compared with downward flow in pipes. The comparison shows differences between downward two-phase flow in annulus and pipes for liquid holdup and flow regimes. The experimental results show that the liquid holdup is consistently higher for two-phase downward flow in annulus than in pipes for the annular flow regime.

After the experimental validation of LAGL unloading and the characterization of two-phase flow through GLVs and annulus, a simulation model is built using a commercial transient flow simulator. The model is initially validated with experimental data from the field-scale test well. Out of 15 validation cases, only two cases showed average error higher than 15%. After the model validation, the simulation model is used to simulate the complete unloading of the well.

1 Introduction

1.1 Problem Background

It is common that some oil wells, in their early life, produce naturally with no need for external energy to lift the fluids to the surface. However, at some point in the "well life", no reservoir will have enough energy to lift fluids to the surface. The lack of energy (or pressure) to carry the fluid to the surface occurs more often in the middle to late lifetime of the well, but it can also be present in the early life of the well. It may be economical at any point in the life of a well to maintain or even increase the production rate by the use of artificial lift techniques.

Artificial lift techniques are used in the oil and gas industry when it is economical to reestablish the production after the well stops flowing or to increase production rates of a flowing well. Many artificial lift techniques are available and can be chosen accordingly to the characteristic of the field that it will be applied to. Gas-lift is one of the most widely used artificial lift methods (Tang *et al.*, 1999). The popularity of the gas-lift technique is inherent to its simplicity, reliability, ability to operate over a wide range of flow rates, and not requiring a large footprint at the surface (Xu *et al.*, 2013).

According to Pittman (1982), gas-lift was first used in the United States for oil production over 130 years ago. Since, it has been widely used and nowadays gas-lift technology is well developed. Many modifications have been proposed since its first use. However, some aspects of gas-lift operations can still be optimized.

The basic concept of gas-lift is to inject continuously (or intermittently) gas at a specific depth in the production string. The injected gas has the function of lightening the fluid present in the production string by reducing the average fluid density. The reduced density results in lower bottomhole pressures, as a consequence of lower hydrostatic pressure. Reduced bottomhole pressure can either reestablish reservoir flow or increase production rate.

Figure 1.1 presents a schematic diagram of a typical gas-lift system. As shown in Figure 1.1, a compressor-facility compresses gas to be injected in the casing/tubing annulus. The injected gas flows downward in the annulus to a depth where the Gas-Lift Valve (GLV) is located. Once the bottomhole annulus pressure is higher than the bottomhole tubing pressure, the injected gas starts to flow through the GLV to the production tubing. The injected gas comingles with the fluid located in the production tubing and, at this point, the gas-lifted oil production starts. In the case of continuous production, the gas is injected at an approximately constant flow rate.
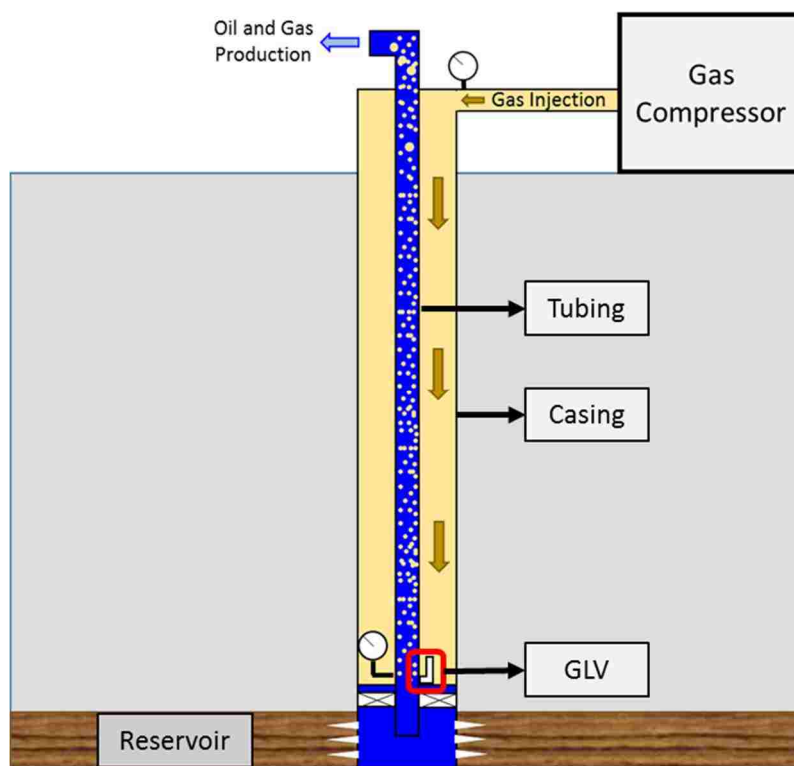
Figure 1.1. Gas-lift concept [adapted from Economides (2013)].

Intermittent gas-lift is applied in wells where continuous production is not required. In the intermittent gas-lift technique, oil periodically accumulates at the bottom of the well, and then a high-volume slug of pressurized gas is injected at the bottom of the well. The injected gas slug lifts the accumulated oil to the surface. After the slug of gas and oil are lifted, oil starts to accumulate again at the bottom of the well, and a new cycle restarts. According to Pittman (1982)

this type of gas-lift should be considered when the reservoir is depleted (e.g., for low reservoir pressures).

Before initiating production for gas-lifted wells or after workover operations, completion and/or formation fluids that are accumulated in the well have to be removed from the production tubing. The process of removing these fluids is known as well "unloading", and it can be considered a critical step for gas-lift operations.

A conventional unloading operation is a transient process where high pressure gas is injected in the annular space between casing and production tubing. Figure 1.2 shows a simplified diagram of the unloading operation in a well with single-point injection. The diagram presented in Figure 1.2 is based on the industry standard practices for gas-lift unloading [adapted from Takács (2005)].
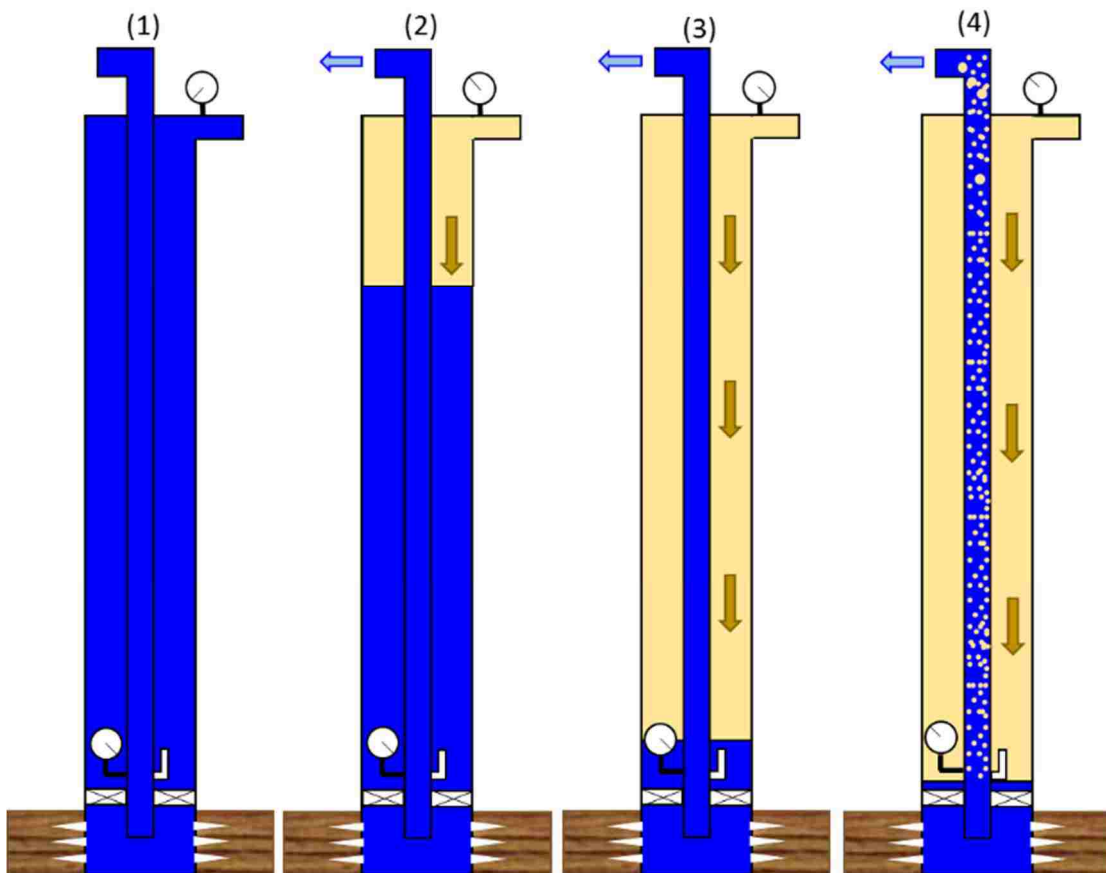

Figure 1.2. Gas-lift unloading process for single-phase single-point of injection.

The process illustrated in Figure 1.2 can be divided in four steps:

- Both annulus and tubing are filled with liquid (heavy fluids). The injection pressure (p_{inj}) is low, and the bottomhole pressure (p_{bh}) is high due to the large hydrostatic pressure of the liquid.

- Gas starts to be injected at the surface in the annulus. The gas injected in the annulus pushes the liquid out of the tubing. Once gas starts to replace the liquid in the annulus, the injection pressure increases to compensate for the difference between gas and liquid density, to maintain the same bottomhole pressure. The bottomhole pressure will be kept constant as long as the production tubing is filled with liquid (if considering negligible friction effects).

- Right before the gas reaches the GLV, the injection pressure reaches its maximum level. At this point, the injection pressure can be obtained using the following expression:

$$p_{inj} = p_{wh} + \Delta p_{GLV} + \Delta p_f + (\overline{\rho_{tb}} - \overline{\rho_{an}})gL \qquad 1.1$$

where, p_{wh} is the tubing wellhead pressure, Δp_{GLV} is the pressure drop through the GLV, Δp_f is the pressure drop due friction effects, g is the acceleration of gravity, L is the depth of the GLV, $\overline{\rho_{tb}}$ is the average density of the liquid in the tubing, and $\overline{\rho_{an}}$ is the average density of gas in the annulus.

- Gas reaches the GLV and starts to be injected in the tubing. At this moment, the tubing bottomhole pressure starts to decrease due the presence of lighter fluid (gas) in the tubing, which lowers the mixture density of the fluid in the tubing ($\overline{\rho_{tb}}$). Once the bottomhole pressure drops below the formation pressure, inflow from the formation to the tubing starts (Takács, 2005). When the unloading process reaches either steady production or cyclic unstable production, then unloading ends and production begins (Tang *et al.*, 1999).

The process presented in Figure 1.2 is a single-point injection example. It is the simplest configuration of a well where continuous gas-lift is deployed. Continuous gas-lift unloading

operations normally requires the use of multiple GLVs. In general, additional valves are required in cases where the gas compression system is not able to deliver enough pressure to push heavy fluid out of the annulus and the production tubing using only the *operating* GLV located at the bottom of the well. In this case, *unload* valves are added above the *operating* valve, and they are used to facilitate the unload process. The unload valves allow a stepwise removal of heavy fluid from the annulus (Takács, 2005).

Most of the *unload* valves are pressure operated, which are designed to stay closed during the regular production operation. However, it is possible that one or more of these valves may malfunction over the life of the well. According to Candido (1989), a problem that can occur in pressure operated valves is the loss of the original fluid pressure in the bellows, which would cause valve malfunctioning. If one of these valves is leaking, it may create the need to stop production for replacement of such defective valves. However, this process would generate additional costs, larger production downtime, and require longer workover rig time.

The replacement of GLVs is conducted through a wireline intervention. Wireline operations can be time consuming and can pose risks to existing well completions (Xu *et al.*, 2013). Production is also negatively affected by the downtime due the installation of the new valve. All these factors combined result in loss of revenue. Based on that, the use of multiple valves may increase well completion and intervention costs.

Another main concern for conventional gas-lift unloading operations is the capital and operating expenses of gas compression facilities. Pittman (1982) stated that the need for an excessive volume of high-pressure gas could make the process uneconomic. Therefore, efforts to lower injection pressure can potentially decrease capital and operational costs for gas-lift operations.

1.2 Motivation

This study proposes the investigation of an alternative technique to perform the gas-lift unloading process. This technique is termed here "Liquid-Assisted Gas-Lift (LAGL)". In LAGL the injection-fluid is a mixture of gas and liquid. The main objective of injecting a gas-liquid mixture is to increase the mixture density of the fluid in the casing annulus, which would consequently decrease the injection pressure for gas to reach a single GLV at the bottom of the well. Figure 1.3 presents the pressure profile during the unloading process for both conventional single point gas-lift unloading (single-phase gas - Figure 1.3a) and LAGL unloading (multiphase mixture - Figure 1.3b). Figure 1.3 is a hypothetical example, and the parameters used to calculate the pressure gradients presented in this figure are listed in Table 1.1.
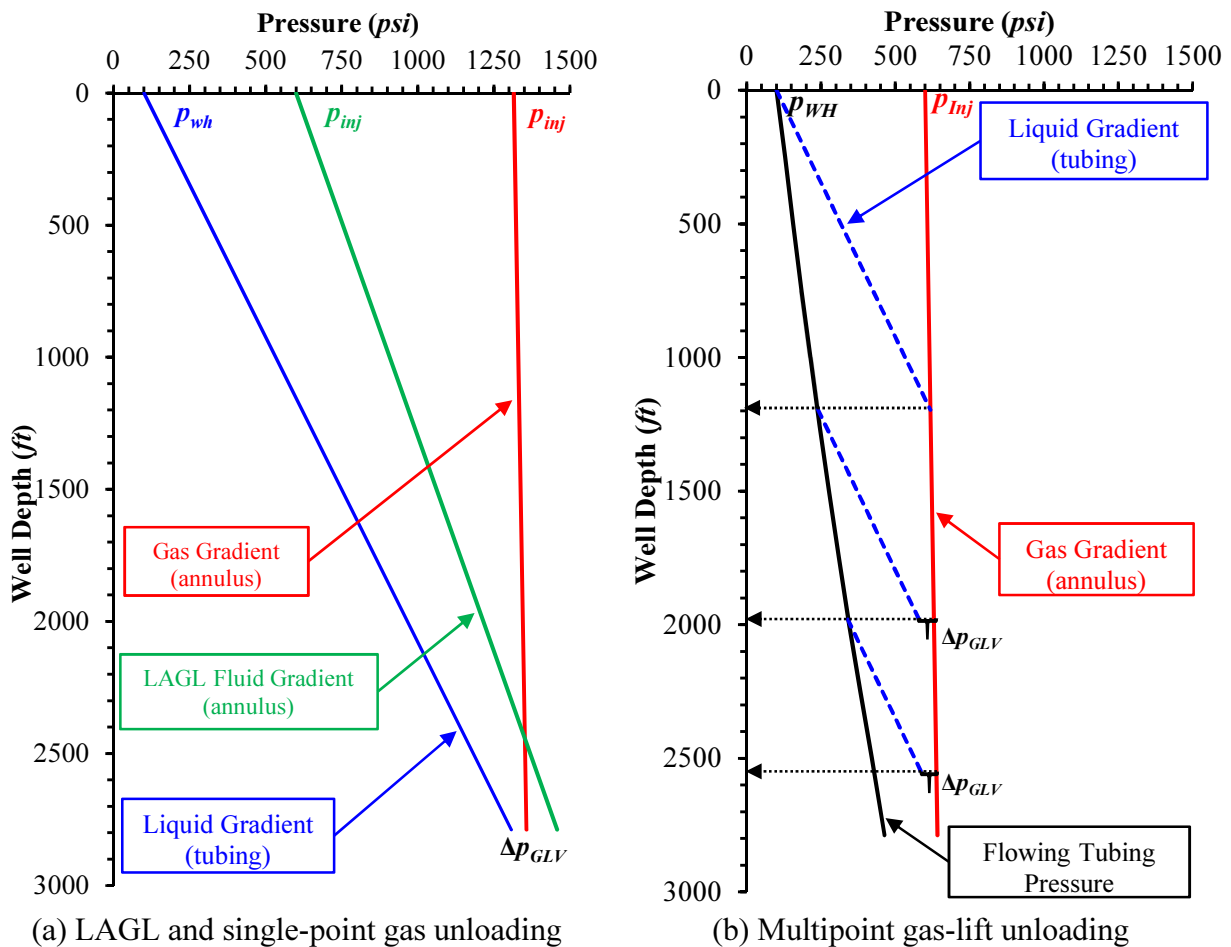

(a) LAGL and single-point gas unloading   (b) Multipoint gas-lift unloading
Figure 1.3. Liquid-assisted gas-lift unloading.

Table 1.1. Parameters used in the schematic drawing presented in Figure 1.3.

Parameter	Unit	Value
Wellhead tubing pressure	*psi*	100
Hydrostatic pressure gradient for the liquid	*psi/ft*	0.433
Hydrostatic pressure gradient for the gas	*psi/ft*	0.015
Pressure drop through GLV for single-phase gas	*psi*	50
Pressure drop through GLV for multiphase (gas and liquid)	*psi*	150

The pressure profile in Figure 1.3 illustrates a theoretical example for the pressure profile for the step 3 in the unloading process as shown in Figure 1.2. This example assumes the geometry of test well used in this study (see Figure 2.1), no friction effects in the flow in the annulus and tubing, non-slip conditions between gas and liquid, using working fluids as natural gas and water, and considering Gas-Volume-Fraction (GVF) of 30%. In this example, the maximum required injection pressure for the LAGL method to unload the well is 950 *psi*. On the other hand, a pressure of 1,340 *psi* is needed to complete the unloading process for conventional single-phase gas injection. The use of LAGL represents a reduction of 29% on the injection pressure compared to single-phase gas injection. This simplified theoretical analysis shows that the injection of multiphase flow during the unloading process has the potential to significantly decrease the lift fluid injection pressure.

The pressure profile in Figure 1.3a (red line) illustrates a theoretical example for the pressure profile for the step 3 of Figure 1.2. The example presented in Figure 1.3 assumes the geometry of the test well used in this study, as shown in Figure 2.1. This example assumes the geometry of test well used in this study (see Figure 2.1), no friction effects in the flow in the annulus and tubing and non-slip conditions between gas and liquid. The work fluids are natural gas and water, and the Gas-Volume-Fraction (GVF) is 30%. In this example, the maximum required injection pressure for the LAGL method to unload the well is 600 *psi*. On the other hand, a pressure of 1,315 *psi* is

required to complete the unloading process for single-point gas injection. The use of LAGL represents a reduction of more than 50% on the injection pressure compared to single-point gas injection. This theoretical analysis shows that the injection of multiphase flow during the unloading process has the potential to decrease the injection pressure for the single-point gas-lift unloading.

Figure 1.3b shows the unloading valve string design for multipoint gas-lift unloading. The example considers that the injection pressure available is 600 *psi* for the design presented in the Figure 1.3b. The design shows that three unloading valves are required to perform the unloading of the well with the available injection pressure. The extra valves would require additional costs. This additional cost can get higher in deep wells or in locations with lower injection pressure available. For the latter case, a larger number of unloading valves would be necessary. Multiple-point gas-lift unloading is a well-developed and consolidated technique. However, in cases where technical (e.g. production of highly corrosive fluids) and economical aspects challenge the applicability of such technique, the LAGL is a viable alternative to unload the well applying low injection pressure using single injection point. The LAGL technique also generates extra cost related to the liquid pumping system, and a case-by-case, economic analysis is needed to make the decision of which technique would be more efficient.

1.3   Liquid-Assisted Gas-Lift Concept

The liquid-assisted gas-lift unloading process is illustrated in Figure 1.4. This process is similar to the conventional unloading process. It can be divided in five steps:

1) Both annulus and tubing are filled with liquid (formation and/or completion fluids). The injection pressure (p_{inj}) is low, and the bottomhole pressure (p_{bh}) is high due to the large hydrostatic pressure of the liquid.

2) Multiphase fluid (gas-liquid mixture) starts to be injected in the annulus pushing part of the liquid out the tubing. Bottomhole pressure would be the same as step 2.

3) Multiphase fluid is injected in the annulus pushing part of the liquid out the tubing. This is the moment right before the two-phase mixture reaches the GLV. At this point bottomhole pressure would be the same as step 2 in Figure 1.2. However, the injection pressure is lower due to the higher fluid mixture density in the annulus, because of the injection of gas and liquid (see Equation 1.1).

4) Gas reaches the GLV and starts to flow upward in the tubing. The presence of gas in the tubing lowers the mixture density of the fluid in the tubing, which consequently decreases the bottomhole pressure.

5) After this point, the Gas-Liquid-Ratio (GLR) of the injected gas-liquid mixture increases slowly to a point when only gas is injected. At this moment, the LAGL unloading process ends.
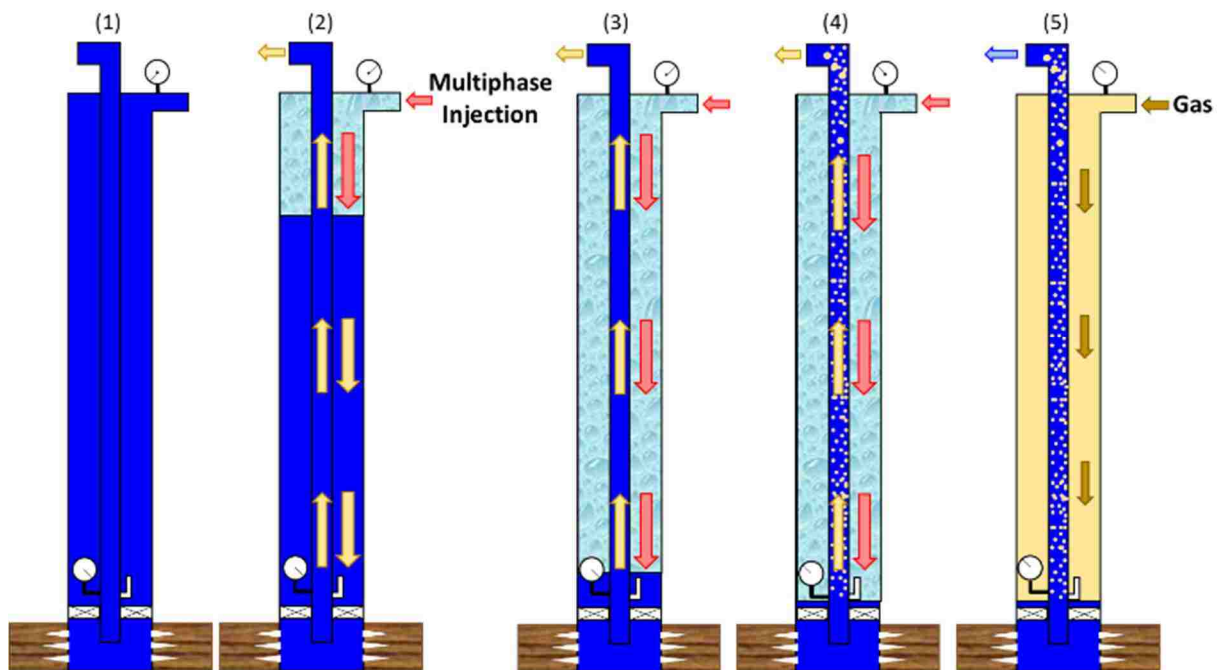

Figure 1.4. Steps of liquid-assisted gas-lift unloading.

1.4   Objectives

This work investigates the use of the LAGL technique as an alternative way to perform well unloading for gas-lifted wells. The two main objectives of this work are (i) to validate the use of LAGL technique to unload wells and (ii) to understand the controlling parameters of the LAGL system that can be used to optimize its efficiency. To accomplish these objectives, the following tasks will be carried out:

1) *Experimentally validate the LAGL concept for unloading applications*: A field-scale test well is used to validate the concept.

2) *Evaluate the effect of two-phase flow through orifice GLVs:* The orifice GLVs are originally designed for single-phase gas flow conditions. However, it is important to evaluate the performance of different orifice GLVs under two-phase flow conditions.

3) *Design and build a flow loop to investigate downward flow in pipe annulus:* The understanding of two-phase downward annular flow is essential for a further understanding of the LAGL concept. There is a lack of experimental studies on downward two-phase flow.

4) *Build a simulation model for the LAGL system:* Combine the knowledge acquired for each sub-system of the LAGL technique to develop a model for the LAGL system. This model will be used to perform system analysis and propose a procedure to perform well unloading using the LAGL technique for different well configurations.

1.5   Structure of the Dissertation

This dissertation is divided in five other chapters.

Chapter 2 presents the proof-of-concept of Liquid-Assisted Gas-Lift unloading technique, using a field-scale test well. Once the viability of the LAGL technique is proven, downward two-phase flow in annulus and two-phase flow through orifice GLVs will be experimentally analyzed.

Chapter 3 describes the experimental and numerical investigation of two-phase flow through Gas-Lift Valves using a multiphase flowloop. The experimental results are then used to evaluate the accuracy of the models available in the literature for two-phase flow through restrictions when applied to GLVs.

Chapter 1 discusses the experimental characterization of downward two-phase flow in an annulus, using a laboratory-scale flow loop. It presents results for flow regimes, liquid holdup and pressure gradients for a wide range of gas and liquid flow rates. Experimental results found in this work are compared to results presented in the literature for two-phase downward flow in tubing.

Chapter 1 presents a comparison of experimental data with a commercial transient flow simulator (OLGA$^®$) for multiphase flow in pipes. The validated simulation model is used to perform system analysis of the LAGL technique for the complete gas-lift unloading operation. A procedure for field deployment of LAGL is presented at the end of this chapter.

Chapter 6 presents an initial economic evolution of the LAGL unloading. In this evaluation, LAGL unloading is compared to single-point gas-lift and multipoint gas-lift unloading.

Chapter 7 presents a summary of the conclusions from this work and suggests future works toward subjects studied in this dissertation.

2   Liquid-Assisted Gas-Lift – Proof of Concept

In this chapter, results from a field-scale test well are used to prove the concept of Liquid-Assisted Gas-Lift unloading. The main objective of the experiments is to access the potential of LAGL unloading to decreases the maximum injection pressure for gas to reach a single GLV at the bottom of the well. Different gas-liquid ratios of the injection fluid are experimentally evaluated and it is observed that, for a constant gas flow rate there is an optimum injection interval for the liquid flow rate. More details about the well configuration and experimental procedures are discussed below.

2.1   Gas-Lift Unloading

It is common that oil wells with natural or gas-lift aided production, at some point during their life, face situations where the production has to be established or reestablished. In general, these situations can occur at the beginning of the well production or after a workover job, oil or completion fluids are found in the wellbore. In many cases, the wellbore liquid has to be pushed out from the wellbore annulus and tubing in order to bring the well back to production. This process of removing liquid out the wellbore is known as *wellbore unloading*.

The application of a conventional gas-lift unloading process for deep wells may require the use of multiple-gas-injection-points in order to keep the well kick off injection pressure at acceptable levels. The kick-off injection pressure is desired to be low enough to save compression power and, therefore, energy (Capucci & Serra, 1991). Often, empirical designs used to space the unloading and operation GLVs result in multipoint injection, unstable production, and low lift efficiency (Tang *et al.*, 1999).

The GLVs used for wellbore unloading are not deployed during the continuous or intermittent gas-lift production process. They are installed exclusively for the unloading process. A common type of unloading valve is the Injection-Pressure-Operated (IPO) valve. IPO valves are designed to stay closed during the production phase. However, it is possible that one or more of these valves present malfunction behavior over the life of the well. According to Candido (1989), a problem that may occur during operations with IPO valves is the loss of the original fluid pressure present in the bellow of these valves. The loss of bellow pressure would cause a malfunctioning of the valve and it would result in undesired leak of injection fluid to the production stream.

If one of the unloading valves starts to leak during regular operation, an uneconomic situation may be created. In such a situation, an excessive gas volume is needed due to an undesired shallower gas injection. Pittman (1982) stated that a primary concern in the daily operation of gas-lift is the cost of the gas compression facilities. Based on that, the presence of a leaky valve may create the need to stop production for its replacement (Kumar & Gupta, 2003).

Replacement of GLVs are conducted through a wireline intervention. Wireline operations can be time consuming and can pose risks to existing well completions (Xu *et al.*, 2013), and sometimes can lead to costly work-over. Production is also negatively affected by the downtime due the installation of the new valves (Elmer *et al.*, 2017). All these factors combined result in loss of revenue. Based on that, the use of multiple valves may increase well completion and intervention costs.

Another concern for conventional gas-lift unloading is the capital and operating expenses of gas compression facilities. Compressor discharge pressures of typically 1400 to 1700 *psi* may be required for single-point unloading, with relatively high throughput and a high compression ratio (Halim & Samad, 2016). Pittman (1982) stated that the need for an excessive volume of high-

pressure gas could make the process uneconomical. Therefore, efforts to lower injection pressure can potentially decrease capital and operational costs for gas-lift operations.

In offshore wells with subsea completions, wireline operations are relatively complex and workover rigs are, in general, extremely expensive (Capucci & Serra, 1991). To overcome problems related to multiple injection points, Candido (1989) proposed the use a booster compressor to perform the unloading operation in offshore wells. The proposed technique does not use multipoint injection to kick off the well. A single injection point (orifice GLV) at the bottom of the well composes the system. To inject high-pressure gas capable of reaching the bottom of the well, a booster compressor is used exclusively to kick-off the well. After the kick-off, the booster compressor is turned off and a main compressor sustains the production gas-lift.

2.2 Field Scale Well Test

The concept of LAGL is validated in this study using a 2,788 *ft* deep test well, located at the Petroleum Engineering Research & Technology Transfer Laboratory (PERTT Lab) at Louisiana State University. The experiments to validate the applicability of LAGL unloading are performed by the injection of a gas-liquid two-phase fluid mixture in the annulus. This allows the evaluation of the maximum injection pressure required to bring the injected fluids to the bottom of the well. Different gas and liquid flow rates are evaluated, and the results are presented at the end of this chapter.

2.2.1 Experimental Procedure

Two different sets of experiments are performed in this study to evaluate the efficiency of the LAGL in field conditions:

1   The first set of experiments has the objective to characterize the flow of single-phase water through the test well system. Tests using water would enable the evaluation of the pressure

drop due to friction in the GLV and flow through annulus and tubing (Δp_{GLV} and Δp_f in

Equation 1.1). For the single-phase flow experiments, the entire well (outer casing, inner casing

and tubing) are filled with water initially. In these experiments, eight different water flow rates

(see Table 2.1) are injected in the inner casing using the gas injection line. The water flows

through the inner casing, through the orifice GLV, flows upwards in the tubing and through

the separator, and then returns to the water storage tanks.

Table 2.1. Test matrix for well tests to evaluate the efficiency of the LAGL concept.

Case #	$q_{G,inj}$ (agpm*)	$q_{G,inj}$ (acfd*)	$q_{G,max}$ (Mscfd)	$q_{G,min}$ (Mscfd)	q_L (gpm)
1	5	962	34	11	20
2	5	962	29	11	30
3	5	962	35	12	40
4	5	962	25	15	50
5	5	962	31	12	60
6	10	1,925	120	11	20
7	10	1,925	70	40	40
8	10	1,925	48	11	45
9	10	1,925	60	15	50
10	10	1,925	53	15	55
11	20	2,887	294	70	20
12	20	2,887	274	80	30
13	20	2,887	229	60	40
14	20	2,887	209	60	50
15	20	2,887	271	90	70

*agpm = actual*** gallons per minute
**acfd = actual cubic feet per day
*** Actual flow rate is the actual volume of fluid at a specific in situ condition (pressure and temperature of the process).

2   The second set of the experiments carried out aims to evaluate if the basic concept of the LAGL

(e.g., injection of gas-liquid mixtures during unloading), which is expected to lower the

injection pressure during the unloading operation. For each experiment, the entire well was

initially full of water (to simulate formation or completion fluids). The inflow line is kept

closed during the experiment and the gas injection line was used to inject the gas-liquid mixture

in the inner annulus. The outflow line is connected to the gas-liquid separator. For each

15

experiment, constant-actual-volumetric flow rates (e.g., volumetric flow rates at pressure and temperature of the injection lines) of water and natural gas are injected in the inner casing. Table 2.1 presents the experimental test matrix. All tests ended when the gas-liquid mixture reached the GLV at the bottom of the well. The tests ended at this stage because the moment the gas-liquid mixture to reach the GLV is when the injection pressure should be the highest during the unloading operation.

The natural gas used in the experiments was supplied from a pipeline from the utilities at university campus, but no fluid composition was available at the time. According to the North American Energy Standards Board (NAESB 2017), natural gas in North America has a typical composition presented in Table 2.2 (NAESB 2017). Table 2.2 shows that, typically, more than 94% in volume of natural gas is composed by methane.

Table 2.2. Typical chemical composition of natural gas (NAESB 2017).

Component	Typical analysis (vol%)	Range (vol%)
Methane	94.9	87.0–96.0
Ethane	2.5	1.8–5.1
Propane	0.2	0.1–1.5
Isobutane	0.03	0.01–0.3
n-Butane	0.03	0.01–0.3
Isopentane	0.01	Trace to 0.14
n-Pentane	0.01	Trace to 0.14
Hexane	0.01	Trace to 0.06
Nitrogen	1.6	1.3–5.6
Carbon dioxide	0.7	0.1–1.0
Oxygen	0.02	0.1–1.0
Hydrogen	Trace	Trace to 0.02

2.2.2 Well Configuration

Figure 2.1 presents the well configuration. This test well includes a 5.50 *inch* OD and 4.89 *inch* ID inner casing, and a 2.88 *inch* OD and 2.44 *inch* ID production tubing. A GLV mandrel is installed in the tubing at the depth of 2,717 *ft*, with a 44/64 *inch* port size orifice GLV. The well is

equipped with temperature and pressure transducers at two different depths (1,648 *ft* and 2,717 *ft*). Pressures and temperatures are also measured in the gas injection line and in the outflow line at the surface. The water flow rate injected in the well was measured using a magnetic flow meter, and the gas flow rate injected was measured using an orifice meter.
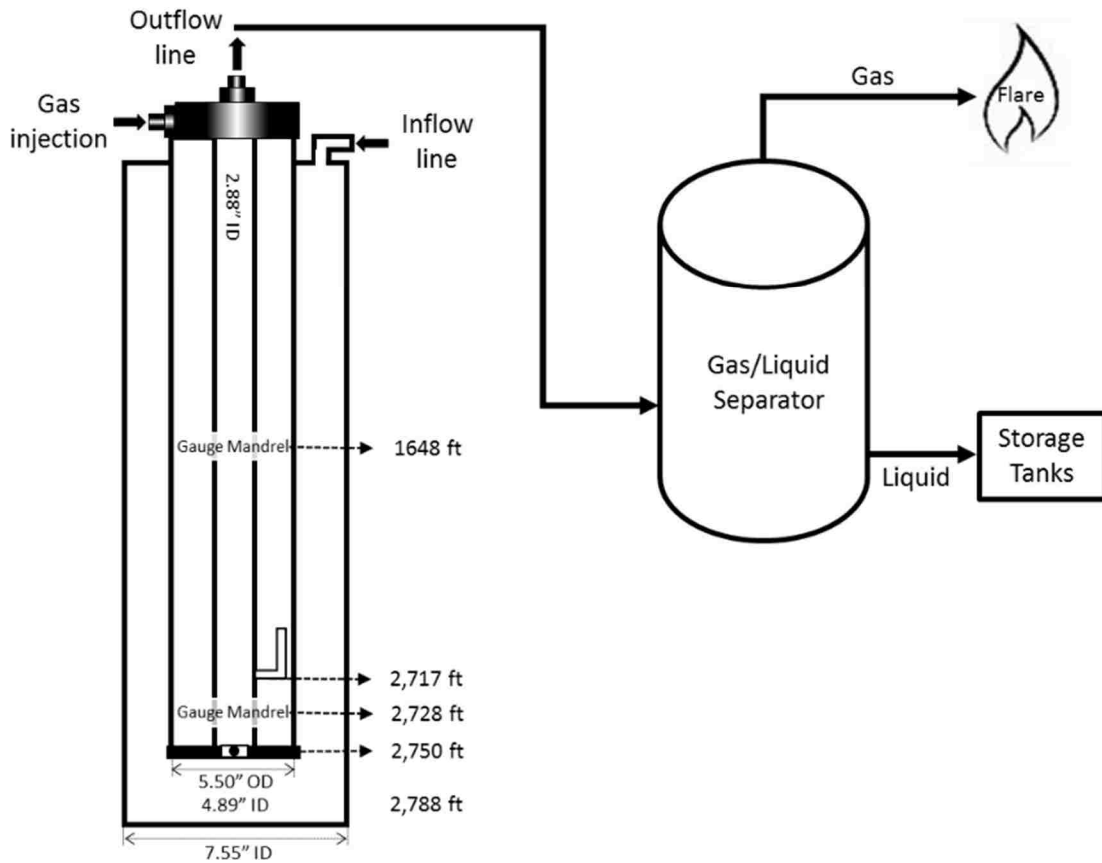

Figure 2.1. Configuration of the test well used in this study.

Natural gas and water were the fluids used in all experiments. After water and gas flow through the well, these fluids were separated downstream to the outflow line in a vertical separator. The natural gas was vented out to the flare, and the water re-circulated to the storage tank. The experiments were performed in 2011 (prior to the author's arrival at LSU), during a partnership between LSU and Shell Production Company. In 2014, Shell and LSU signed a new project and one of the main roles of this project was to analyze the data obtained during the 2011 project.

2.3   Results for Field-Scale Test Well

2.3.1   System characterization for single-phase water

The first component of the system that is analyzed with the single-phase water flow tests is the pressure drop through the GLV. Figure 2.2 shows the experimental results for the pressure drop through the GLV for the injection in the well at different water flow rates. The subtraction of the pressure at the bottom of the inner casing and the pressure at the bottom of the tubing (see Figure 2.1) results in the experimental pressure drop across the GLV. Figure 2.2 shows the pressure drop increasing with the water flow rate. These results are in accordance with other studies in the literature (Surbey *et al.*, 1989).
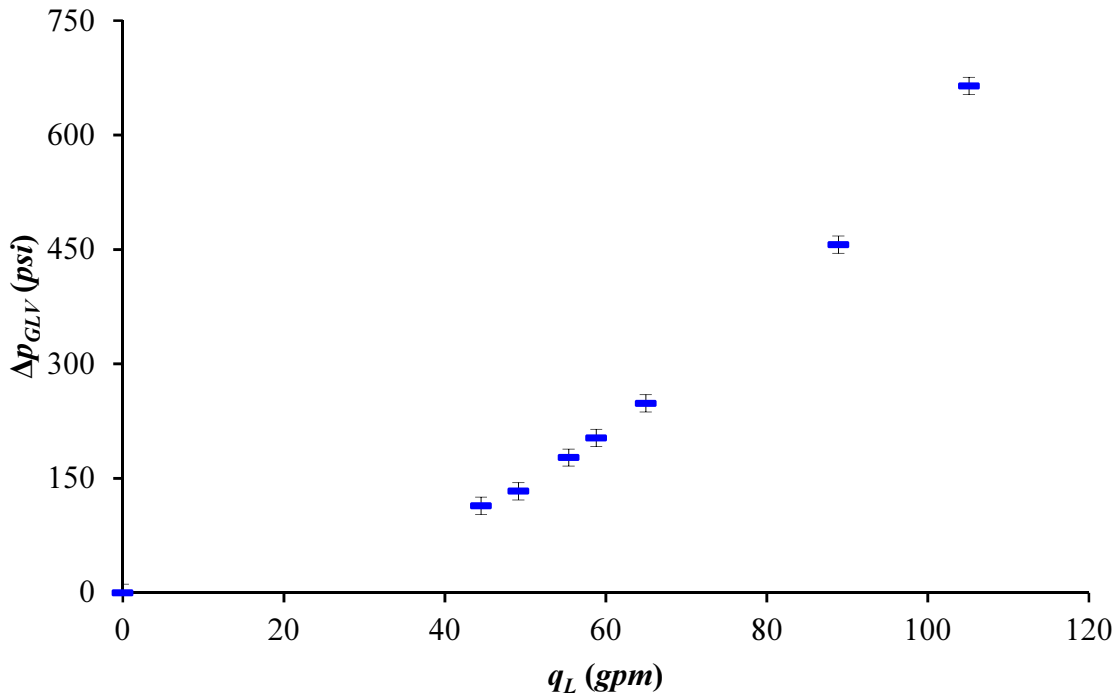

Figure 2.2. Differential pressure across GLV as a function of water flow rate through the GLV.

The downward flow in the annulus is another important part of the LAGL system, as it significantly affects the injection pressure. Figure 2.3 shows the experimental results for the total pressure drop in the downward water flow through the annulus, and through the GLV. The results

presented in Figure 2.3 show the contribution to the total pressure drop from the pressure drop through the GLV, hydrostatic effects and friction effects. The sum of these three components results in the total pressure drop.

As shown in Figure 2.3, for the single-phase water flow test in the well, the hydrostatic effect accounts for more than 90% of the pressure change for the flow in the casing annulus. The friction loss is smaller for lower water flow rates, and it increases for larger water flow rates. However, even for the higher flow rates tested, the friction effects in the annulus and tubing are negligible when compared to the hydrostatic and accelerational effects. Figure 2.3 also show that the single-phase water flow through the GLV has a relevant contribution to the total pressure drop. This contribution is small for low water rates, but it becomes significant for high water flow rates.
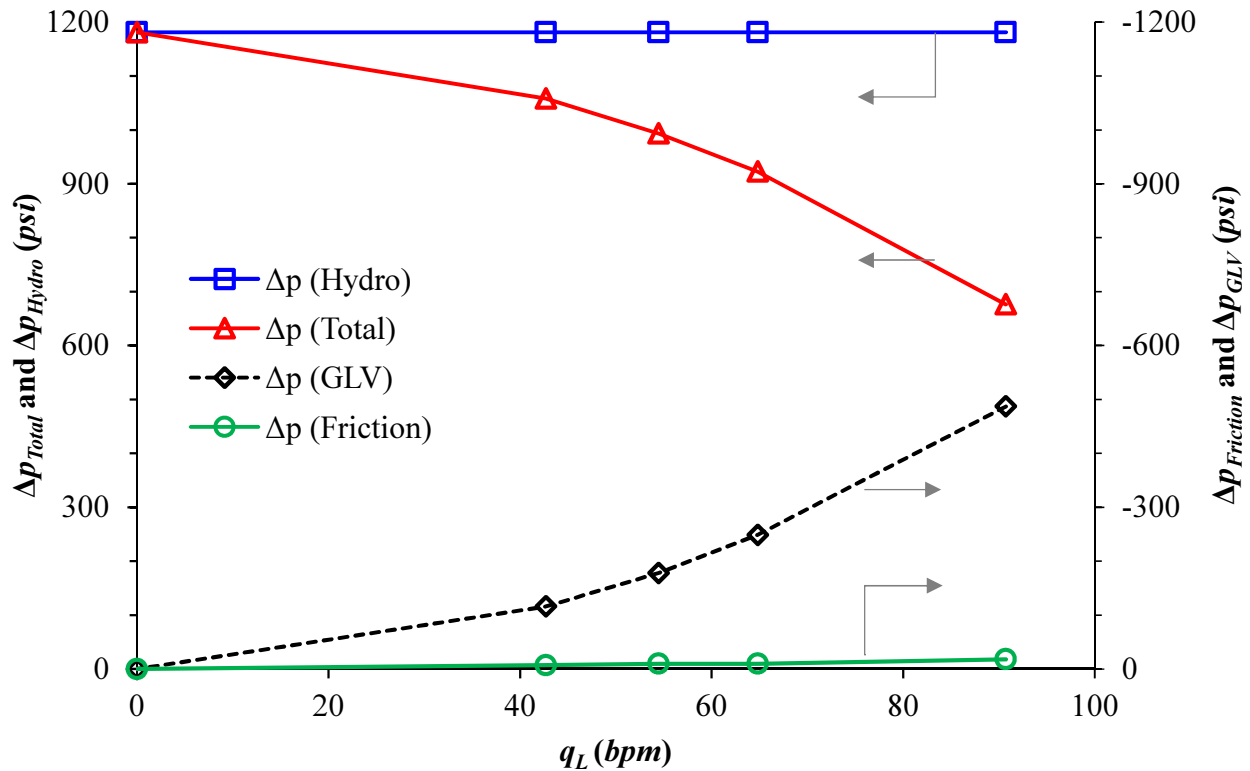

Figure 2.3. Pressure drop for the downward flow and flow trough the GLV.

### 2.3.2 *Proof of concept using a field-scale test well*

In order to analyze the applicability of LAGL for unloading operations, a series of experiments were conducted using the field-scale test well described in Figure 2.1. The main objective behind the concept of LAGL is to decrease the injection pressure by injecting a gas-liquid mixture rather than single-phase gas (conventional gas-lift concept). Figure 2.4 shows the relationship of the injection pressure as a function of time for six combinations of gas and water flow rates, while using the concept of LAGL. Figure 2.4 shows the results for two constant water flow rates of 50 and 40 *gpm*, and for three different actual-volumetric gas flow rates: 5, 10 and 20 actual *gpm* (*agpm*).

As shown in Figure 2.4, at the beginning of each experiment, the injection pressure is constant. During this period of constant injection pressure, single-phase water is injected and it has a constant flow rate. This initial single-phase water injection is important to guarantee that no trapped gas is in the well. After this initial period of single-phase water injection, gas injection starts.
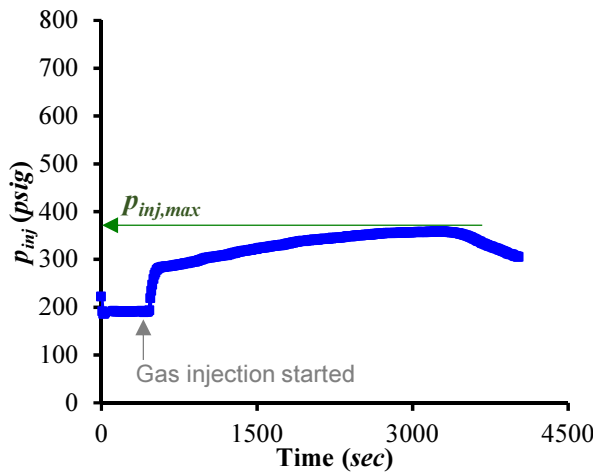
Once gas injection into the well is initiated, the injection pressure starts to increase due to a decrease in the mixture density in the annulus (see Equation 1.1). Over the entire experiment, the actual gas and water flow rates are constant. The injection pressure keeps increasing as the gas phase goes deeper in the well, up to a point in time when the gas phase reaches the GLV and enters the tubing. When the gas phase reaches the GLV, it starts flowing upward through the tubing, and consequently, the injection pressure starts to decrease (gas in the tubing lowers the mixture density of the fluid in the tubing, which consequently decreases the injection pressure – see Equation 1.1). At this point, the experiment ends.
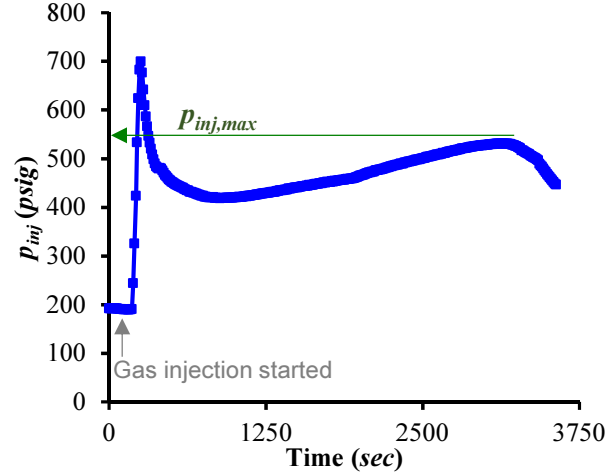
(a) q_L = 50 *gpm* and q_G = 5 *agpm*

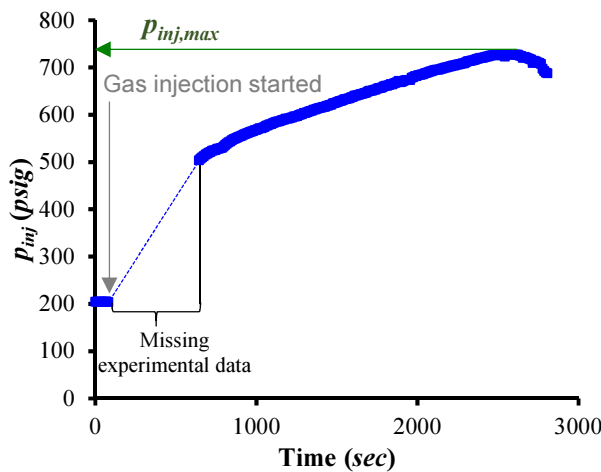(b) q_L = 50 *gpm* and q_G = 10 *agpm*
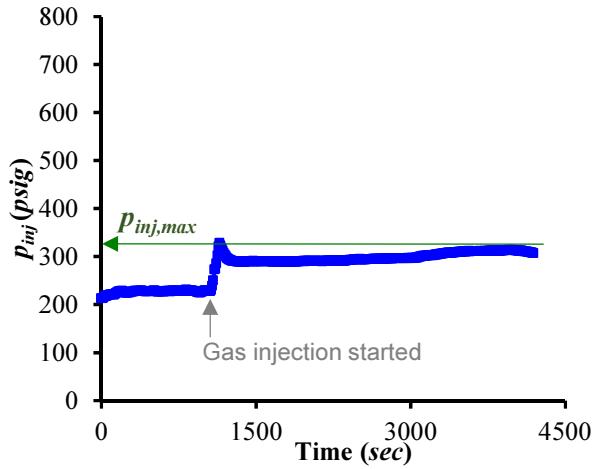
(c) q_L = 50 *gpm* and q_G = 20 *agpm*
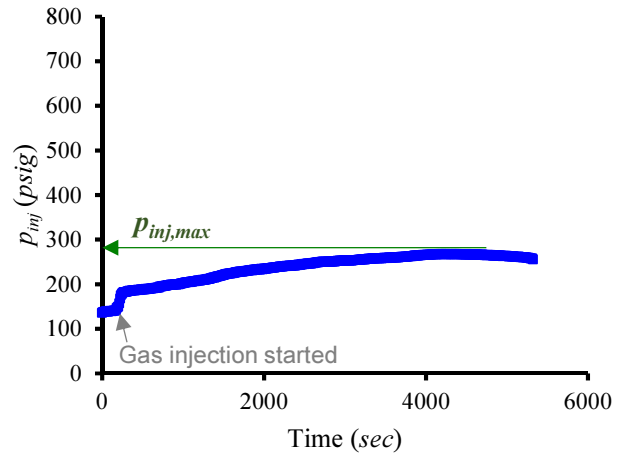
(d) q_L = 40 *gpm* and q_G = 5 *agpm*

(e) q_L = 40 *gpm* and q_G = 10 *agpm*
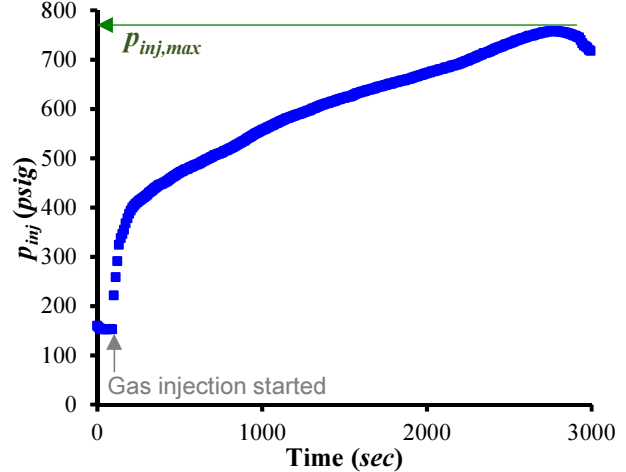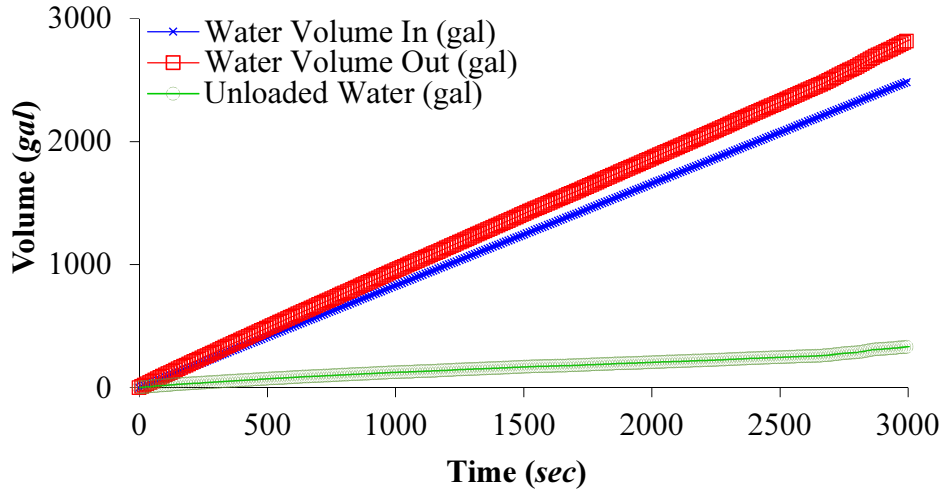
(f) q_L = 40 *gpm* and q_G = 20 *agpm*

Figure 2.4. Relationship of the injection pressure as a function of time for six combinations of gas and water flow rates while using the concept of LAGL.

The main result obtained in each experiment is the maximum injection pressure ($p_{inj,max}$) necessary to initiate gas injection in the tubing. Graphically, $p_{inj,max}$ is identified by the maximum pressure towards the end of the test. Some experiments have a time interval with no data (e.g. Figure 2.4c). A malfunctioning in the data acquisition system during a minor time interval caused the missing data. However, the missing data do not affect the main objective of the test, which is to obtain the $p_{inj,max}$ experimental value.

The GLR of the injection fluid increases from Figure 2.4a to Figure 2.4c. The analysis of these three figures indicate that, during the unloading process, higher GLR for the injection fluid would increase the injection pressure. For a lower water flow rate injection (40 *gpm*), the same analysis can be obtained from Figure 2.4d to Figure 2.4f. When comparing the results for maximum injection pressure presented in Figure 2.4a and Figure 2.4d, it is observed that the increase of the liquid flow rate (from 40 gpm to 50 gpm) reduces the maximum injection pressure necessary to reach the bottom of the well. It happens because as the liquid flow rate increases, the mixture density for the injection fluid also trends to increase, which would result in lower injection pressure (see Equation 1.1). The same analysis can be performed for Figure 2.4b and Figure 2.4e, and Figure 2.4c and Figure 2.4f.

Figure 2.5 shows experimental results for the volume of water injected, removed, and unloaded (e.g., the difference between the removed and injected amount) from the well as a function of time for three combinations of water and gas flow rates. The time zero in Figure 2.5 represents the moment of the beginning of injection of the gas and water into the well. These experimental results are plotted for times up to the maximum injection pressure reaches its maximum value.

(a) $q_L = 50$ *gpm* and $q_G = 5$ *agpm*
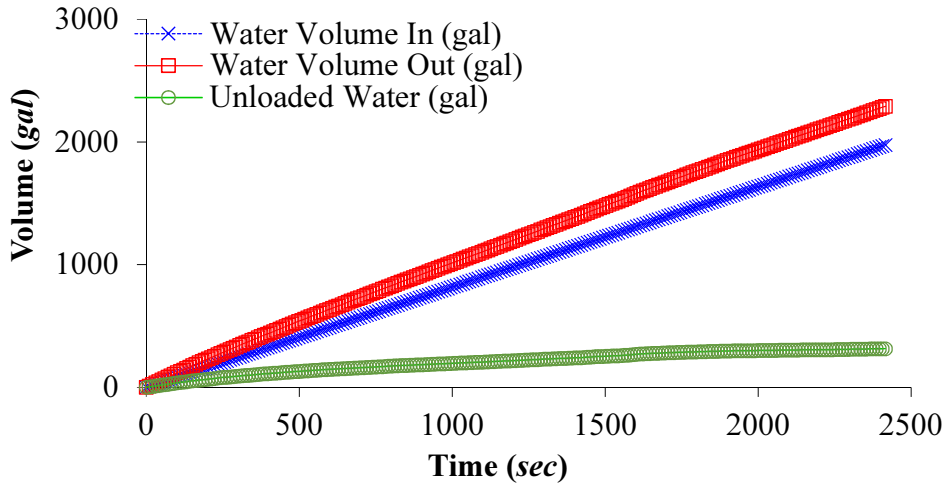
(b) $q_L = 50$ *gpm* and $q_G = 10$ *agpm*
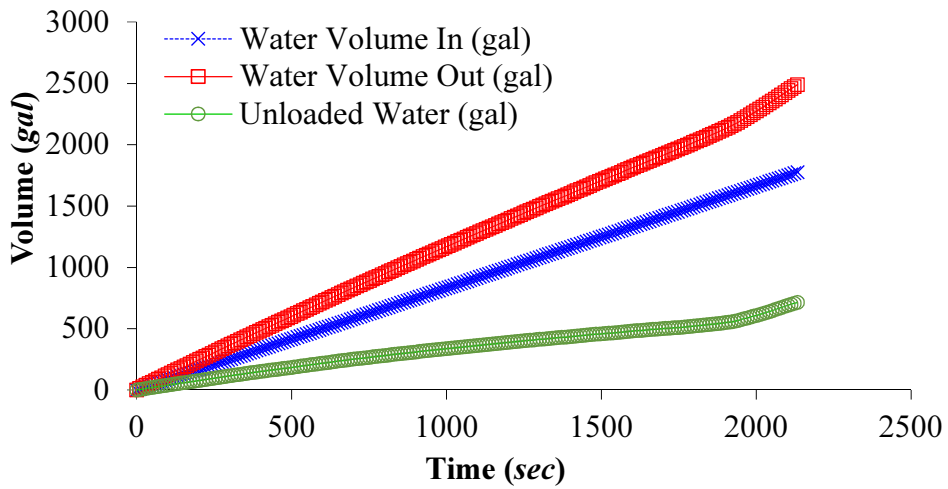
(c) $q_L = 50$ *gpm* and $q_G = 20$ *agpm*

Figure 2.5. Experimental water volume injected, removed, and unloaded as a function of time, for three combinations of gas and water flow rates while using the concept of LAGL.

23

As shown in all three plots in Figure 2.5, the volume of water removed (red dotted line) present values always higher than the injected water volume (blue dashed line). It indicates that the volume of water that was originally in the well is unloaded (the difference between the volume removed and injected), since the unloaded water values are always positive for all three cases. For Figure 2.5a (q_L = 50 *gpm* and q_G = 5 *agpm*), the unloaded volume is around 330 *gal*, while for Figure 2.5b and c the values are around 320 and 710 *gal*, respectively. The volumes of unloaded water in Figure 2.5 indicate the effectiveness of the LAGL unloading process.

Figure 2.6 shows the experimental results for the maximum injection pressure as a function of the water flow rate for a constant gas flow rate of 20 *agpm*. As can be seen from this figure, low and high water rates result in high maximum injection pressure, but intermediate water flow rates yields a point of minimum injection pressure. This behavior on the maximum injection pressure can be explained by using Equation 1.1 and the experimental results from Bhagwat and Ghajar (2012).
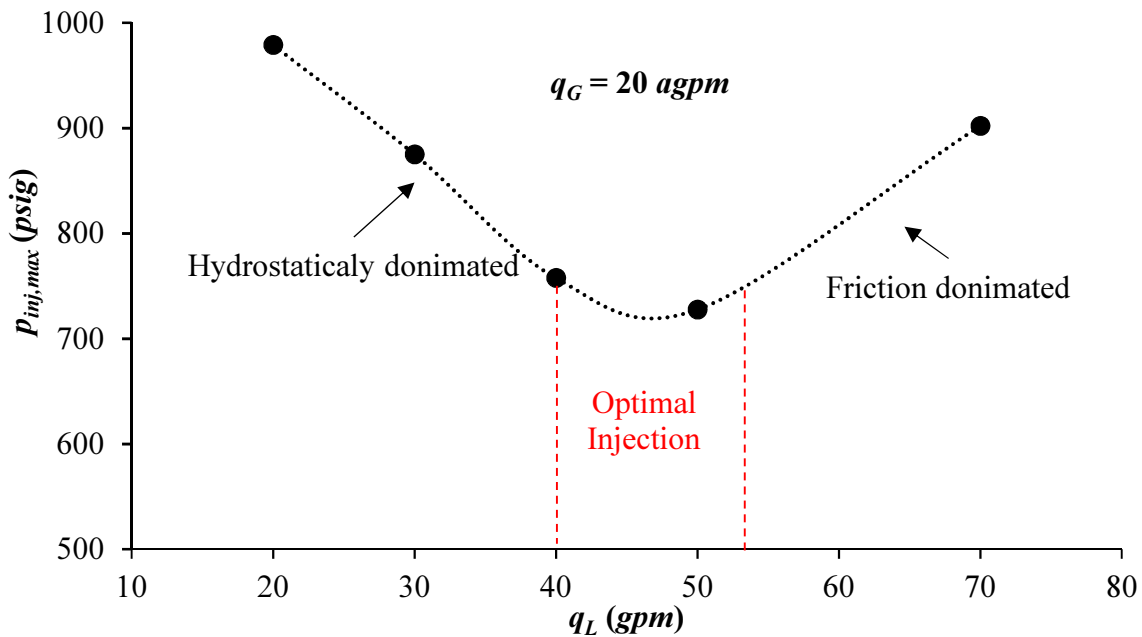

Figure 2.6. Maximum injection pressure as a function of water flow rate for gas injection rate of q_G = 20 *agpm*.

24

For lower water flow rates (labeled as hydrostatically dominated flows in Figure 2.6), void fraction in the casing annulus decreases as water flow rates is raised, due to an increase in the fluid mixture density. If the flow rate changes do not significantly affect the friction and accelerational (GLV) terms, Equation 1.1 shows that higher fluid mixture density in the annulus will decrease injection pressure. Bhagwat and Ghajar (2012) shows that void fraction increases exponentially with slip ratio (u_{sG}/u_{sL} or q_G/q_L) for downward two-phase flows. However, as the water flow rate keeps increasing (for a constant gas flow rate), friction effects start to become dominant in Equation 1.1, and the injection pressure starts to increase for higher water flow rates. For water flow rates higher than about 45 *gpm* in Figure 2.6, the pressure drop through the GLV dominates the pressure drop due to friction and accelerational components. The friction pressure drop due to the flow through the casing annulus is negligible for the conditions tested in this study, when compared to the pressure drop in the GLV (see Figure 2.3).
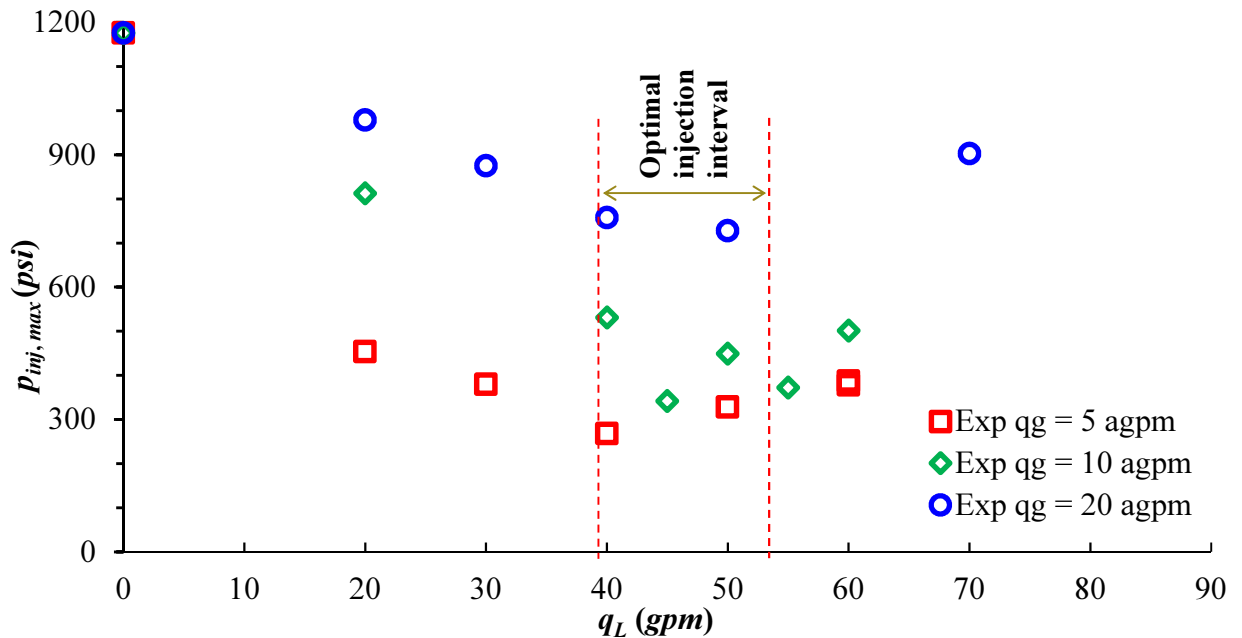

Figure 2.7. Maximum injection pressure as a fuction of water flow rate for different gas injection rates.

Figure 2.7 presents the maximum injection pressure as a function of the water injection rate for all cases tested. This figure presents the experimental results for three gas injection flow rates (5, 10 and 20 *agpm*). The experimental results for all multiphase injection curves have their profiles similar to the one presented in Figure 2.6. For the three gas rates that are tested in this study, the water injection rate that provides the minimum injection pressure (optimal injection interval) is within the range of water flow rate between 40 and 53 *gpm*.

Table 2.3. Actual gas and liquid flow rates, standard gas flow rate at maximum injection pressure and maximum injection pressure. The lines highlighted indicate the conditions from the tests, which shows the lowest injection pressure for a constant water flow rate.

Case #	q_G (agpm)	q_L (gpm)	q_L (Mscfd @ $p_{inj,max}$)	$p_{inj,max}$ (psi)
1	5	20	34	454
2	5	30	29	379
3	**5**	**40**	**35**	**268**
4	5	50	25	328
5	5	60	31	378
6	10	20	120	742
7	10	40	70	531
8	**10**	**45**	**48**	**342**
9	10	50	60	449
10	10	55	53	372
12	20	20	294	979
13	20	30	274	875
14	20	40	229	758
15	**20**	**50**	**209**	**728**
16	20	70	271	902

One major conclusion from this analysis is that there is a narrow range for the water flow rate required to obtain the optimal injection pressure. This narrow range for liquid injection rates may increase the challenge for field application of the LAGL concept, as it would require monitoring and control of liquid flow rate with a narrow margin to deploy effectively this technique in the field.

2.4   Power Requirement Analysis

Figure 2.8 presents the calculated horsepower required to compress the gas and to pump the water for single-phase gas injection and LAGL. This section evaluates the power requirement for both techniques as a function of the gas flow rate. Two curves are presented for each plot: the red dotted curve represents the power requirement for injection of single-phase gas (no liquid injected), and the blue dashed curve represents the power requirement for the injection of liquid and gas. The liquid injection flow rate selected (q_L = 50 *gpm*) is based on the optimal liquid injection interval that is shown in Figure 2.7. The injection pressure is 1,300 *psi* for the single-phase case (q_L = 0 *gpm*) in both plots in Figure 2.8, which is the maximum injection pressure required for the single-point gas injection during the unloading operation. For the LAGL case (q_L = 50 *gpm*), two different injection pressure are plotted: Figure 2.8a shows the results for an injection pressure of 300 *psi*, and Figure 2.8b shows the results for an injection pressure of 700 *psi*.

(a) LAGL injection pressure: 300 *psi*   (b) LAGL injection pressure: 700 *psi*
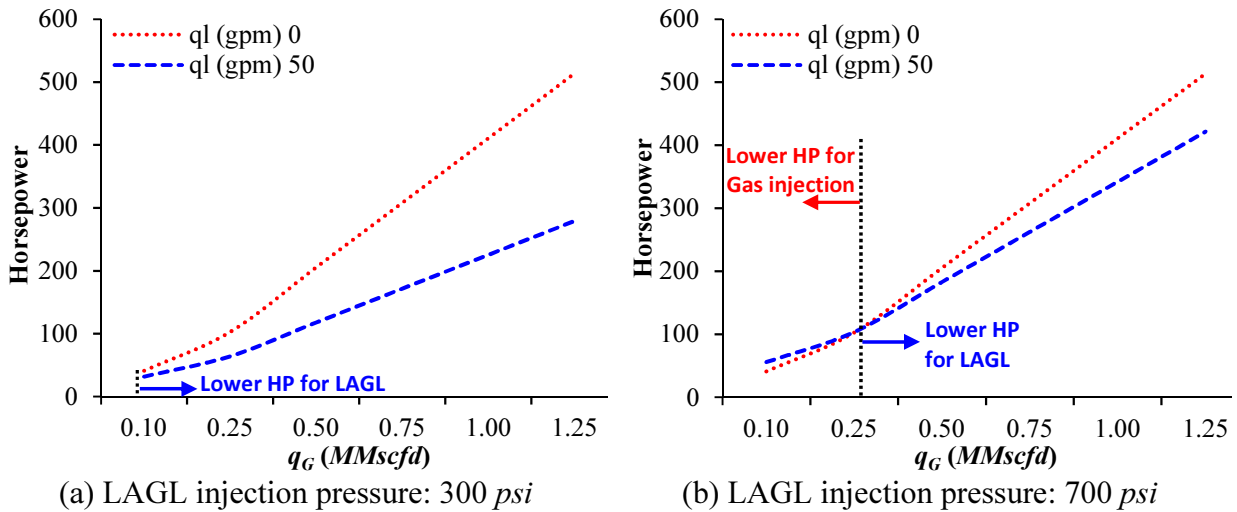Figure 2.8. Total horsepower (gas compressor + liquid pump) for combinations of liquid flow rates (q$_L$ in *gpm*) and gas flow rates (q$_G$ in *MMscfd*). Single phase gas injection pressure is 1,300 *psi*.

The results presented in Figure 2.8a show that, for gas flow rates higher than 0.1 *MMscfd*, the use of the LAGL would require lower horsepower than single-phase single-point gas injection. If the injection pressure for the LAGL is 700 *psi* (Figure 2.8b), the LAGL would require lower horsepower for gas flow rates higher than 0.25 *MMscfd*. Thus, Figure 2.8 shows that the use of the LAGL is thermodynamically more efficient than the single-phase single-point injection in conditions that require high gas flow rates. The requirement of higher gas flow rates during the unloading operations is defined primarily by the tubing diameter. Larger tubing diameters would require larger gas velocities to lift the liquid to the surface (Turner *et al.*, 1969).

To minimize the injection pressure during the unloading for the case of Figure 2.6, the experimental results in this figure shows that the optimum liquid and gas flow rate injection are 50 *gpm* and 0.2 *MMscfd*, respectively. The maximum injection pressure for this case is about 700 *psi*. Comparing experimental results in Figure 2.6 with the plot presented in Figure 2.8b leads to the conclusion that the LAGL technique requires slightly higher horsepower than the conventional single-point injection for this particular case. However, the injection pressure is lower for the LAGL than the pressure required for single-phase single point injection to unload the well. It is important to notice that, although the horsepower requirement for the case in Figure 2.6 is higher for the LAGL than for single-phase gas injection, the maximum injection pressure is still lower for the LAGL. These results clearly show that the use of LAGL is not always beneficial. However, the use of the LAGL can allow the well unloading using a compressor with lower pressure specifications. In fact, the gas compressor available in the facility where the well tests were carried out for this study would only be able to unload the well using the LAGL technique, since the maximum working for this compressor was 1,000 *psi*.

2.5 Conclusions

This chapter presented a new technique for gas-lift unloading operations, termed in this study as the Liquid Assisted Gas-Lift (LAGL). The main idea behind this new concept is to inject a gas-liquid mixture during the unloading process to lower injection pressure, and then enable the use of a single gas-lift valve at the bottom of the well, while reducing compression and GALV replacement costs. Conventional gas-lift unloading operations use multiple valves and injection of single-phase gas. The use of single GLVs during unloading operations would decrease the number of potential leak points between casing and production tubing, by eliminating the multiple gas-lift valves required on conventional unloading processes.

This study evaluates the LAGL concept in using a field-scale test well. This well has a vertical depth of 2,788 ft. The working fluids used during the experimental tests are natural gas and water. The experimental results show that the use of LAGL technique has potential to reduce significantly the injection pressure during unloading operations. The use of the LAGL technique can enable the reduction of the injection pressure from 1,300 psi (when injecting single-phase gas) to approximately 300 psi (when injecting gas-liquid mixtures). Field trials are still needed to truly prove the concept.

The experimental results also show that the injection pressure is only reduced significantly for gas-liquid flow rate ratios (q_G/q_L) lower than 2. For gas-liquid flow rate ratios higher than 2, there is the appearance of the annular flow regime (falling liquid film) in the downward two-phase flow in the casing annulus, which generate high void fraction flow in the annulus. As a consequence of the high void fraction in the annulus, the fluid mixture density decreases and larger injection pressures are required during the unloading process. Other studies in the literature about downward two-phase flow in vertical pipes support these results. The main idea behind the concept of the LAGL is to increase the mixture fluid density in the annulus to enable lower injection pressures.

29

For a better understanding of the flow behavior in the different components of LAGL system, it is suggested here to investigate the following topics: downward two-phase flow in annulus (e.g., flow regime map, pressure gradient, liquid holdup), two-phase flow through gas-lift valves (performance curves), and full simulation of the LAGL unloading process. The next chapters of this dissertation discusses these topics.

3   Two-Phase Flow through Gas-Lift Valves

The successful development of the LAGL unloading technique depends on the understanding and characterization of the behavior of all components of the LAGL system. Gas-lift valves play an important role in traditional gas-lift operations, and it is not different for the LAGL unloading technique. The design of traditional gas-lift operations takes in consideration the performance curves of unloading and operating GLVs under single-phase gas flow conditions. Studies on the characterization of GLVs for single-phase gas flow have been conducted for many years, and nowadays many experimental and numerical characterization studies are available in the literature (Pittman, 1982; Winkler & Camp, 1987; Decker, 1993; Hepguler *et al.*, 1993; Hall & Decker, 1995; Faustinelli & Doty, 2001; Decker, 2007). However, there is a lack of investigation on the experimental and numerical characterization of two-phase flow through GLVs. This lack of studies is explained by the fact that conventional gas-lift systems are not designed to handle two-phase flow through the GLV. Nevertheless, for the LAGL unloading, the presence of two-phase flow through the GLV is expected throughout the unloading process.

Due to the importance of characterization of the pressure variation in GLV during the LAGL unloading process, this work presents an experimental characterization of methane-water two-phase flow through two orifice GLVs. This work also evaluates the applicability of currently available numerical models for two-phase flow through restrictions to predict the performance of GLVs under two-phase flow conditions.

3.1   Introduction

Some authors (Neely et al., 1974; Steele, 1976; Laing, 1989, 1991) have previously described the importance of experimental characterization of gas-lift valves (GLVs) for the successful design of gas-lifted wells.

The gas-lift valve is the central piece of gas-lift operations. These valves directly control well production rates and their performance is used to establish the technical and economic parameter of fluid lifting (Takács, 2005). Over the years, different types of GLVs were designed and today a wide number of valves, with different features and operating principles, are available in the market. In traditional gas-lift operations, there are two main categories of GLV:

- Unload valves: valves used during the unloading process.

- Operating valves: valves used during the regular gas-lift operation.

One of the most common designs of GLVs used during continuous gas-lift operations is the orifice GLV. Orifice GLVs have the simplest design among all GLVs available in the market. As shown in Figure 3.1, an orifice GLV includes four main components:

    i)   inlet port
    ii)   orifice port
    iii)   a reverse flow check valve
    iv)   outlet port

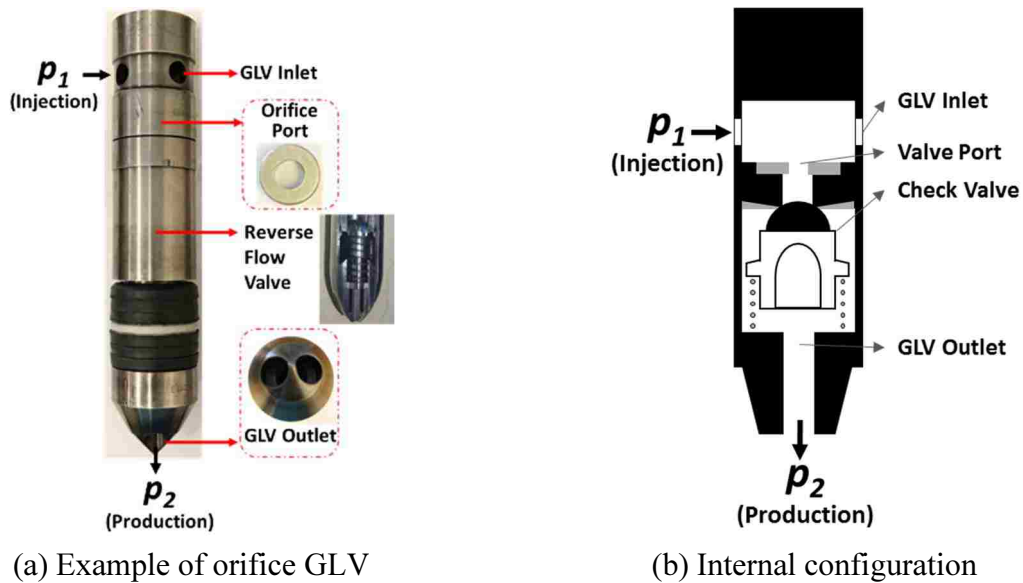(a) Example of orifice GLV   (b) Internal configuration
Figure 3.1. Orifice gas-lift valve.

The orifice port size dictates the performance curve of the valve (flow rate across the orifice as a function of pressure ratio). Figure 3.2 illustrates the performance curve for an orifice GLV when submitted to single-phase gas flow at a constant upstream pressure (p_1) and temperature. Figure 3.2 shows that the performance curve for an orifice GLV can be divided in two flow regions: critical and subcritical. At zero gas flow rate, the pressure ratio is one. As the pressure ratio across the orifice valve decreases at a constant upstream pressure (p_1), the gas flow rate increases. The region where a variation in the pressure ratio affects the gas flow rate through the valve is called subcritical flow region. If the pressure ratio across the valve is slowly reduced, the fluid flow reaches the sonic velocity and, at this point, the transition between subcritical and critical flow will occur. According to Green and Perry (2007), for air with pressure and temperature approximate to standard conditions, the critical pressure ratio is approximately 0.53.
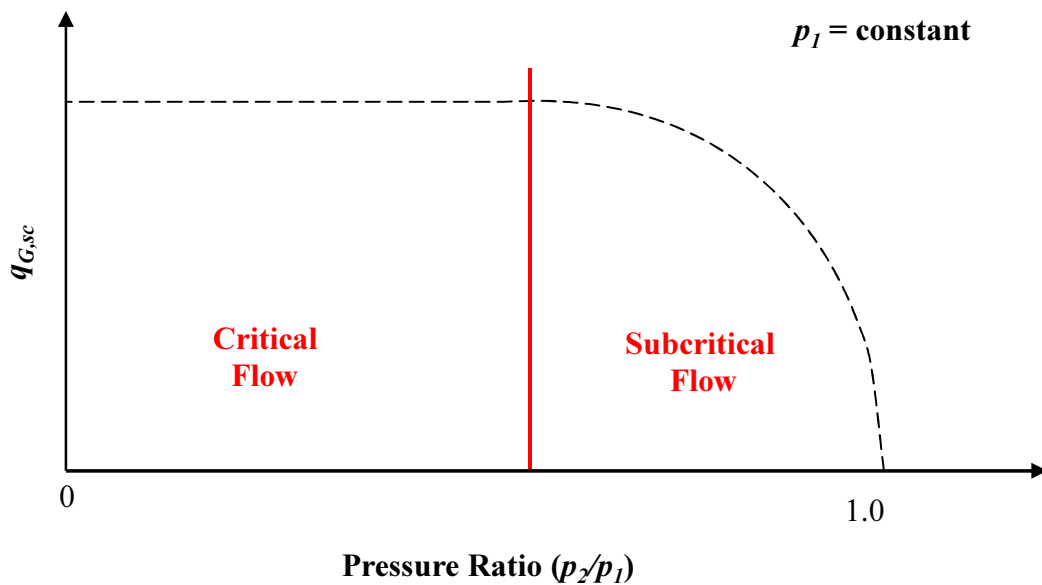

Figure 3.2. Performance curve for single-phase gas flow through an orifice valve with a constant injection pressure.

During gas-lift unloading and regular gas-lift operations, GLVs may be submitted to flow of single-phase gas or single-phase liquid. Including the proposed new technique to unload wells

called Liquid-Assisted Gas-Lift (Coutinho *et al.*, 2018). Therefore, understanding the valve performance under single- and two-phase flow is essential for the correct design (valve port sizing) of the unloading and oil production processes for regular gas-lift operations and for the newly proposed LAGL unloading method (Coutinho *et al.*, 2018).

The dynamic performance of GLVs for single-phase gas flow has been extensively investigated in the last three decades, and reliable test procedures and simulation models are available in the literature (Pittman, 1982; Winkler & Camp, 1987; Decker, 1993; Hepguler *et al.*, 1993; Hall & Decker, 1995; Tang *et al.*, 1999; Faustinelli & Doty, 2001; Decker, 2007). However, no studies can be found in the literature on two-phase flow through GLVs. In liquid-assisted gas-lift operations, gas-liquid two-phase flow through operating GLVs will occur during the well unloading, and the performance of these valves under two-phase flow is essential on the optimization of the design of LAGL unloading operations (Coutinho *et al.*, 2017). Before the development of LAGL unloading by Coutinho *et al.* (2018), there was no clear need for understanding the performance of GLV under two-phase flow. This is likely the main reason why studies about the performance of GLVs under two-phase flow cannot be found in the literature.

There are few studies on gas-liquid two-phase flow through orifices that can be potentially used to understand and predict the behavior of two-phase flow through orifice GLVs. However, the presence of the reverse check valve, inlet and outlet ports may significantly affect the flow in GLVs. Therefore, the two main objectives of this chapter are:

- Experimentally characterize two-phase through GLVs, for a wide range of gas-liquid-ratio (from 600 to 11000 *scf/bbl*) and pressures (from 140 to 450 *psi*);
- Evaluate the performance of models developed for two-phase through only orifices/restrictions but applied to orifice GLVs.

3.2 Two-Phase Flow through Orifices/Restrictions

Similar to single-phase flow through restrictions, gas-liquid two-phase flow through orifices may occur in either critical or subcritical flow regime. In critical flow, the flow rate reaches its maximum value for a given set of upstream pressure and gas-liquid ratio, which means that the fluid mixture flowing through the orifice reach sonic velocity. During critical flow, disturbances in the downstream pressure do not propagate upstream to the orifice throat.

According to Sachdeva *et al.* (1986), if the downstream pressure is progressively increased, the upstream pressure and flow rate will remain constant until the flow reaches the critical-subcritical pressure ratio boundary. Once the critical-subcritical pressure ratio boundary is reached, any small increase in the upstream pressure results in changes in both flow rate and upstream pressure. For upstream pressure below this boundary, the flow is in subcritical flow, and mixture fluid velocity through the choke is sub-sonic. In subcritical flow, flow rate depends on the pressure deferential through the orifice, and oscillations in the downstream pressure will affect the upstream pressure.

Therefore, to predict the two-phase flow performance in orifices, it is first necessary to predict the pressure ratio boundary between critical and subcritical flow. Critical-subcritical pressure ratio boundary definition for two-phase flow is more complex than for single-phase flow (Brill & Mukherjee, 1999). The use of a wrong pressure ratio boundary would cause the use of a critical flow model for subcritical flow situations or vice-versa, and it would result in a miss-prediction of the flow behavior.

As can be seen in Figure 3.3, this work uses the subscript 1 for conditions upstream to the orifice, the subscript 2 for conditions downstream and the subscript *bean* refers to the orifice size (or equivalent diameter). The velocity of two-phase flow through orifices, for both critical and subcritical flow, is greatly dependent on the gas fraction, and the critical pressure ratio (p_2/p_1) can

be as low as 0.225 (Fortunati, 1972). Fortunati (1972) also shows that the pressure ratio for two-phase flow is always lower than for single-phase gas flow (~0.53 for air and water).
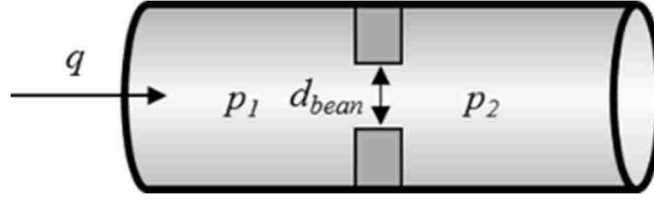

Figure 3.3. Orifice flow schematic.

During the development of flow models to predicted two-phase flow through orifices, some researchers consider the assumption that the slippage effect is not relevant in the orifice and, consequently, the velocity is the same for both gas and liquid through the orifice (Ros, 1959; Fortunati, 1972; Ashford & Pierce, 1975).

3.2.1   *Models for Prediction Critical Pressure Ratio*

Ashford (1974) proposed a model to establish the critical pressure ratio for two-phase through choke valves. The work performed by Ashford (1974) is a modification and extension of the work initially proposed by Tangren et al. (1949) and lately extended by Ros (1959). In the model of Ashford (1974) it is assumed that the gas expands polytropically, the liquid is incompressible, and there is a uniform dispersion of gas in the liquid phase.

According to Ashford (1974), the critical pressure ratio (y_c) can be defined using the Equation 3.1. This is an implicit equation of y_c and its solution requires an iterative process.

$$y_c = \left(\frac{\frac{2R_1}{k\left(1 + R_1 y_c^{\frac{-1}{k}}\right)}\left(\frac{R_1}{b}(1 - y_c^{b}) - y_c + 1\right)y_c^{-e} - 1}{R_1} \right)^{-k} \qquad 3.1$$

and,

$$b = \frac{k-1}{k}$$ 3.2

$$e = \frac{k+1}{k}$$ 3.3

where R_1 is the in-situ GLR at upstream conditions, and k is the ratio of specific heats (C_p/C_v).

A similar approach was presented by Ashford to characterize two-phase flow through subsurface safety valves (Ashford & Pierce, 1975), with orifice sizes from 14/64 to 20/64 inch. In their work, Ashford and Pierce (1975) concluded that "the model may be used to estimate two-phase pressure drops through restrictive beans in safety valves of other internal geometrical configurations". This conclusion indicates that their model may be applied for GLVs.

Fortunati (1972) proposed an empirical correlation based on the assumption that when flowing through orifices, both gas and liquid have the same velocity. Fortunati (1972) stated that this assumption is only valid for: (i) mixture velocity larger than 32.8 *ft/sec*, and (ii) Froude number ($F_r = \frac{u^2}{gd}$) > 600. Fortunati used experimental results obtained by Guzov and Medviediev (1962) for p_2 = 19.9 *psia* as shown in Figure 3.4, and suggested that the mixture velocities for production pressures (p_2) other than 19.9 *psia* can be estimated applying the following relationship:

$$u = u_{plot} \left(\sqrt{\frac{p_2}{p_{2plot}}} \right)^K$$ 3.4

and,

$$K = (1 - \lambda_{G2}^3)^{0.38}$$ 3.5

$$\lambda_{G2} = \frac{q_{G2}}{q_{G2} + q_{L2}}$$ 3.6

where u is the mixture velocity corresponding to the actual pressure (ft/sec), u_{plot} is the mixture velocity (*ft/sec*) in Figure 3.4, $p_{2plot} = 19.9$ *psia* is the orifice downstream pressure used in the experimental curve presented in Figure 3.4, and p_2 is the actual orifice downstream pressure (*psia*).
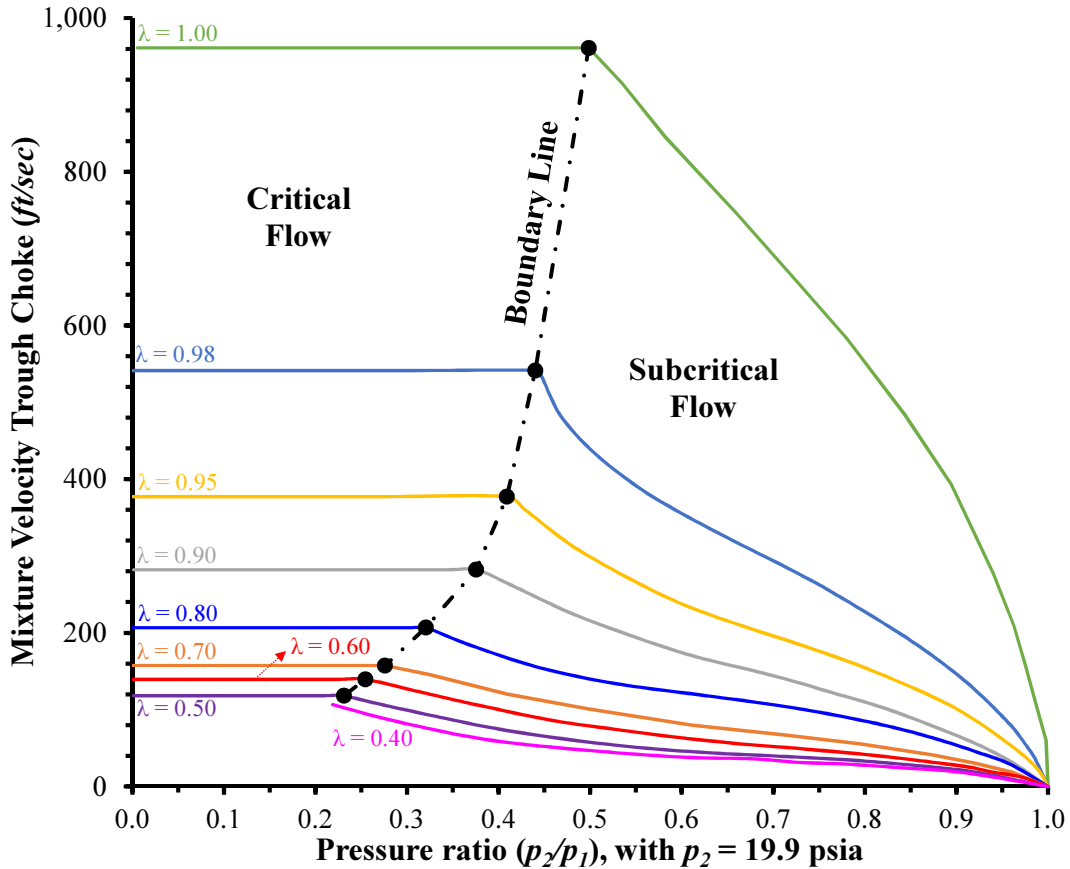

Figure 3.4. Relationship between mixture velocity the critical pressure ratio for two-phase flow through choke valves [modified after Fortunati (1972)].

Sachdeva et al. (1986) performed an experimental and numerical study to characterize two-phase flow through chokes. They proposed a model based on the conservation of mass, momentum and energy for two-phase flow through orifices. For the model development, these authors assumed one-dimensional flow, equal phase velocities in the orifice (no-slip), predominance of the acceleration term for the pressure, constant gas fraction, and incompressible liquid phase. Based on that, the pressure ratio at the critical-subcritical boundary is obtained by iterating and converging y_c using Equation 3.7.

$$y_c = \left(\frac{b + \dfrac{(1 - x_1)V_L(1 - y_c)}{x_1 V_{G1}}}{b + \dfrac{n}{2} + \dfrac{n(1 - x_1)V_L}{x_1 V_{G2}} + \dfrac{n}{2}\left(\dfrac{(1 - x_1) * V_L}{x_1 V_{G2}}\right)^2} \right)^b \qquad 3.7$$

and,

$$x_1 = \frac{w_{G1}}{w_{G1} + w_{L1}} \qquad 3.8$$

$$b = \frac{k}{k - 1} \qquad 3.9$$

$$n = 1 + \frac{x_1(C_p - C_v)}{x_1 C_v + (1 - x_1)C_L} \qquad 3.10$$

where V is the specific volume, n is the polytropic exponent given by Ros (1959), x_1 is the in-situ gas mass fraction at upstream condition, w_{G1} and w_{L1} are the mass flow rate for gas and liquid at upstream condition, C_p and C_v are the specific heat of the gas at constant pressure and constant volume, and C_L is the specific heat of the liquid.

The critical pressure ratio as a function of the GLR for the three models described in this section is shown in Figure 3.5, where ratio of specific heat for the gas is used as $k = 1.4$. As can be seen from this figure, the Ashford and Sachdeva models have similar critical pressure ratios (approximately 0.53) for GLR higher than 50 *scf/scf*. For GLR lower than 50 *scf/scf*, the y_c for both models starts to deviate from each other. For the Ashford model, the critical pressure ratio stays approximately constant for GLRs as low as 1 *scf/scf*. For GLR lower than 1, y_c decreases as the GLR is reduced. The critical pressure ratio curve obtained through Fortunati's model presents a trend similar to the Ashford curve, but it starts to deviate from the other two models for GLR lower than 100 *scf/scf*.
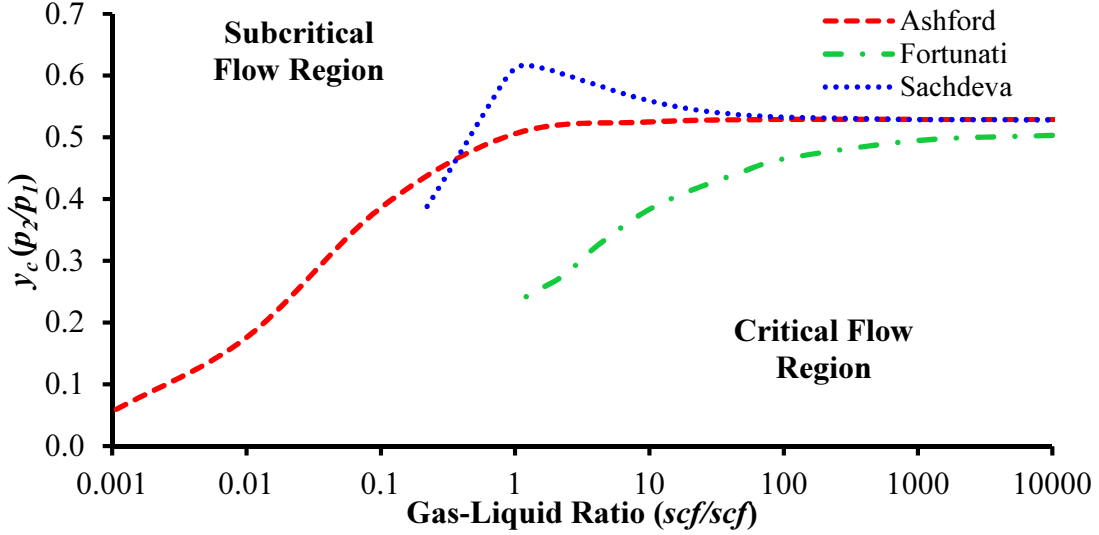
Figure 3.5. Critical pressure ratio as a function of the gas-liquid-ratio for $k = 1.4$.

3.2.2 Models for Flow Rate Prediction in Subcritical and Critical Flow

According to Brill and Mukherjee (1999), experimental and field tests confirm that prediction of subcritical two-phase flow rate through orifices is very difficult. Al-Attar (2010) stated that only few models are available for subcritical flow prediction. Two of the most popular models were proposed by Ashford and Pierce (1975) and Sachdeva *et al.* (1986). The model proposed by *Ashford & Pierce* can be used to predict the flow rate for both critical and subcritical flow, which is given by the following expression,

$$q_o = a_1 \sqrt{p_1} \frac{\sqrt{1 - y + R_L \frac{1 - y^{a_2}}{a_2}}}{1 + R_L y^{-\frac{1}{k}}} \frac{1}{\sqrt{B_o + F_{wo}}} a_3 \qquad 3.11$$

$$a_1 = \frac{c_1 C_D (d_{bean})^2}{\sqrt{c_2}} \qquad 3.12$$

$$a_2 = \frac{k - 1}{k} \qquad 3.13$$

$$a_3 = \frac{\sqrt{\gamma_o + c_3 \gamma_G R_s + F_{wo} \gamma_w}}{\gamma_o + c_3 \gamma_G R + F_{wo} \gamma_w} \qquad 3.14$$

and,

40

$$R_L = T_1 Z_1 * \frac{R - R_s}{198.6 P_1}$$

3.15

where $c_1 = 3.51$; $c_2 = 198.6$; $c_3 = 0.000217$, B_o is the oil formation volume factor (*bbl/stb*), F_{wo} is the water-oil ratio, R_s is the solution GLR (*scf/stb*), R is the production GLR (*scf/stb*) and C_D is the discharge coefficient.

The main assumptions in this model are as follow: polytropic expansion of gas-liquid mixture, equal gas and liquid velocities at the throat, incompressible liquid phase, liquid dispersed in a continuous gas phase and negligible friction losses.

Using the *Sachdeva et al. (1986)* model to predict flow rate in critical and subcritical flow is based on the same premises of the flow model developed by *Sachdeva et al. (1986)* for predicting the critical pressure ratio. The model is presented in Equation 3.16, where liquid flow rate for either critical or subcritical flow is obtained by,

$$q_{L_{sc}} = a_4 \left(p_1 \rho_{m2}^2 \left(\frac{(1 - x_1)(1 - y)}{\rho_{L1}} + \frac{x_1 k (1 - y^{a_2})}{\rho_{G1}(k - 1)} \right) \right)^{0.5}$$

3.16

$$a_4 = \frac{0.525 C_D d_{ch}^2}{C_{m2}}$$

3.17

and,

$$\rho_{m2} = \left(\frac{x_1}{\rho_{G1} y^{\frac{1}{k}}} + \frac{(1 - x_1)}{\rho_{L1}} \right)^{-1}$$

3.18

3.2.3 Models for Flow Rate Prediction in Critical Flow

When flowing through orifices, the critical flow condition exists if pressure ratio, y, is smaller than the critical pressure ratio, y_c, which implicates that the mixture velocity is higher than the critical velocity. The number of studies available in the literature that characterize two-phase critical flow in orifices is considerably higher than for subcritical flow. A precursor and classical

study in critical flow behavior was carried out by *Gilbert (1954)*. This author developed an empirical correlation to calculate the pressure upstream restrictions, given by the following expression,

$$p_1 = \frac{A q_{L_{sc}} GLR^B}{d_{bean_{64th}}^C} \qquad\qquad 3.19$$

where *A*, *B* and *C* are coefficients and the values are presented in Table 3.1 and d_{bean} is the orifice diameter in 64th of an *inch*.

Table 3.1. Coefficients A, B and C for Equation 3.19 suggested by different researchers.

Researchers	A	B	C
Gilbert (1954)	10.00	0.55	1.89
Ros (1959)	17.40	0.50	2.00
Baxendell (1957)	9.56	0.55	1.93
Achong (1961)	3.82	0.65	1.88

Equation 3.19 correlates the upstream pressure with the GLR (in *scf/stb*) and liquid volumetric flow rate at standard condition (q_{Lsc} in *stb/day*). The proposed equation neglects the fluid properties and does not consider the effect of p_2, since Equation 3.19 is recommended only for *y* < 0.7 (e.g., critical flow).

Some authors developed further work with experimental and field data and proposed adjustments in the three coefficients originally proposed by Gilbert (1954), as presented in Table 3.1. The most cited studies that proposed modifications for the coefficients originally developed by Gilbert are presented in this Table 3.1.

3.3   Models from Commercial Simulators for Two-Phase Flow through Valves

Two commercial flow simulators (OLGA, 2015; PIPESIM, 2015) widely used in the oil and gas industry are also included in the present study in the evaluation of models to simulate two-phase flow in orifice GLVs. Both mechanistic models presented in this section are used in the commercial flow simulator used here to predict two-phase flow conditions through orifice GLVs.

For a complete description of both models, the references cited in the simulator should be consulted (Brill & Beggs, 1991; Selmer-Olsen *et al.*, 1995).

3.3.1 PIPESIM® (2015) model

The PIPESIM (2015) model, the GLVs is represented by a choke valve with bean size similar to the orifice port in the GLVs evaluated in the experiments (0.50 and 0.69 *inch*). A mechanistic flow model (Brill & Beggs, 1991) was chosen for both subcritical and critical flow pressure drop predictions, which is given by the following expression:

$$\Delta p = \lambda_L \Delta p_L + \lambda_G \Delta p_G \qquad \qquad 3.20$$

The pressure drop for liquid and gas phases are given by Bernoulli's equation, and are presented in Equations 3.21 and 3.22, respectively:

$$\Delta p_L = \frac{\rho_m}{2c}\left(\frac{u}{C_{vL}\,Z_L}\right)^2 \qquad \qquad 3.21$$

$$\Delta p_G = \frac{\rho_m}{2c}\left(\frac{u}{C_{vG}\,Z_G}\right)^2 \qquad \qquad 3.22$$

$$u = \frac{q}{A_{bean}\,\rho_m} \qquad \qquad 3.23$$

where u is the mixture velocity flowing through the orifice, with area A_{bean}, given by,

$$A_{bean} = \frac{\pi\,d_{bean}^2}{4} \qquad \qquad 3.24$$

$$\rho_m = \lambda_L \rho_L + \lambda_G \rho_G \qquad \qquad 3.25$$

$$Z_L = 1 \qquad \qquad 3.26$$

$$Z_G = 1 - \frac{0.41 + 0.35\delta^2}{k}\cdot\frac{\Delta p}{p_1} \qquad \qquad 3.27$$

Thus, the total pressure drop in the PIPESIM® model for two-phase flow through the orifice is given by,

$$\Delta p = \frac{\rho_m \, u^2}{2c} \left(\frac{\lambda_L}{(C_{vL} \, Z_L)^2} + \frac{\lambda_G}{(C_{vG} \, Z_G)^2} \right)$$

<div align="right">3.28</div>

where ρ_m is the no-slip density; c is a conversion factor for engineering units ($c = 144g$); u is the mixture velocity through the orifice; A_{bean} is the orifice area; λ_L and λ_G are the liquid and gas flowing fraction; Z_L and Z_G are liquid and gas compressibility factors; k is the ratio of specific heats; C_{vL} and C_{vG} are liquid and gas flow coefficients.

The flow coefficients, c_{vL} and c_{vG}, can either be specified or calculated from the discharge coefficient (C_D) (default = 0.6). The flow coefficients for the liquid and gas phases are often calculated by,

$$C_v = \frac{C_D}{\sqrt{1 - \delta^4}}$$

<div align="right">3.29</div>

$$\delta = \frac{d_{bean}}{d_1}$$

<div align="right">3.30</div>

3.3.2   OLGA® (2015) model

In the OLGA (2015) model, an orifice valve represents the GLV, and the Hydrovalve™ model was selected for both critical and subcritical two-phase flow. The Hydrovalve™ model was developed by Selmer-Olsen et al. (1995), and it provides a relationship between multiphase mass flow rate, M, and the pressure drop through the restriction. The model was developed for a circular-symmetric flow geometry similar to the one illustrated in Figure 3.6. The conservation equations for mass, momentum and total energy equation were applied considering steady-state flow.
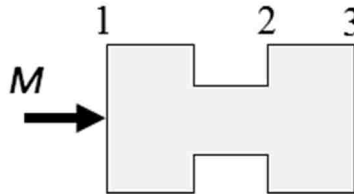

Figure 3.6. Geometry of Hydrovalve™ flow model.

The model proposed by Selmer-Olsen *et al.* (1995) assumes that the flow is in thermodinamic non-equilibrium with nonslip conditions. The four main equations for the Hydrovalve™ model are Equations 3.31 to 3.34. The subscripts 1, 2 and 3 in the equations are related to the positions specified in Figure 3.6. For solving the Hydrovalve™ model, it is first necessary to solve Equation 3.31 for the critical mass flow rate for the mixture, M_C, and the pressure $p_2 = p_{C.}$,

$$M_C = \frac{A_1^2 C_T^2}{\frac{d}{dp}\left(\frac{1}{\rho_{m2}}\right)} \frac{1}{\left(\frac{1}{C_D} - 1\right)^2 + 1} \tag{3.31}$$

$$\frac{1}{\rho_m} = \left[\frac{w_G}{\rho_G} + S\frac{1 - w_G}{\rho_L}\right]\left[w_G + \frac{(1 - w_G)}{S}\right]^{-1} \tag{3.32}$$

where A is the cross sectional area of the flow geometry, C_T is the valve throttling coefficient (A_1/A_2), ρ_m is the mixture density based on the net momentum flow through a control column (Chisholm, 1983), S is the slip ratio and w is the mass fraction. After solving the critical equation, equations 3.33 and 3.34 are solved for the subcritical mass flow rate (M) and pressure (p_2) and, in case a solution is found for these two equations, the flow is considered to be in subcritical condition. If there are no roots available for Equations 3.33 and 3.34, the flow is considered to be in the critical condition. In this case, $M = M_C$ and $p_2 = p_C$ (calculated in the first step).

$$\int_1^2 \frac{\rho_{m1}}{\rho_m} dp = \frac{M^2}{2A_1^2\rho_{m1}}\left[1 - \left(\frac{\rho_{m1}}{\rho_{m2}}\right)^2 \frac{1}{C_T^2 C_D^2} + 2\left(\frac{\rho_{m1}}{\rho_{m2}}\right)^2 \frac{1}{C_T^2}\left(\frac{1}{C_D} - 1\right)\right] \tag{3.33}$$

$$(p_3 - p_B) + C_T C_X(p_B - p_2) = \frac{M^2}{A_1^2\rho_{e1}}\left[\frac{\rho_{m1}}{\rho_{m2}}\frac{C_X}{C_T} - C_X^2\frac{\rho_{m1}}{\rho_{m3}}\right] \tag{3.34}$$

3.4   Experiments

The experimental characterization of two-phase flow through GLVs is performed in this study using a multiphase flow loop located at Louisiana State University. During the experimental campaign, two GLVs with 32/64 and 44/64 *inch* port sizes were tested. The experimental data

generated using these two valves are used to evaluate the models presented previously in this work for both critical and subcritical flow. Both valves are tested for GLR ranging from 600 to 11,000 *scf/bbl*, and pressures from 140 to 450 *psi* and temperature ranging from 80 to 100 °*F*.

3.4.1 Experimental Apparatus

A schematic diagram of the flow loop designed to test the GLVs is shown in Figure 3.7. This state-of-art flow loop includes a 300 *bbl* tank, with a maximum working pressure of 720 *psi*. This tank is used to store both liquid and gas, and the liquid level is monitored in the tank using a differential pressure transducer (*LT-100*), which translates the hydrostatic pressure into liquid level. The top section of the tank is connected to the suction line of an electric powered compressor. The bottom section of the tank is connected to a diesel-engine triplex pump. A picture of the flow loop in shown in Figure 3.8.
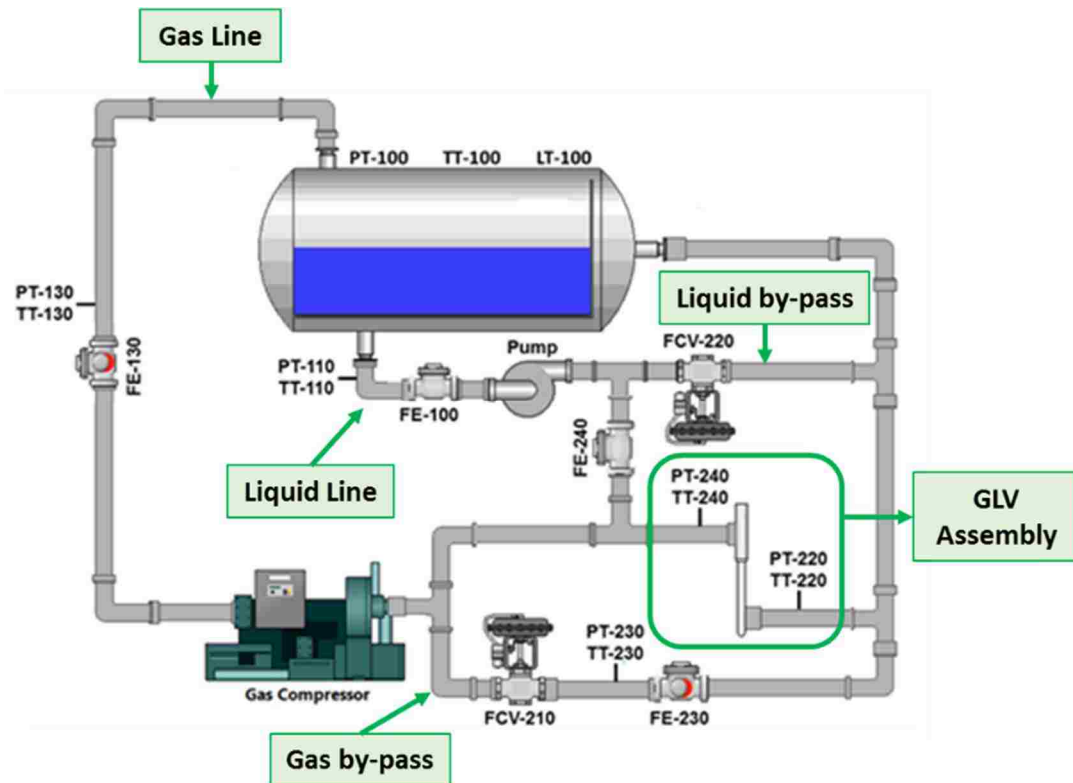
Figure 3.7. Experimental apparatus schematic.
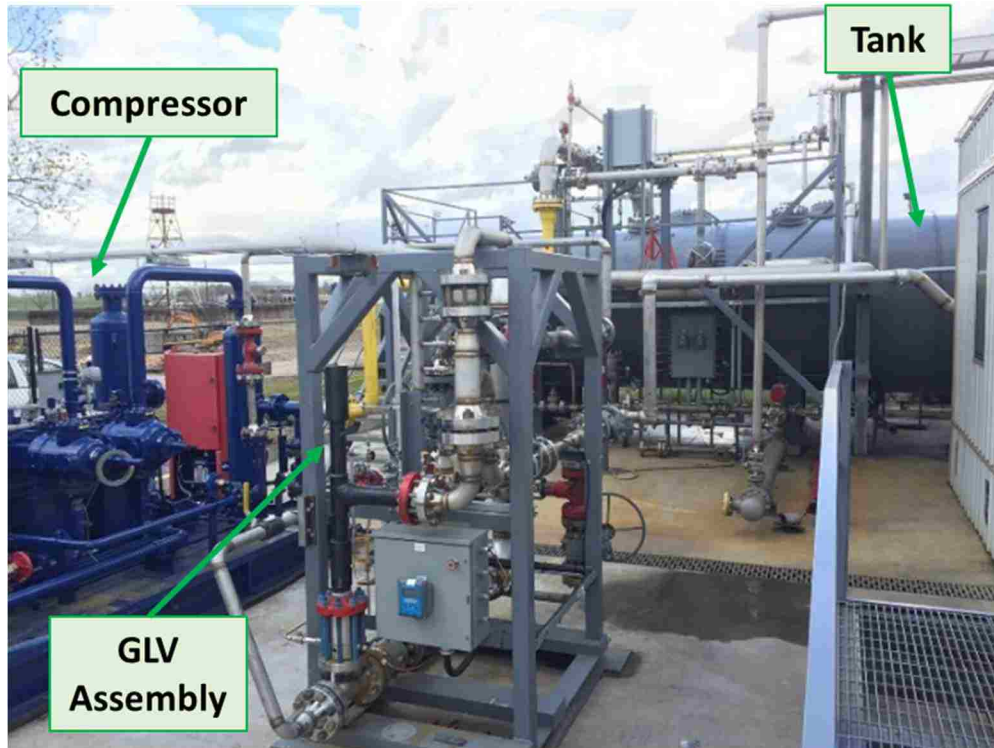
Figure 3.8. Picture of the experimental apparatus.

On the liquid line (see Figure 3.7), a turbine flow meter (*FE-100*) measures the liquid flow rate upstream to the pump. The pump discharge flows to the gas-lift valve assembly. The water flow rate through the gas-lift valve assembly is controlled using a pneumatic flow control valve (*FCV-220*) located at the by-pass line. A second turbine flow meter (*FE-240*) measures the liquid flow through the test section.

On the gas line, a rotary gas flow meter (*FE-130*) measures the gas flow rate flowing through the gas compressor. The high-pressure gas discharged from the compressor flows either to the test section or through the gas by-pass. The flow rate through the gas by-pass is controlled using a pneumatic flow control valve (*FCV-210*), monitored by a second rotary flow meter (*FE-230*) with the same specification of the one in the suction line of the gas compressor (*FE-130*).
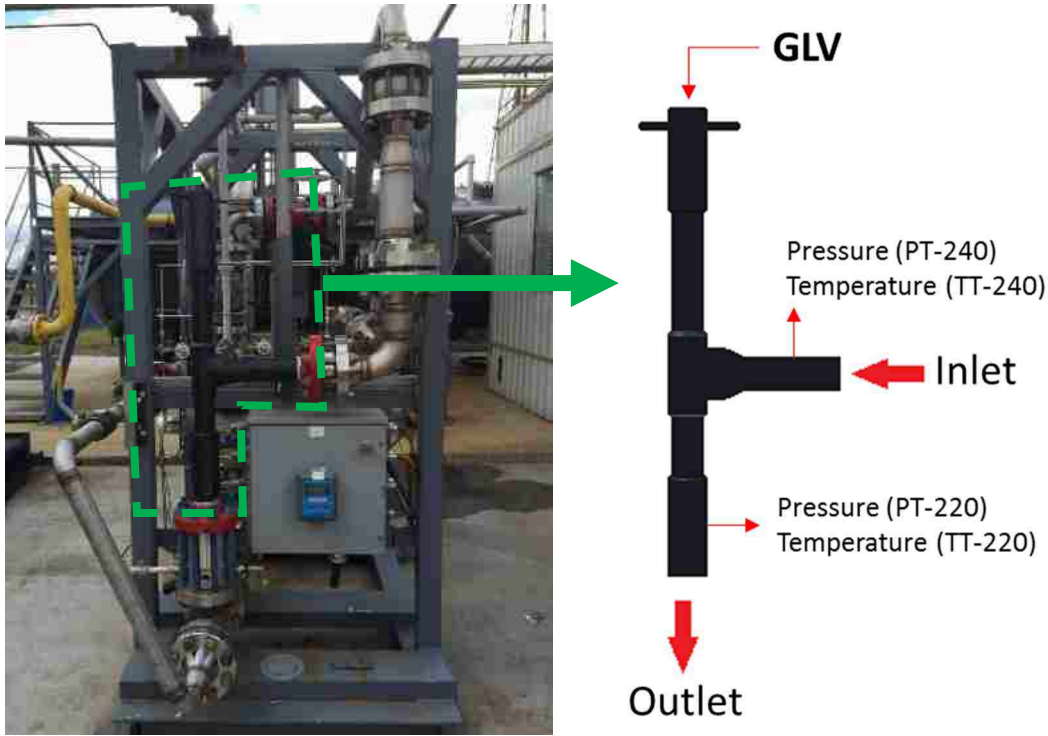
Figure 3.9. Gas-lift valve assembly used in the experimental apparatus.

Upstream to the gas-lift valve assembly, the liquid and gas streams are mixed in a "mixing Tee". This fluid mixture, with a known GLR, then flows through the gas-lift valve assembly. The gas-lift valve assembly is shown in more details in Figure 3.9, where it indicates how the GLV is installed for testing. In the gas-lift valve assembly pressure and temperature are measured upstream (*PT-240* and *TT-240*) and downstream (*PT-220* and *TT-220*) to the GLV. The maximum operating pressure in the test section is 1,400 *psi*.

Pressure and temperature are also monitored at the tank (*PT-100* and *TT-100*), in the water suction line (*PT-110* and *TT-110*), and at upstream to each rotary flow meter. A data acquisition system is used to acquire the data, and control the pneumatic valves and water pump. The flow loop is fully operated using a computer-based interface and no manual operation is required during the test. A complete list of the pressure, temperature, and flow measurement equipment is presented in Table 3.2. The uncertainty of each instrument is also included in this table.

Table 3.2. Instruments specification.

Nomenclature in Figure 3.7	Model	Accuracy	Range
PT-100 PT-110 PT-130	AST 4400-A	±0.25% of full range	0 to 800 *psi*
PT-220 PT-230 PT-240	AST 4400-A	±0.25% of full range	0 to 2000 *psi*
TT-10o TT-110 TT-130 TT-220 TT-230 TT-240	RTD PR-21SL-3-100-A	$\pm(0.15 + 0.002*T{\circ}_C)$	-58 to 500 °*F*
FE-100	B132-300	±1% of reading	60 to 600 *gpm*
FE-230	B132-200	±1% of reading	15 to 180 *gpm*
FE-130 FE-230	Rotary 11M1480	±1% of reading	0 to 11 *acfh*

3.4.2 Experimental Procedure

For the two-phase flow tests, two orifice GLVs with 32/64 and 44/64 port size (Figure 3.10) were used to analyze the pressure drop through the valve for different GLRs. The working fluids used for the two-phase tests are natural gas (methane) and water. During the tests, the pressure downstream (p_2) to the GLV is kept constant and the upstream pressure (p_1) varies with the change in the gas and water flow rates. For each upstream pressure (p_1), experimental data is acquired for about three minutes, with an acquisition rate of 0.3 *Hz*. The key measured parameters in the experiments are volumetric gas and liquid flow rates (q_G and q_L), pressures and temperatures at the inlet and outlet of the GLV.

(a) 32/64 port size   (b) 44/64 port size
Figure 3.10 . Orifice GLV (a) 32/64, (b) 44/64.

For the valve with 32/64 port size, the experiments were performed for two constants pressures downstream to the GLVs (140 and 310 *psi*). For the 44/64 port size valve, one extra pressure

49

downstream to the GLV was evaluated (450, 260 and 160 *psi*). During the tests, the gas by-pass is fully closed and the water flow rate is increased from zero to the flow rate that results in a pressure upstream to the GLV (p_1) around 1,100 *psi*. The water rate is controlled using both the water by-pass valve (*FCV-220*) and pump speed.

3.5 Experimental Results and Discussions

Figure 3.10 presents the experimental results in the two GLVs. At a constant downstream pressure (p_2), the pressure ratio across the GLV increases with the GLR. This means that, if it is assumed there is a constant gas flow, an increase in the water flow rate reduces the pressure ratio, which correspond to an increase in the pressure drop. The increase in the pressure drop is caused by the increase in the mixture velocity and mixture density, which are related to the acceleration component in the pressure drop calculation. It is also important to notice from the results in Figure 3.11 that the relationship between *y* and GLR does not to depend on the downstream pressure for both port sizes.
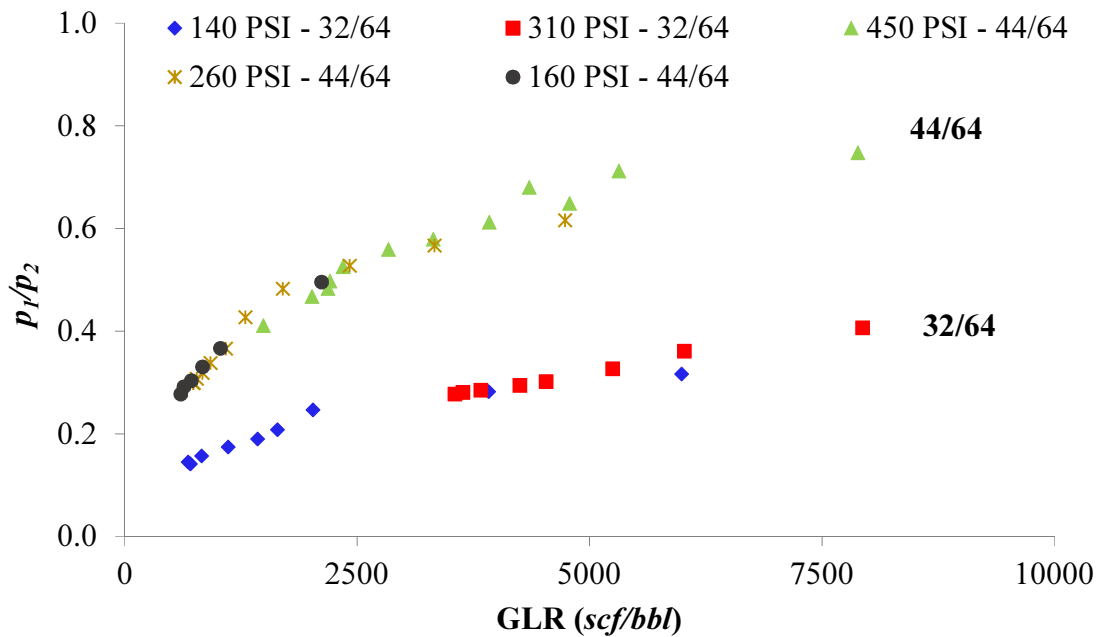
Figure 3.11. Pressure ratio as a fucntion of the gas-liquid-ratio for GLVs with different port sizes (32/64 and 44/64) and downstream pressures (p_2).

For similar GLRs, the pressure ratio is consistently higher for the data obtained testing the 44/64 valve. This behavior is expected because a larger orifice would result in a lower pressure drop across the valve.

3.5.1 Evaluation of the Models for Two-Phase through Orifices

Initially, the critical-subcritical pressure ratio boundary are calculated using the three models described in Section 3.2 (Fortunati, 1972; Ashford, 1974; Sachdeva *et al.*, 1986). After obtaining the pressure ratio boundary between critical and subcritical flow from the theory, the experimental data is compared to the calculated boundaries to define if the data is either in the critical or subcritical region. Then, the models for critical and subcritical flow are applied to simulate experimental pressure drop through the GLVs. The models available in the commercial flow simulators (OLGA, 2015; PIPESIM, 2015) are also compared to experimental data.

3.5.2 Model Results for Critical Pressure Ratio

The first step to evaluate the models for two-phase through orifices is to determine the pressure ratio boundary between the critical and subcritical flow region, to determine in which region the experimental data is. Figure 3.12 presents the critical pressure ratio (y_c) that represents the boundary between the critical and subcritical flow conditions, calculated using three correlations: (Fortunati, 1972; Ashford, 1974; Sachdeva *et al.*, 1986), which are previously described in Section 3.2.2. All experimental results are presented in Figure 3.12.

As shown in Figure 3.12, the experimental data for the valve with 32/64 port size is entirely in the critical flow region. The experimental data for the GLV with port size 44/64 are in both critical and subcritical flow region. It is also important to notice that the experimental data is shown for a GLR range where the y_c calculated with Ashford and Sachdeva model is approximately constant around 0.53. For the same GLR range, y_c obtained with Fortunati method is between 0.47 and 0.50.
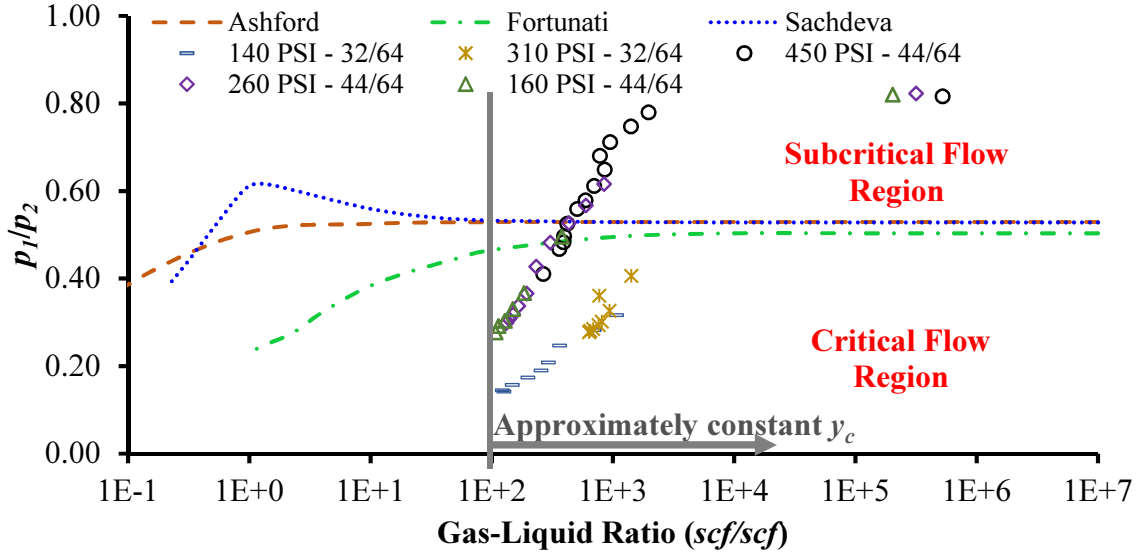
Figure 3.12. Numerical critical pressure ratio and experimental pressure ratio.

Considering that Ashford and Sachdeva models are semi-empirical and that Fortunati's model is empirical, the y_c of 0.53 will be used as the pressure ratio boundary between the critical and subcritical flow for the experimental data presented in this study, assuming that semi-empirical models can provide better results when extrapolating the empirical conditions which these models where validated.

3.5.3 Models Results for Pressure Drop Prediction in Critical Flow

The model proposed by Gilbert (1954), which was later modified by Baxendell (1957), Ros (1959), and Achong (1961), is used here to predict the pressure drop in the GLV for the experimental data in the critical flow region. Figure 3.13 shows a comparison between the experimental pressure upstream to the GLV (p_1) and the predictions using Gilbert (1954) model and the other three models adapted from his work.

Figure 3.13(a) and Figure 3.13(b) present results for the valve with port size of 32/64 inch, and Figure 3.13(c) to (e) present the results for the valve with port size 44/64 inch. For all plots presented in Figure 3.13, the values predicted with the model of Gilbert (1954) show a better agreement with the experimental data (13% averaged absolute error). On the other hand, the values

predicted using Ros (1959) and Baxendell (1957) modification are the ones with highest errors (26% averaged absolute error) among the four models analyzed in this study.
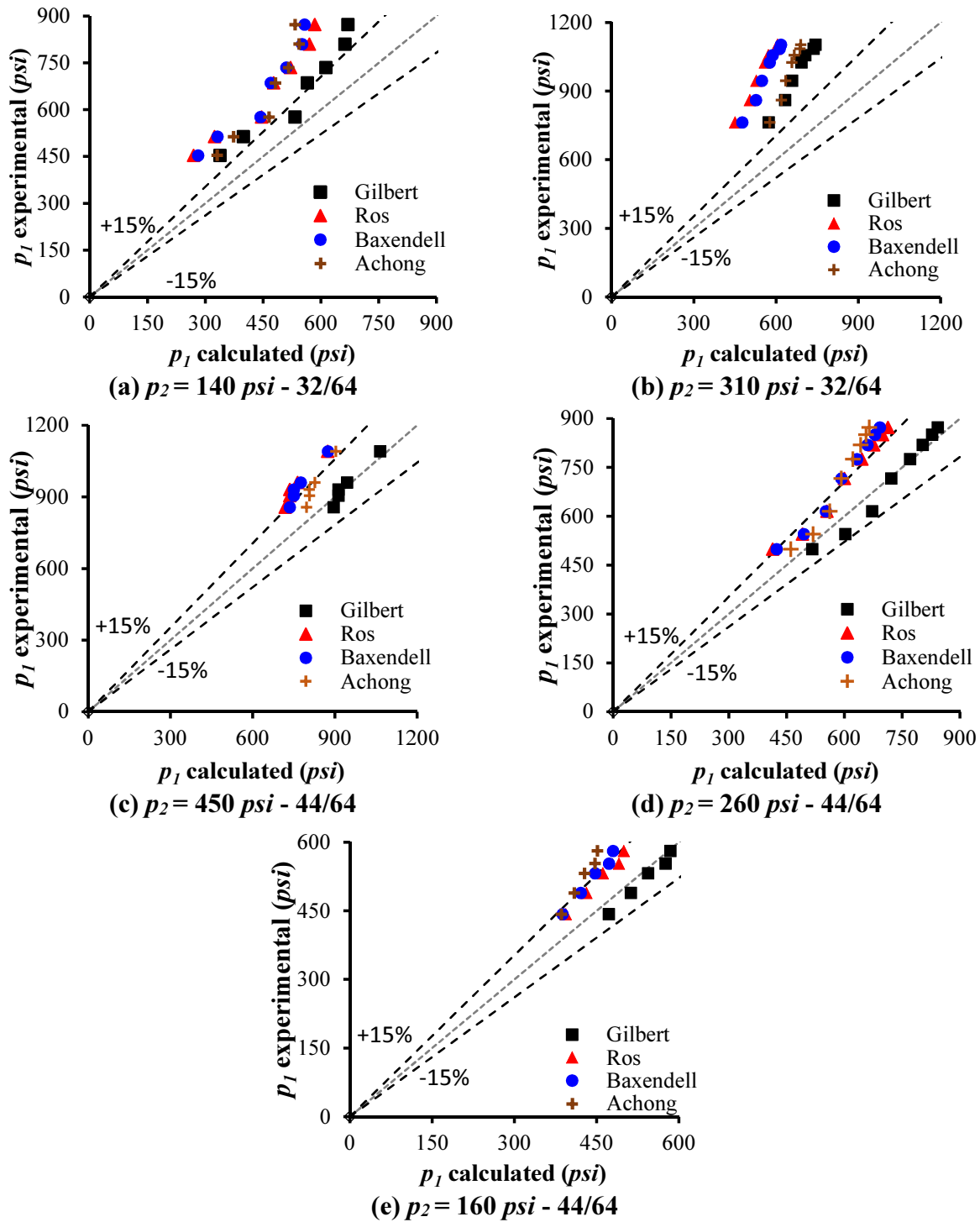

(a) $p_2 = 140$ *psi* - 32/64

(b) $p_2 = 310$ *psi* - 32/64

(c) $p_2 = 450$ *psi* - 44/64

(d) $p_2 = 260$ *psi* - 44/64

(e) $p_2 = 160$ *psi* - 44/64

Figure 3.13. Comparisons between experimental upstream pressures and critical flow model results. The results are presented for two different port sizes (32/64 and 44/64), at pressure ranging from 140 to 450 *psi*.

Another important point is that the model predictions for the 32/64 port size are not as accurate as for the 44/64 port size. As shown in Table 3.3, the model of Gilbert (1954) has an averaged absolute error of 24% for the 32/64 port size, and this error drops to 3% for the 44/64 port size. Similar trend occurs with all the other models.

One possible cause for the difference is the difference in the geometry of the valves. Because it is an empirical model, Gilbert's model is expected to give high errors when applied in conditions other than the model was validated. The model proposed by Gilbert (1954), and posteriorly adjusted by the other authors, is an empirical model that was originally proposed and validated for choke valves with openings ranging from 6/64 to 18/64 *inch*.

Table 3.3. Averaged error for critical flow data presented in Figure 3.13.

Averaged absolute error (%)	Gilbert (1954)	Ros (1959)	Baxendell (1957)	Achong (1961)
Total	13	26	26	23
32/64 port size	24	37	37	32
44/64 port size	3	16	16	16

It is also observed that the results obtained with Ros (1959), Baxendell (1957) and Achong (1961) are close to each other when compared to Gilbert (1954). Similar results were observed by Al-Attar (2010) for two-phase flow through choke valves. In his study, Al-Attar (2010) compared field data for 32, 34, 40, 48 and 64/64 choke size with results obtained using models proposed by Gilbert (1954), Ros (1959), Baxendell (1957) and Achong (1961), and he found errors as high as 28%.

3.5.4 *Models Results for Flow Rate Prediction in Critical and Subcritical Flow*

The comparison between experimental and numerical results using both Ashford and Pierce (1975) and Sachdeva *et al.* (1986) models are presented in Figure 3.14 and Figure 3.16. For both models, GLR and pressures upstream and downstream to the GLVs are given, and the flow rates

are calculated considering the fluid properties and valve geometry. Model results for the liquid

flow rate prediction for all five cases are analyzed experimentally for the following conditions:

- <u>GLV with port size 32/64</u>: at downstream pressures of 140 and 340 *psi*

- <u>GLV with port size 44/64</u>: at downstream pressures of 160, 260 and 450 *psi*

    The experimental results are presented in Figure 3.14 for Ashford and Pierce (1975) model

and in Figure 3.16 for the Sachdeva *et al.* (1986) model. As can be seen in Figure 3.14, the

comparison between experimental data and the numerical predictions using the Ashford and Pierce

(1975) model for the 32/64 port size GLV indicates errors within the 15% for most of the data

points. The averaged absolute error obtained for the cases with 44/64 port size was 5% and the

maximum error was 21%. For the case with 450 *psi* downstream pressure and larger orifice port

size (44/64 *inch*), the errors for some data points were slightly higher than 15%, and the absolute

averaged error was 10%.
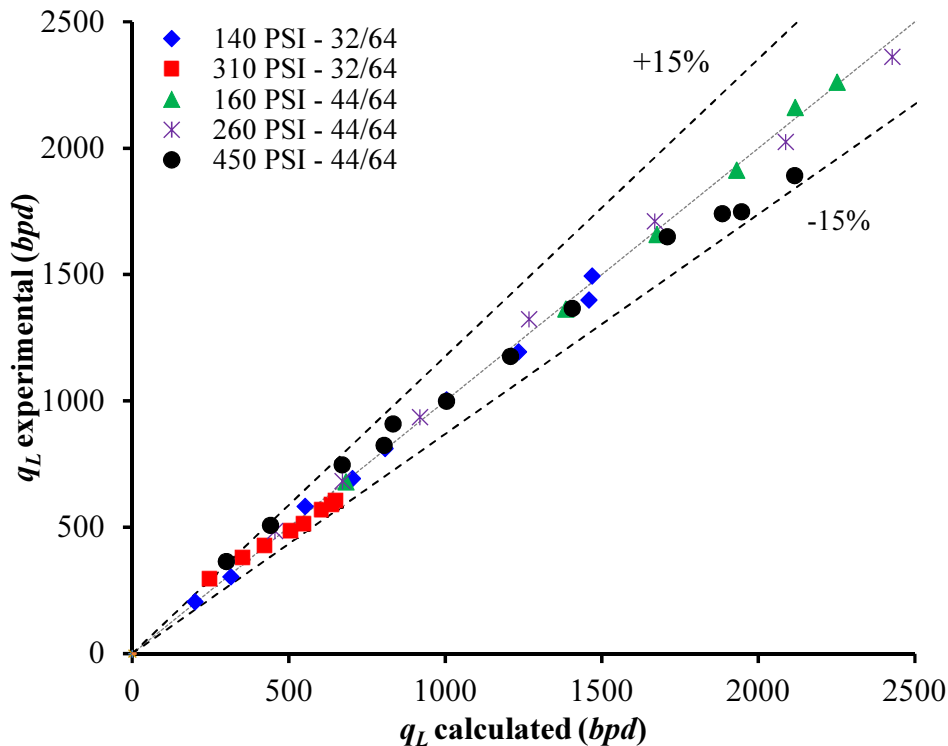
Figure 3.14. Comparison between experimental data and calculated liquid flow rate using the critical Ashford and Pierce (1975) model for all data points.

The discharge coefficient used to calculate the theoretical liquid flow rates presented in Figure 3.14 were 0.85 for the 32/64 valve and 0.88 for the 44/64 valve. The latter discharge coefficients are the ones that result in the smaller errors for the predicted liquid flow rate after the C_D is calibrated with the experimental data. Figure 3.15 presents the average absolute error (between calculated and experimental liquid flow rate) as a function of the discharge coefficient, when using Ashford and Pierce (1975) model presented in Equations 3.11-3.15. As shown in Figure 3.15, the use of non-calibrated discharge coefficients may generate high errors. When experimental data is not available to determine the calibrated discharge coefficient, Ashford and Pierce (1975) suggest the use of $C_D = 1.0$. If the discharge coefficient is considered to be 1.0 for the valves used in this work, the error will be around 18% for the 32/64 valve and 15% for the 44/64 valve.
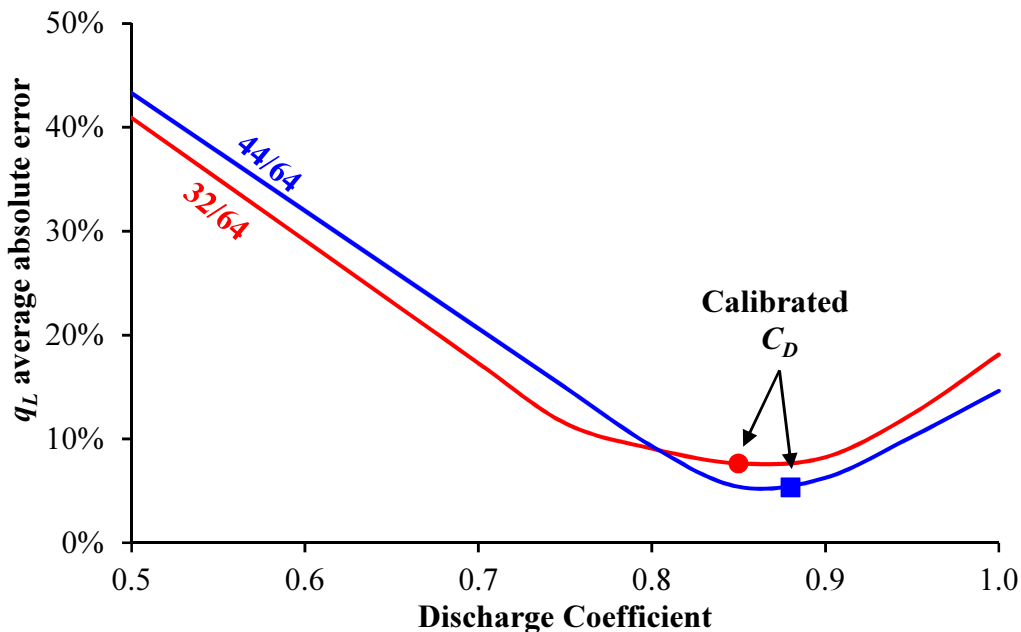
Figure 3.15. Liquid flow rate error as a function of the discharge coefficient for the Ashford and Pierce (1975) model.

Figure 3.15 illustrates the results for the Sachdeva *et al.* (1986) model, and the results are similar to the ones observed for Ashford and Pierce (1975) model. The model prediction was satisfactorily accurate, with an averaged absolute error of 7%. The averaged absolute error for the

44/64 valve was 4% and for the 32/64 valve was 12%. The averaged absolute error considering all data points obtained with Sachdeva model is 7%, which is slightly higher than the error obtained using Ashford and Pierce (1975) model.
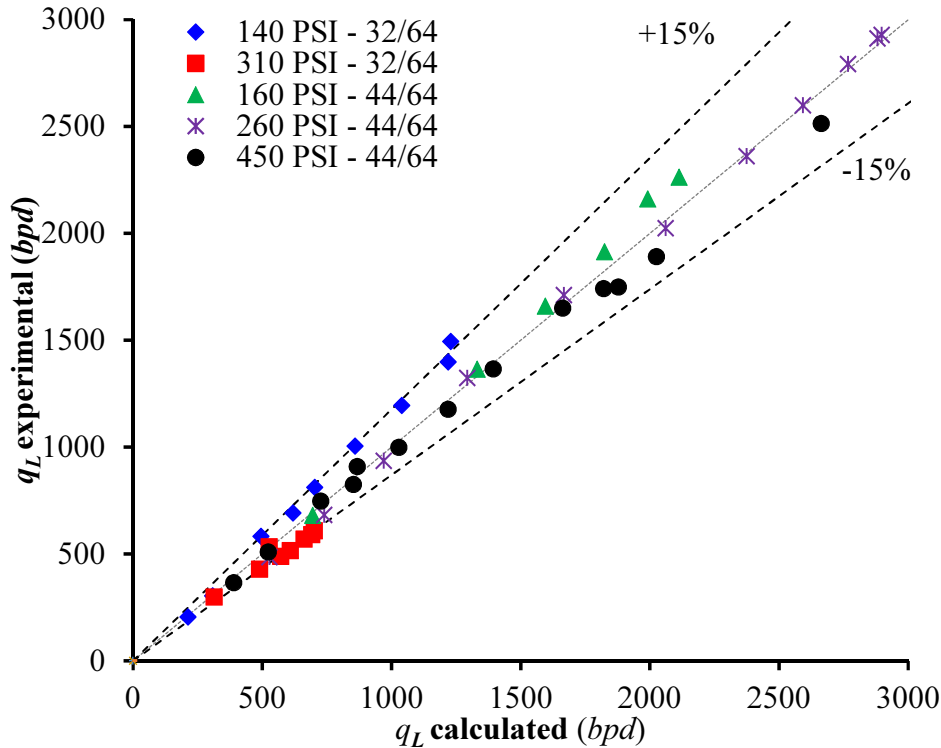

Figure 3.16. Comparison between experimental data and calculated liquid flow rate using the critical Sachdeva et al. (1986) model for all data points.

The calibrated discharge coefficients used to calculate the liquid flow rates presented Figure 3.16 were $C_D = 0.72$ for the 32/64 port size valve, and $C_D = 0.78$ for the 44/64 port size valve. Figure 3.17 presents the average absolute error (between calculated and experimental liquid flow rate) as a function of the discharge coefficient when using Sachdeva *et al.* (1986) model presented in Equations 3.16-3.18. According to Sachdeva *et al.* (1986), C_D values in the interval of 0.75 and 0.85 are expected for wellhead choke valves. The C_D values obtained in this work for GLVs are in accordance to the values suggested by Sachdeva *et al.* (1986).
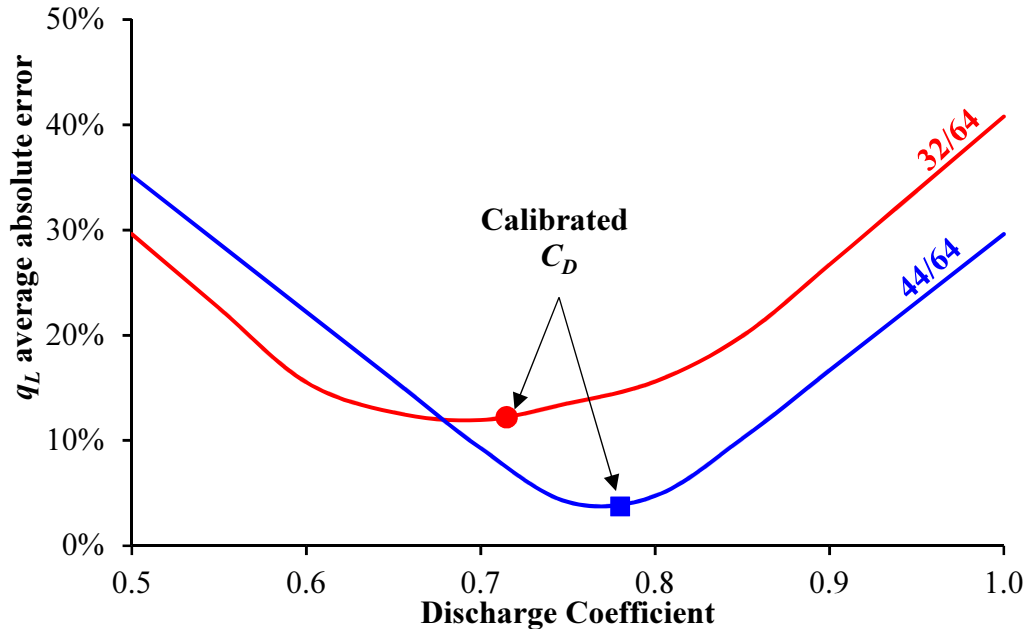
Figure 3.17. Liquid flow rate error as a function of the discharge coefficient for Sachdeva *et al.* (1986) model.

A summary of the averaged absolute errors for all five cases is presented in Table 3.4. Both Sachdeva and Ashford & Pierce models presented similar errors. It is also included in Table 3.4 the results for the mechanistic models used in the PIPESIM® and OLGA® simulations, which also showed errors approximately the same as Sachdeva and Ashford & Pierce. More details about the results of commercial flow simulators will be discussed in the next section.

Table 3.4. Summary of averaged absolute error for all five cases analyzed with Ashford & Pierce and Sachdeva model.

Model	Averaged absolute error (%)					
	32/64		44/64			Total
	140 *psi*	310 *psi*	160 *psi*	260 *psi*	450 *psi*	
Ashford & Pierce	5	10	2	4	8	6
Sachdeva	11	13	5	3	4	7
Mechanistic (PIPESIM®)	7	15	8	6	3	8
Mechanistic (OLGA®)	3	12	5	3	1	5

It is important to notice that the results for the case with 32/64 port size valve and 310 *psi* downstream pressure presented errors considerably higher when compared to all other cases. Similar behavior was observed in the analysis of the critical flow only models.

3.5.5 Results for Commercial Simulator Models

The simulation results obtained using the mechanistic model for two-phase flow through orifices in OLGA® and PIPESIM® are presented in this section. Figure 3.18 to Figure 3.22 show simulation and experimental results for all the experimental runs in this study. Error bars for the uncertainty of the experimental pressure measurements are also included in Figure 3.18 to Figure 3.22. The uncertainty estimation was obtained using the accuracy of the pressure transducer as shown in Table 3.2.

For the commercial simulator models used in this study, the discharge coefficient needs to be adjusted before the prediction of the pressure drop through the GLV. Thus, simulations were performed to determine the discharge coefficient (C_D) that should be used in the valve that represents the GLVs tested in this study. During this process, C_D was initially set at 0.3 and simulations were performed for each case in each simulator. The average absolute error was calculated for each valve port size. After this initial simulation, the C_D for each valve was gradually increased in 0.1 increments. The C_D selected for each valve port size and flow model (OLGA® or PIPESIM®) was the one with lower average absolute error.

For the 32/64 port size valve, the calibrated C_D for the orifice valve used in the OLGA® model was 0.57, and for the valve used in the PIPESIM® model was 0.55. It is important to mention here that the C_D obtained from the adjustment from the experimental data is very similar to the default C_D suggested by the commercial simulators ($C_D = 0.6$).
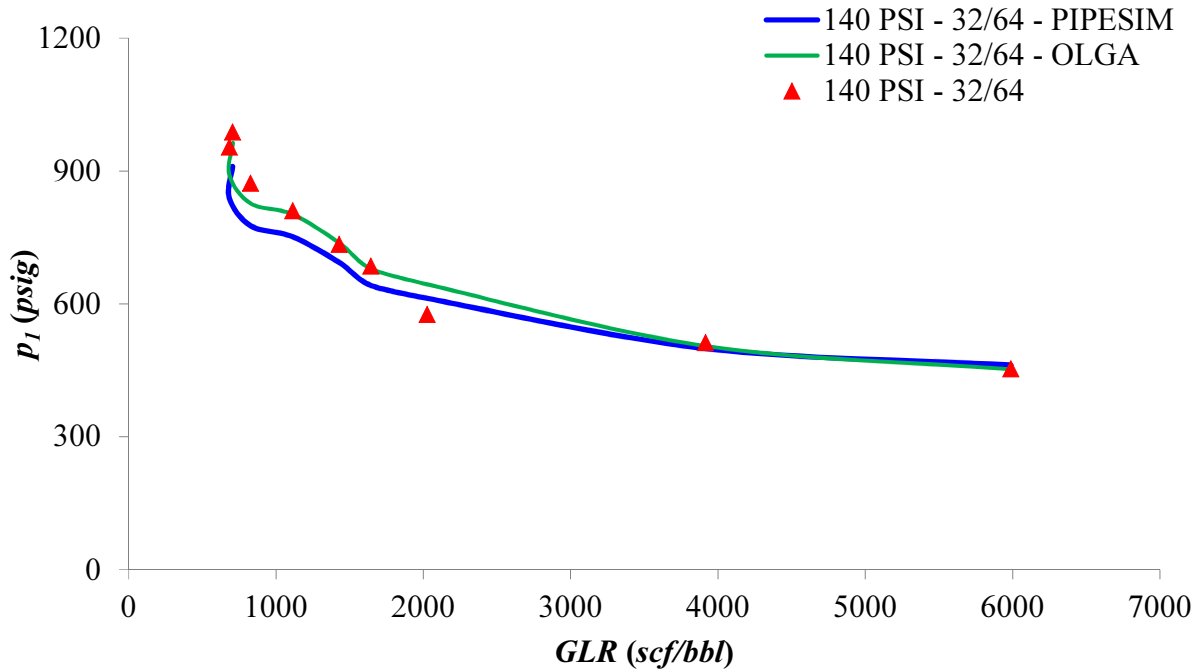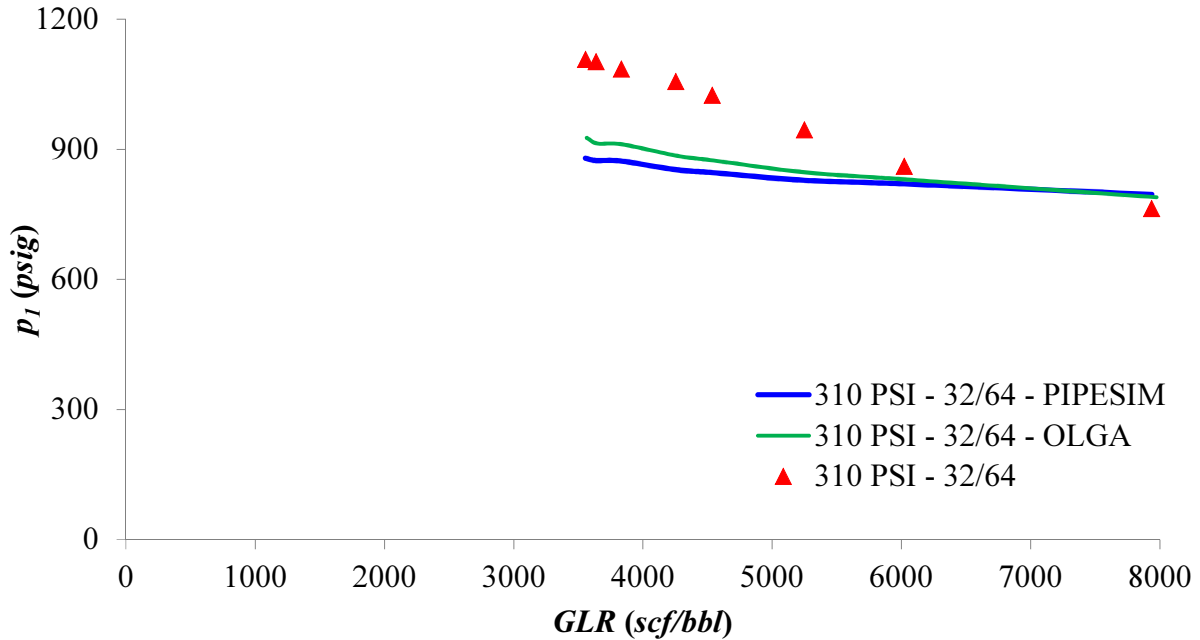
Figure 3.18. Comparison between PIPESIM® and OLGA® results and experimental upstream pressure for the GLV with 32/64 *inch* port size and constant downstream pressure of 140 *psi*.

Figure 3.18 shows that both simulation models were able to predict upstream pressures similar to the ones obtained in the experiment, with averaged absolute errors of 7% for the PIPESIM® model and 3% for the OLGA® model. For high GLR (above 3,500 *scf/bbl*) the model can be considered the same. However, as the GLR gets higher, the PIPESIM® model trends to underestimate the upstream pressure, while the OLGA® model presents better pressure estimation.

Figure 3.19 presents the results for the case with 310 *psi* downstream pressure. The simulation results present a small difference when compared to each other. At high GLR, the difference between the models is practically inexistent and it gets higher as GLR decreases. When comparing theoretical results with experimental results, it is clear that the models under predicts in more than 16% the results for lower GLRs. As discussed in the previous section, this behavior was observed for all the models used in this work, and it can be an indication of experimental errors.
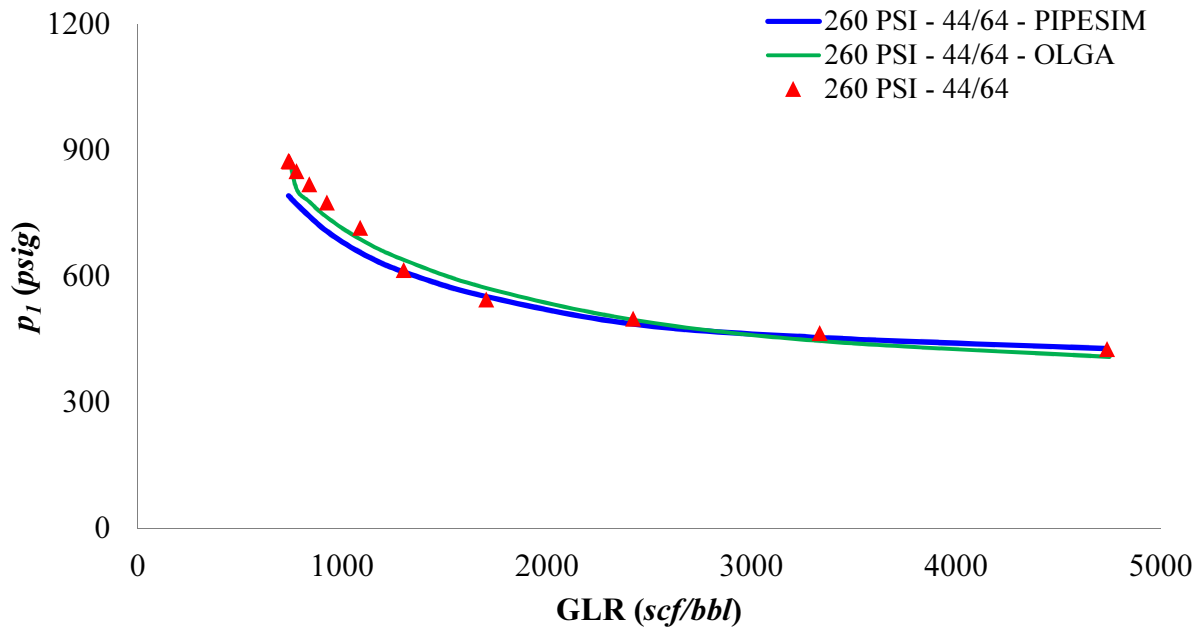
Figure 3.19. Comparison between PIPESIM® and OLGA® results and experimental upstream pressure for the GLV with 32/64 *inch* port size and constant downstream pressure of 310 *psi*.

For the 44/64 port size valve, the calibrated C_D for the orifice valve used in the OLGA® model was 0.70 and for the valve used in the PIPESIM® model was 0.64. Figure 3.20, Figure 3.21 and Figure 3.22 present simulation and experimental results for the cases performed with 44/64 *inch* downstream pressure with, respectively, 160, 260 and 450 *psi* downstream pressure.

The simulation results for all three cases presented for the 44/64 port size valve present averaged absolute errors smaller than 8%. A summary of the averaged absolute errors for all cases presented in Table 3.4. The total averaged absolute error, which considers all data points for the five cases studied, is slightly lower for the OLGA® model (5%) than for the PIPESIM® model (8%).

The cases presented in Figure 3.20 and Figure 3.21 present similar behavior of the cases evaluated for the 32/64 port size valve. The results for both cases show that at high GLRs the differences between the simulation results and experimental data is less than 2%, and both models present accurate results in the prediction of the experimental data (errors lower than 5%). As the

GLR decreases lower, the OLGA® model presents a higher accuracy in the prediction of experimental data, and the PIPESIM® model trend to underestimate the upstream pressure.

Figure 3.20. Comparison between PIPESIM® and OLGA® results and experimental upstream pressure for the GLV for 44/64 *inch* port size and constant downstream pressure of 160 *psi*.
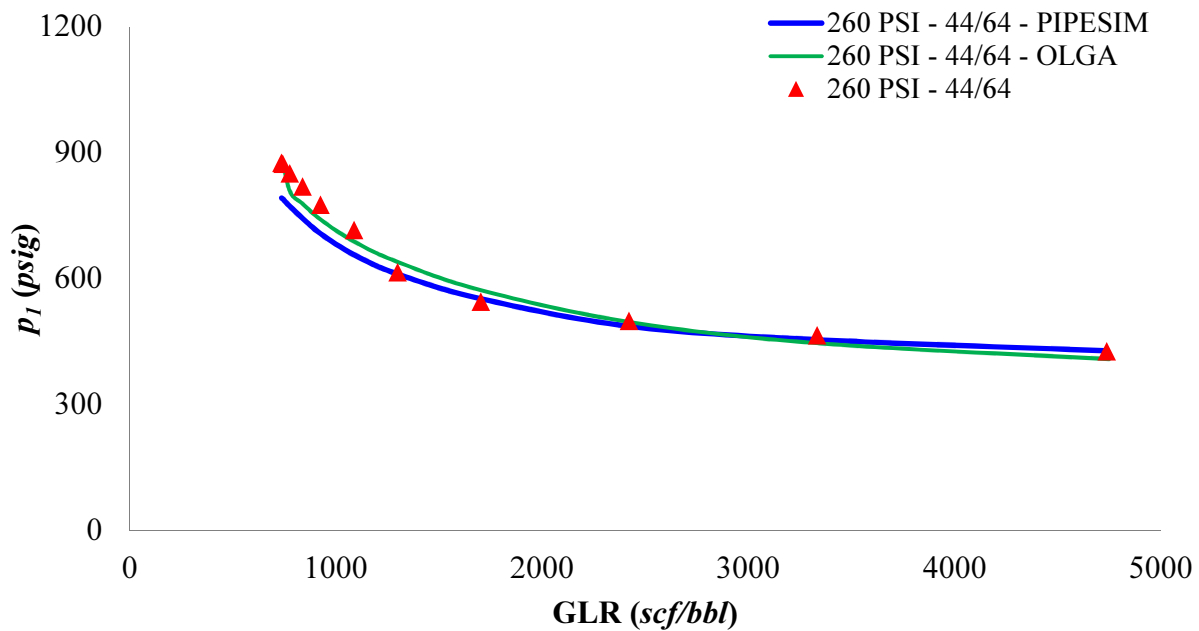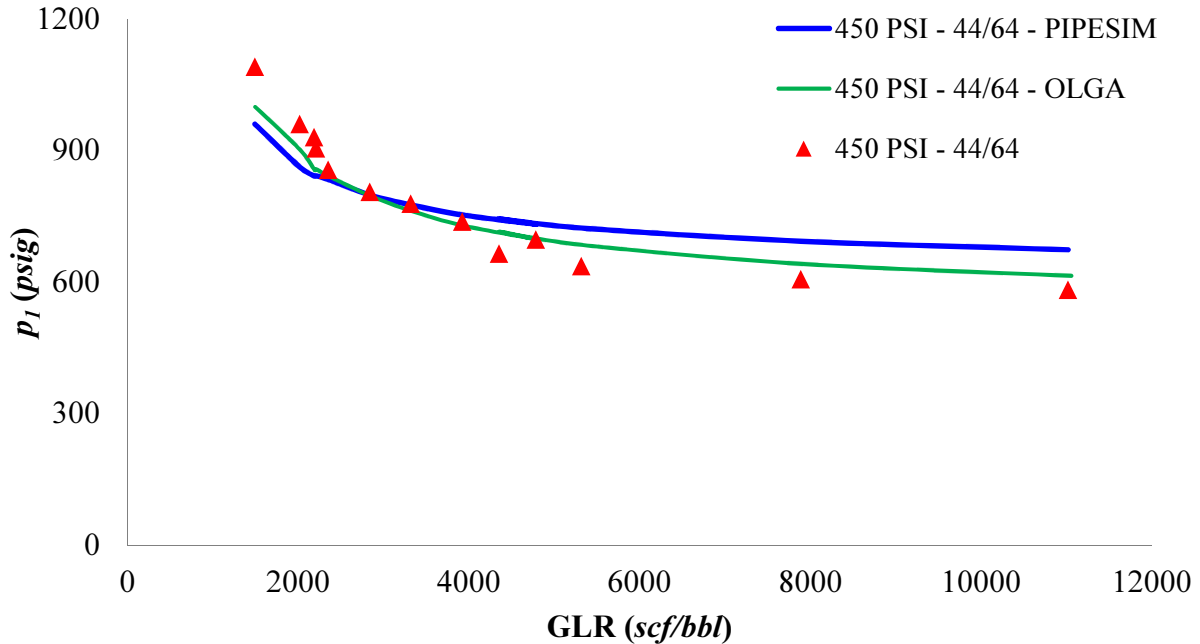

Figure 3.21. Comparison between PIPESIM® and OLGA® results and experimental upstream pressure for the GLV for 44/64 *inch* port size and constant downstream pressure of 260 *psi*.

Figure 3.22. Comparison between PIPESIM® and OLGA® results and experimental upstream pressure for the GLV for 44/64 *inch* port size and constant downstream pressure of 450 *psi*.

The cases presented in Figure 3.19 to Figure 3.21 show that the OLGA® model predicted the experimental upstream pressure with higher accuracy than the PIPESIM® model for both high and low GLR. For high GLR the PIPESIM® model over predicted the upstream pressure more than 15% and for low GLR the model under predicted the pressure in more 10%.

The results presented in this section are summarized in Figure 3.23 and Figure 3.24, where the upstream pressure predicted using the numerical models are plotted against the experimental upstream pressure. The results for the PIPESIM® model (Figure 3.23) and OLGA® model (Figure 3.24) show that the models predicted the upstream pressure with errors lower than 15% for most cases. Only the case for the 32/64 port size valve and 310 *psi* downstream pressure presented errors higher than 15%.
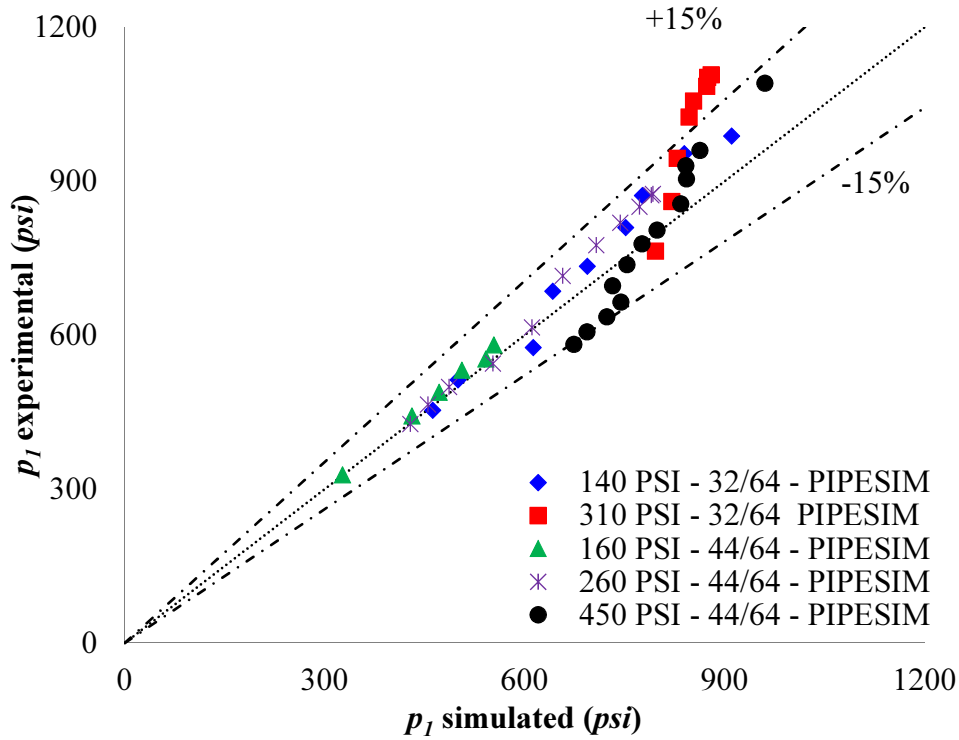
Figure 3.23. Comparison between experimental data and calculated upstream pressure using PIPESIM® model for all data points.
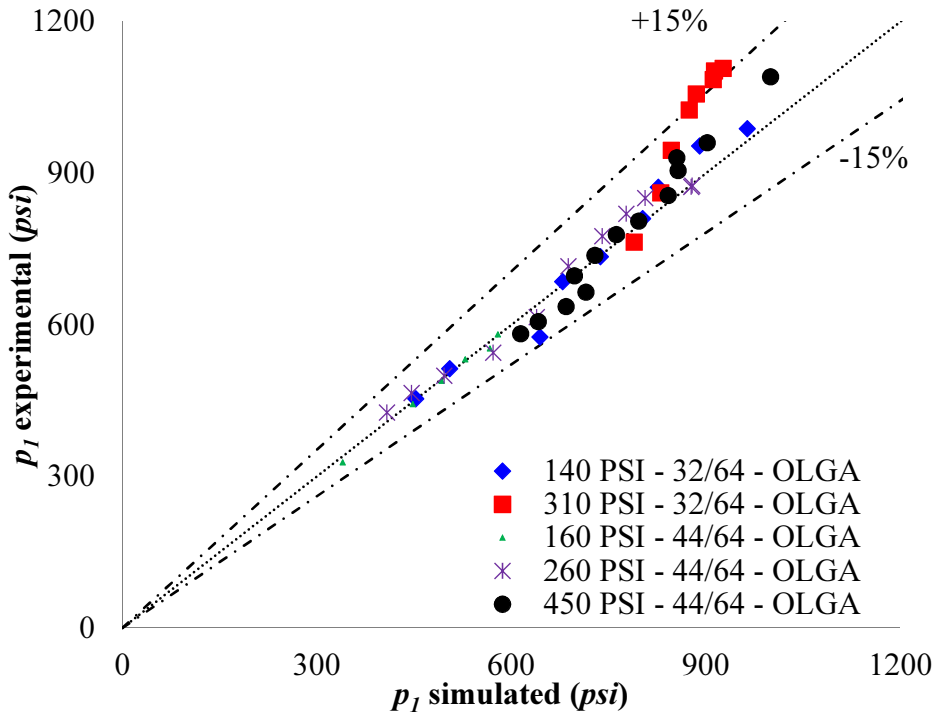

Figure 3.24. Comparison between experimental data and calculated upstream pressure using OLGA® model for all data points.

The results presented in this section showed that the mechanistic models used in PIPESIM®
and OLGA® were able to predict the experimental results with error in the 15% range. It is
important to mention that the discharge coefficients obtained in this study are only valid for the
combination of theoretical model and GLV design used for each C_D calibration. In case a new
valve or a different model for two-phase flow in orifice is used, a new C_D has to be obtained.

3.6 Conclusions

It was observed in this work that some models developed for the two-phase flow through
restrictions can be applied to characterize the performance of two-phase flow through GLVs.
However, some models present higher accuracy than others. For instance, Gilbert (1954) model
showed a superior performance compared to other empirical critical flow models such as Ros
(1959), Achong (1961) and Baxendell (1957). The results showed that, among the latter models,
Gilbert (1954) predicted the experimental results with the lower averaged absolute error (13%).
The other three models resulted in averaged absolute errors around 25%. The errors obtained with
the empirical critical flow models for the valve with 32/64 inch port size were higher than the
errors obtained for the 44/64 inch port size. For some cases, the errors for the smaller valve was
20% higher than the error for the larger valve.

The models for both critical and subcritical flow, proposed by Sachdeva *et al.* (1986) and
Ashford and Pierce (1975), presented satisfactory results with errors lower than 10% for most of
the experimental data points. Only one of case presented errors higher than 10%. Both Sachdeva
et al. (1986) and Ashford and Pierce (1975) models could be applied to predict the critical pressure
ratio and flow rate for critical and subcritical two-phase flow through GLVs. However, it is
necessary first to experimentally determine the C_D for the each particular GLV to obtain errors
lower than 20%.

The mechanistic models available in commercial flow simulators showed a reasonable prediction of the experimental results as well. However, both models require an experimental calibration of the discharge coefficient for each valve. Once the C_D was determined, the OLGA® model predicted the experimental results with the best accuracy, when compared to the other models evaluated in this work. The total averaged errors for OLGA® model was 5%, and for some cases the error was as low as 1%.

The model proposed by Brill and Beggs (1991), which is available in PIPESIM®, also presented acceptable errors (around 8%), but it was noticed that this model often underestimated the upstream pressure for low GLRs. The Hydrovalve™ model implemented in OLGA® is the one with lowest errors for predicting critical and subcritical flow for both small and larger port size valve analyzed in this work. Based on that, this model is the one recommended to be applied in future works for modeling two-phase flow through orifices GLVs. The C_D presented in this work for both valves is only valid for that type of valve with the same port size and internal geometry tested in the experiments in this study. In case it is needed to model other GLV with different geometry, a new C_D has to be determined.

4 Experimental Investigation of Vertical Downward Two-Phase Flow in Annulus

One point that requires special attention in the LAGL unloading is the two-phase downward flow in the casing annulus. During the injection of a gas-liquid two-phase fluid mixture to perform the unloading of the well, the injected two-phase mixture will flow downward in the annular space between casing and tubing. Understanding the characteristics of the downward two-phase flow in annulus is essential to define the optimum injection rates for liquid and gas. During the two-phase injection, it is important to have either bubbly or intermittent downward flow in the annulus to enhance the gain in the hydrostatic pressure due the addition of liquid in the injection fluid.

This chapter presents an experimental characterization of downward gas-liquid flow in vertical annulus for a wide range of superficial gas and liquid velocities, using air and water, to obtain experimental characterization of flow regimes, liquid holdup and pressure gradient. Some comparisons are also performed between experimental data from others studies for downward flow in vertical pipe.

4.1 Introduction

Since the early 1960s, a significant number of studies have been performed to characterize two-phase flow in vertical pipes. Most of these studies are focused on upward flow in pipes, while not much attention has being given to downward two-phase flow. From the knowledge of the author, there are no studies in the literature about downward two-phase flow in annular pipes. Nevertheless, studies in downward two-phase flow in pipes can be found in the literature [Barnea *et al.* (1982a); Barnea *et al.* (1982b); Hasan (1995); Hernandez *et al.* (2002); Almabrok *et al.* (2016); Usui and Sato (1989); Usui (1989); Bhagwat and Ghajar (2012)].

Table 4.1 shows that downward gas-liquid flow in vertical pipes exhibits essentially three flow regimes: bubbly (or dispersed bubble), intermittent (including slug and froth), and annular (or failing film). These flow regimes are observed for tubing diameters ranging from 0.5 to 4 *inch*, superficial gas velocities from 0.07 to 285 *ft/sec*, and superficial liquid velocities from 0.03 to 69 *ft/sec*.

Table 4.1. Survey of published experiments of co-current downward gas-liquid flow in vertical pipes.

Study	Fluids	ID (*inch*)	u_{sg} (*ft/sec*)	u_{sl} (*ft/sec*)	Flow Regimes Observed
Barnea *et al.* (1982b)	Air/Water	1 & 2	0.16 to 285	0.03 to 69	Dispersed bubble, Slug and Annular
Hernandez *et al.* (2002)	Air/Water	2	1.15 to 36	0.13 to 9.8	Bubbly, Slug and Annular
Almabrok *et al.* (2016)	Air/Water	4	0.49 to 98	0.23 to 4.9	Bubbly, Intermittent and Annular
Usui and Sato (1989)	Air/Water	0.6, 1, 1.26, 1.5	0.06 to 69	0.29 to 4.9	Bubbly, Slug and Annular
Bhagwat and Ghajar (2012)	Air/Water	0.5	0.26 to 7.2	0.13 to 66	Bubbly, Slug, Froth, Falling film and Annular

Although no study can be found in the literature on downward two-phase in annulus, one can argue that this lack of experimental investigation on this topic is because two-phase flow in vertical pipe and annulus are expected to be similar. However, the experimental investigation of Caetano *et al.* (1992) for upward flow in vertical annulus has reveal that the characteristics of the flow regimes can be substantially different between flow in pipes and annulus. Therefore, an experimental characterization of downward two-phase flow in annulus is needed to determine the similarities and differences between downward flow in pipes and annulus.

4.2 Experimental Setup

Figure 4.1 presents the schematic diagram for the experimental apparatus used in this study to characterize two-phase downward flow in vertical annulus. The pressures used during the experiments are not higher than 30 *psi*, using water and air as the working fluids. During the

operation, water is pumped from a water storage tank (1) using a centrifugal water pump (2). The water flows through a magnetic flow meter (3) and is directed to the mixing tee (10) located at the inlet of the vertical test section. The flow rate of the water is controlled adjusting the pump speed and the automated flow control valve (4) located upstream to the water flow meter.
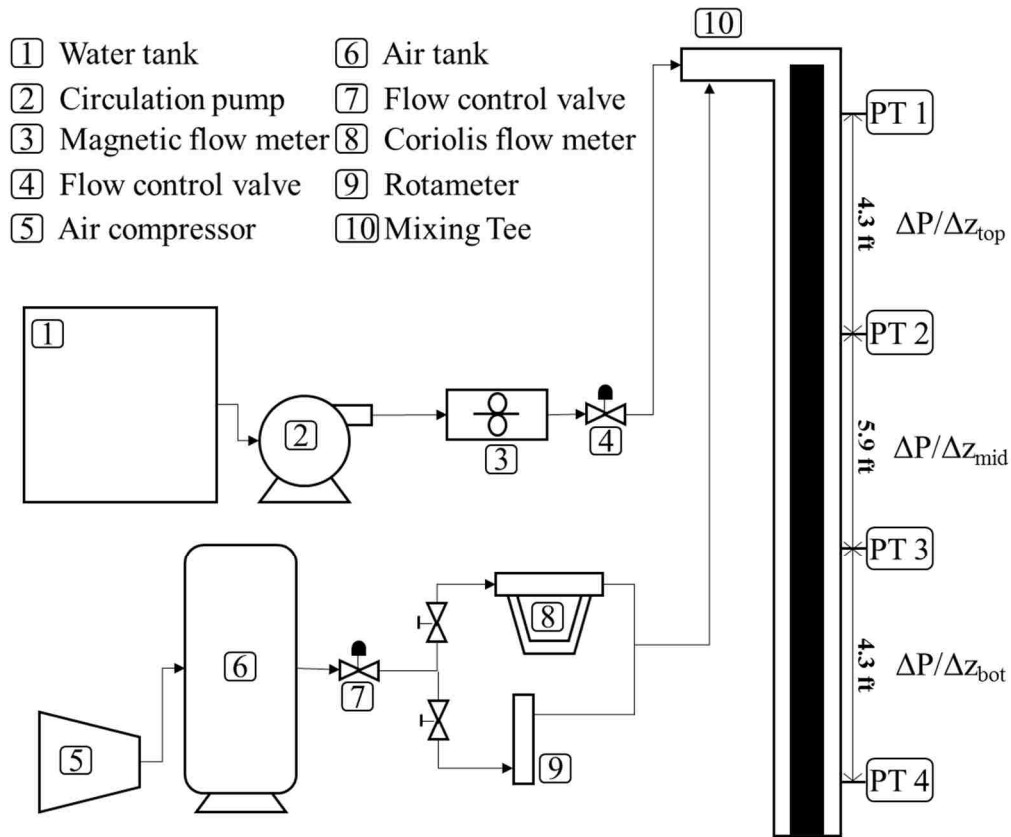

Figure 4.1. Low pressure flow loop.

A centrifugal compressor (5) supplies the air for the experimental facility. The air from the compressor is stored in an air tank (6) to reduce the pressure fluctuation from the compressor. Although is not showed in the schematic diagram, the air from the compressor flows through a filter and a dryer to eliminate moisture from the air before going to the storage tank. An automated flow control valve (7) located in the upstream to the air tank regulates the rate of air flowing through the test system. Two flow meters are used to monitor the gas flow rate, a Coriolis flow meter is used for flow rates higher than 0.07 ft^3/sec and a Rotameter is used for flow rates from 0

to 0.07 ft^3/sec. After flowing through one of the flowmeters, the gas is directed to the mixing tee (10), where it is mixed with the water and injected in the vertical test section.

The test section consists of a 16.4 ft long vertical annular section composed by a 4 $inch$ ID transparent PVC outer pipe and a 3 $inch$ OD aluminum inner pipe. The inner pipe is positioned in the center of the outer pipe using a three-screw centralizer (Figure 4.2) at the top and bottom of the test section, to guarantee that there is no eccentricity between inner and outer pipes. The bottom of the vertical test section is open to the atmosphere. Pressure is monitored in four locations of the vertical section.
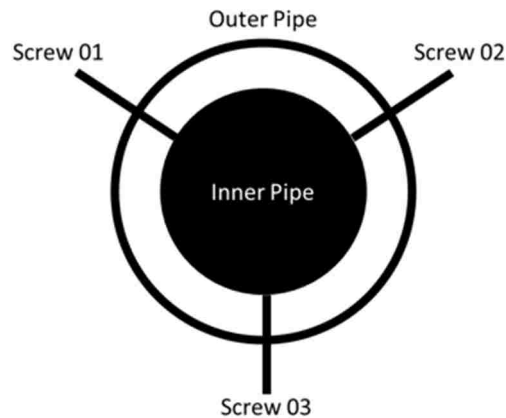
Figure 4.2. Top view of three-screw centralizer.

A high-speed camera is used to visually investigate the flow pattern in the test section. The camera is positioned one meter above the bottom of the tests section. The pressures measurements and high-speed camera results are used to build flow regime maps for downward flow in vertical pipes and to analyze the pressure gradient for different conditions of flow. The liquid holdup measurements are performed at the end of each experiment. The liquid holdup is measured by stopping the water injection to the vertical test section and, simultaneously, collecting the water volume in the test section. Because the test section has a known volume, the liquid holdup is calculated using the following expression,

$$H_l = \frac{V_L}{V_{total}} \hspace{6cm} 4.1$$

Where H_l is the liquid holdup, V_L is the volume of liquid in the test section and V_{total} is the total volume of the test section.

The liquid holdup measurements carried out in this study show some data scattering, particularly for the bubbly flow regime. This scattering is related to the effect of flow development and to the uncertainty of the technique used to measure the liquid holdup. When measuring the liquid holdup, the water injection at the inlet of the test section is shut at the same time that the water in the test section outlet is collected. If there is a small delay between the valve shut at the inlet and the start of collation of water at the test section outlet, variation on liquid holdup may occur. As presented in the results and discussion section of this work, the flow is considered fully developed in the lower three quarters (3/4) of the test section. The effect of flow development in the upper first quarter (1/4) of the test section may create some deviation in the liquid holdup measurement. To account for this deviation related to flow development in the liquid holdup, an uncertainty of ±5% is added in the liquid holdup measurement. This uncertainty is based on the variation of pressure gradient in the first quarter of the test (where the flow is not fully developed) to the other three quarters of the test section, where the flow is considered fully developed.

To quantify the random uncertainty of the liquid holdup measurements, two operators performed liquid holdup measurements for the same experimental conditions. The results are presented in Figure 4.3, where the measurements obtained for the operator 1 is presented in the "x" axis and for the Operator 2 in "y" axis. As can be seen in Figure 4.3, the maximum difference between the operators is around 15%, and it is considered the uncertainty of the liquid holdup measurements presented in this work.
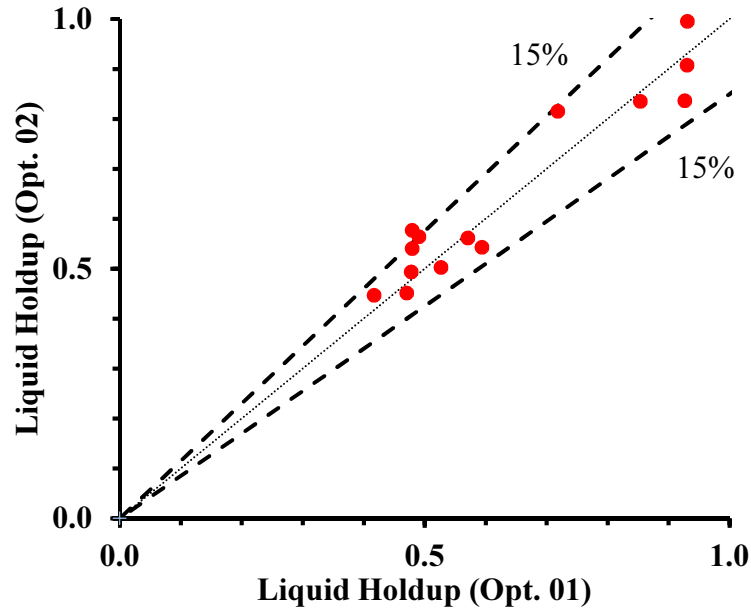
Figure 4.3. Liquid holdup uncertainty for different operators.

Equation 4.2 defines how the total pressure gradient was calculated in this study. The pressure gradient presented in Equation 4.2 is a combination of frictional, acceleration and hydrostatic pressure gradients. It is important to notice that, for downward flow in vertical annulus, the hydrostatic portion of the pressure gradient is always positive and the frictional portion is always negative.

$$\frac{\Delta p}{\Delta z} = \frac{p_{bottom} - p_{top}}{z}$$

4.2

where p_{top} is the pressure at the top of the interval where the pressure gradient is evaluated, p_{bottom} is the pressure at the bottom of the interval and z is the length of the evaluation interval.

Pressure gradients for the top (between PT 1 and PT 2), middle (between PT 2 and PT 3) and bottom (between PT 3 and PT 4) of the vertical test section (Figure 4.1) are calculated in for each test run. A data acquisition system is used to acquire the experimental measurements, and operate the flow control valves. Table 4.2 presents a list of the pressure and flow instruments used in this work.

Table 4.2. Instruments specification.

Name in Figure 4.1	Instrument	Model	Range
PT 1, PT 2, PT 3 & PT 4	Pressure Transducer	Gems Series 2200 0.25% Accuracy	Vac to 14.5 psi
3	Liquid Flowmeter	Rosemount 8705 Magnetic Flowmeter 0.25% Accuracy	9.89 to 600 ft^3/h
8	Gas Flowmeter	Dwyer Series RM	0 to 4.8 ft^3/min
9	Gas Flowmeter	Micro Motion F050S ±0.5% of rate Accuracy	0 to 1252 ft^3/min

4.2.1 Experimental Procedure

Prior to starting the test runs, any liquid present in the vertical test section is removed. Once the test section is completely dry, the pressure transducers are calibrated to the zero point, and this calibration is recorded in the data acquisition system.

The experiment starts with the injection of gas at a constant flow rate, followed by the injection of liquid also at a constant flow rate. Both liquid and gas injection shall be stable (not varying more than 10% of the target value) throughout the experiment, and the data is recorded. The recording time for each test run is about 120 sec.

Five liquid flow rates were evaluated in this work and, for each liquid flow rate, ten to thirty runs with different gas flow rates were evaluated. This work evaluates a total of 114 runs for different combinations of liquid and gas flow rates. Table 4.3 presents a summary of the test matrix.

Table 4.3. Summary of the test matrix.

q_L (ft^3/sec)	u_{sl} (ft/sec)	q_G (ft^3/sec)	u_{sg} (ft/sec)
0.067	1.61	0.003 to 0.812	0.07 to 20
0.089	2.17	0.003 to 0.812	0.07 to 20
0.111	2.69	0.003 to 0.812	0.07 to 20
0.133	3.22	0.003 to 0.812	0.07 to 20

4.3 Results and Discussions

This section presents the experimental results for flow regime maps, liquid holdup and pressure gradient for two-phase downward flow in pipe annulus. The results are presented for five

73

superficial liquid velocities and a wide range of superficial gas velocities. The experimental data obtained in this work is compared to data available in the literature for downward flow in vertical pipes with the same hydraulic diameter. This work calculates the hydraulic diameter for pipe annulus as described in Equation 4.3.

$$D_H = ID_{outer} - OD_{inner} \hspace{4cm} 4.3$$

where D_H is the hydraulic diameter, ID_{outer} is the inner diameter of the outer pipe and OD_{inner} is the inner diameter of the outer pipe

4.3.1 Flow Regime Map

Three flow regimes were observed in this study: bubbly, intermittent and annular flow, which are similar to the experimental observations described by Barnea *et al.* (1982b) and Almabrok *et al.* (2016) for downward two-phase flow in vertical pipes. Figure 4.4 shows the pictures of the typical flow regimes observed during the experimental runs. The flow regime for each experimental run was assessed using a high-speed camera. The high-speed videos were recorded at 960 frames per second.

(a) Bubbly   (b) Intermittent   (c) Annular
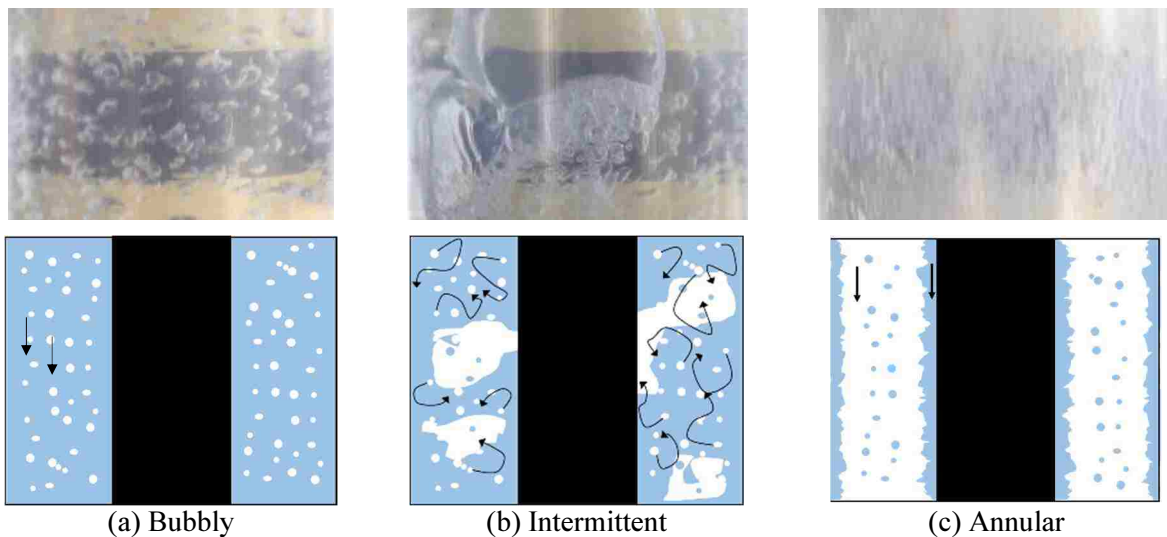
Figure 4.4. Flow regimes in downward flow in annulus

Each flow regime observed during the experimental runs can be briefly described as follows:

Bubbly flow: The bubbly flow regime is characterized by a continuous liquid phase flowing downward and carrying a discontinuous gas phase. The gas phase is distributed as discrete bubbles of small diameter (e.g., diameters no larger than the hydraulic diameter of the annulus). This flow regime occurs for low gas velocities and high liquid velocities.

Intermittent flow: The intermittent flow is characterized by the presence of large gas bubbles with irregular shape flowing downward and liquid phase with small gas droplet in chaotic movements. Large bubbles here means gas bubbles with equivalent diameter significantly larger than the hydraulic diameter of the annulus.

Annular flow: a gas core with entrained droplets flows downward with a liquid film adjacent to the pipe walls (both tubing and casing walls). Gas bubbles are also entrained in the downward liquid film.

Figure 4.5 presents the flow regime map (liquid superficial velocity, u_{sl}, versus gas superficial velocity, u_{sg}) obtained with the experimental results. The intermittent flow regime is not observed for u_{sg} lower than 0.33 *ft/sec*, and the transition between bubbly and annular flow occurs when u_{sg} is around 2 *ft/sec*. As the liquid superficial velocity gets higher than 2.60 *ft/sec*, intermittent flow regime is observed when the superficial gas velocity is in the range of 0.4 to 3.4 *ft/sec*.
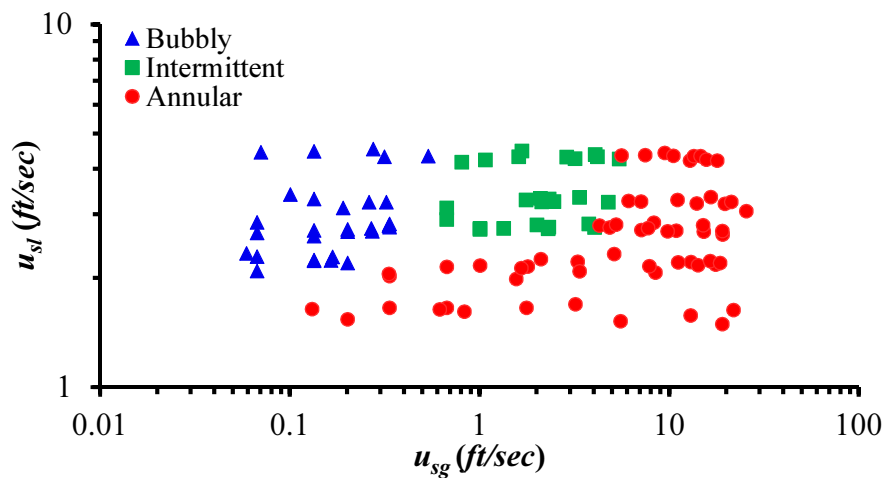
Figure 4.5. Flow regime map prepared from experimental observations.

Similar to what was observed by Barnea *et al.* (1982b) for two-phase downward flow in pipes, annular flow regime is observed for a wide range of superficial liquid and gas velocities. On the other hand, bubbly and intermittent flow is observed for a narrow range of conditions, only for superficial liquid velocities higher than 2 *ft/sec* and superficial gas velocities lower than 3.28 *ft/sec*.

Figure 4.6 shows the comparison of the flow regime map for downward two-phase flow in annulus developed in this work and the flow regime map developed by Usui and Sato (1989) for downward flow in pipes. Both experimental studies were developed with the same hydraulic diameter (1 *inch*).
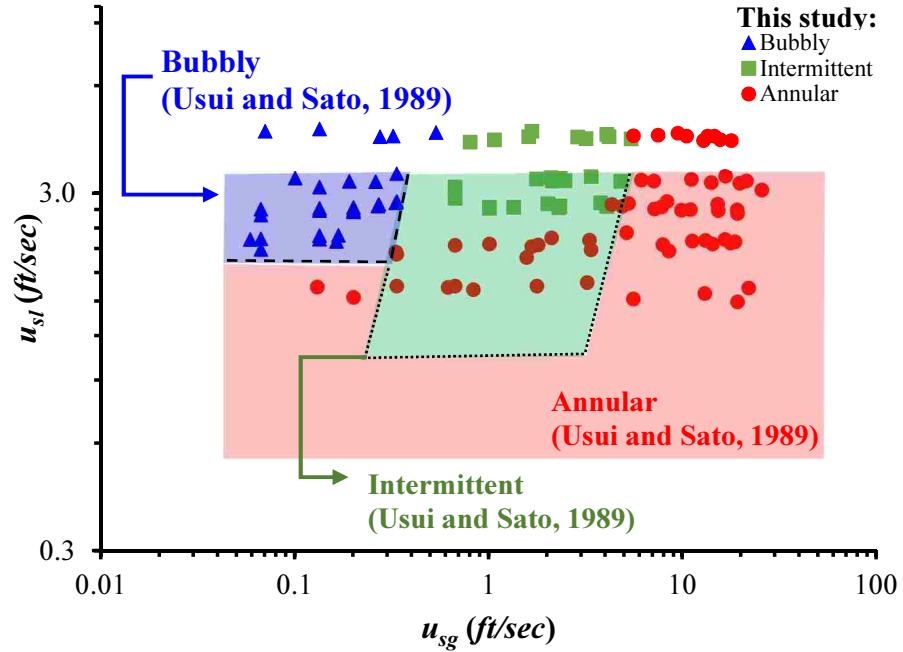
Figure 4.6. Comparison of the experimental observations for this study (data points) and the flow regime map for downward two-phase flow in a 1 *inch* ID pipe (shaded areas) developed by Usui and Sato (1989).

In Figure 4.6, the experimental data from Usui and Sato (1989) is presented by the background-shaded areas and dotted lines, which indicates the transitions between the flow regimes, while the observations from this work (from Figure 4.5) are represented as points. Usui and Sato (1989) described the existence of slug and churn flow regimes for flow in pipes. However,

in this work these two flow regimes are represented as intermittent flow. For this reason, the experimental observations from Usui and Sato (1989) for slug and churn flow are combined in Figure 4.6 and compared to the intermittent flow regime. Figure 4.6 shows that the bubbly flow region is very similar for flows in both pipes and annulus. It also shows that the annular flow region is mostly in agreement for both geometries. However, intermittent flow is observed for lower superficial liquid velocities in flow in pipes.

The disagreement between the experimental observations of this work and Usui and Sato (1989) are possibly a consequence of the difference in flow behavior between flow in pipes and annulus and/or a consequence of divergences on experimental characterization of flow regimes for different authors. Two-phase flow regime characterization is still predominantly obtained visually, and different authors may classify the same flow regime differently. Nevertheless, the experimental liquid holdup and pressure gradient results presented in the sections 4.3.2 and 4.3.3 also indicate differences for the intermittent flow transition between the observations from Usui and Sato (1989) (flow in pipes) and in this study (flow in annulus).

4.3.2 *Liquid Holdup*

The experimental liquid holdup results are presented in Figure 4.7 for five different liquid superficial velocities. This figure also correlates the observed flow regime during the liquid holdup measurements.

Figure 4.7(a) presents the results for the lowest liquid superficial velocity investigated in this study. In Figure 4.7(a), the liquid holdup results present values lower than 0.45. It is the only case, among all cases presented in Figure 4.7, that the liquid holdup does not get higher than 0.5. Liquid holdup lower than 0.5 is a characteristic of annular flow regime for downward flow in pipes, as it was also observed by Usui and Sato (1989). Based on this information, the liquid holdup results are in agreement with the visual flow regime observations
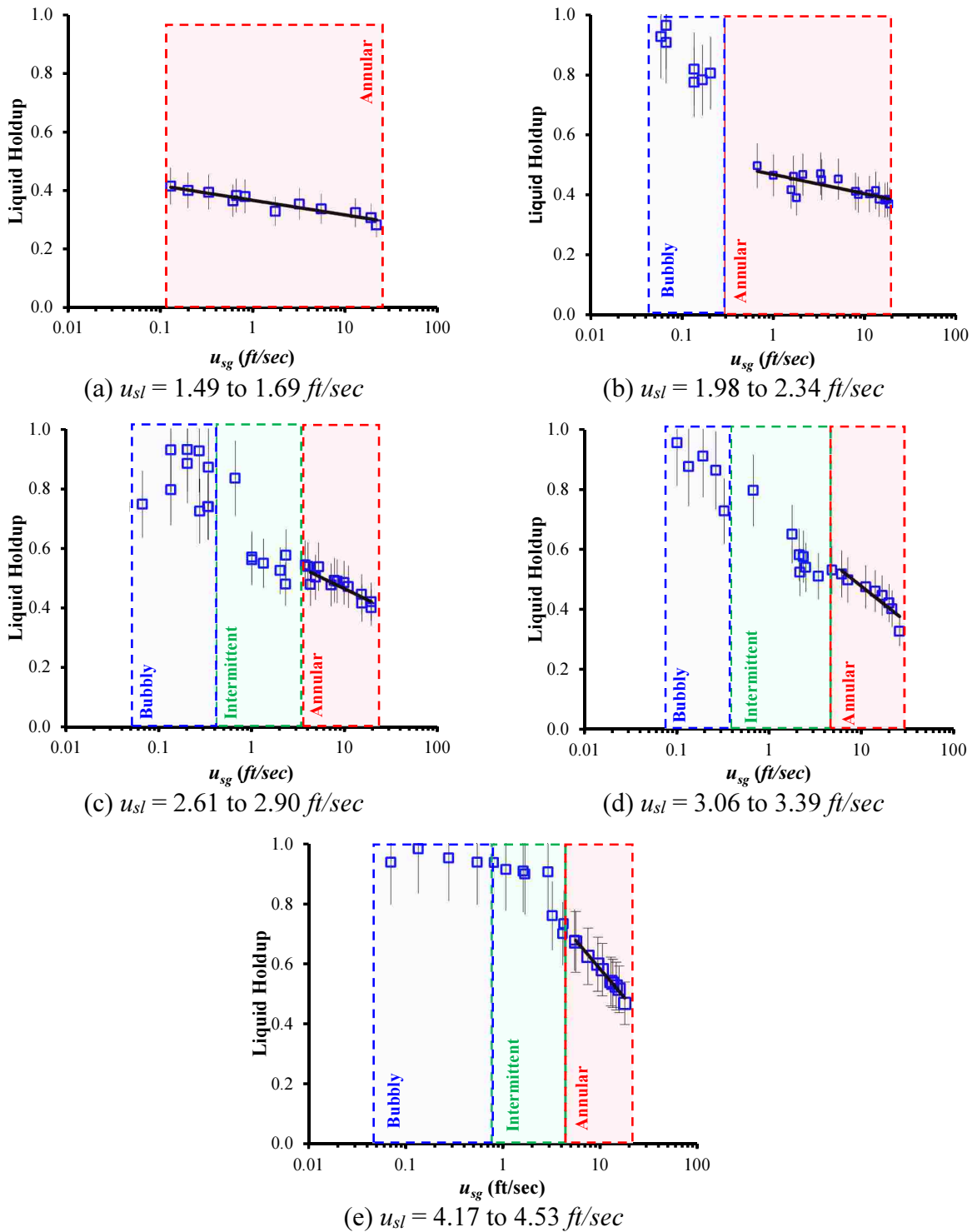
(a) u_{sl} = 1.49 to 1.69 *ft/sec*

(b) u_{sl} = 1.98 to 2.34 *ft/sec*

(c) u_{sl} = 2.61 to 2.90 *ft/sec*

(d) u_{sl} = 3.06 to 3.39 *ft/sec*

(e) u_{sl} = 4.17 to 4.53 *ft/sec*

Figure 4.7. Liquid holdup as a function of gas superficial velocity for five liquid superficial velocities intervals: (a) u_{sl} = 1.49 to 1.69 *ft/sec*; (b) u_{sl} = 1.98 to 2.34 *ft/sec*; (c) u_{sl} = 2.61 to 2.90 *ft/sec*; (d) u_{sl} = 3.06 to 3.39 *ft/sec* and (e) u_{sl} = 4.17 to 4.53 *ft/sec*.

For the bubbly flow region, the liquid holdup is between 0.75 and 1.0, which are shown in Figure 4.7(b) to (e). According to the bubble-packing theory, liquid holdup values higher than 0.73 are estimated for bubbly flow. In agreement to what is observed in this work, Taitel *et al.* (1980) adopted in their work the critical liquid holdup of 0.75 for the transition between bubbly and slug flow regimes in pipes. As expected, with the increase of superficial liquid velocity, the liquid holdup values reached values closer to 1.0. For annular flow, the maximum liquid holdup observed for all cases is around 0.6. It is observed that liquid holdup results for the annular flow region presents a linear trend (with "x" axis in log scale), and the slope of the line tends to increase for higher superficial liquid velocities. It indicates that the variation in the liquid holdup with the increase of gas superficial velocity, during the annular flow, is accentuated for higher liquid velocities. For most of the cases, the results for the liquid holdup also show a shift close to the transitions between different flow regimes, which corroborates the visual observations of these flow regime transitions.

Figure 4.8 presents the comparison of liquid holdup for downward two-phase flow in vertical pipes obtained by Usui and Sato (1989) and in annulus obtained in this work, for two similar liquid velocities. The flow in pipes and annulus have similar hydraulic dimeter (1 inch). The technique used for liquid holdup measurement in Usui and Sato (1989) work is different from the technique used in this work. It is important to mention that the definition for hydraulic diameter for pipe annulus used in this work is described in Equation 4.3, and the use of a different definition of hydraulic diameter may impact the results for the comparison between tubing and annulus. The dotted-vertical lines in Figure 4.8 represents the flow regime transitions from Usui and Sato (1989). The flow regime observed in this work is represented by the data points with the letters "A" for annular, "I" for intermittent and "B" for bubbly flow. In the study of Usui and Sato (1989),

the flow regimes are classified as bubbly, slug, churn and annular flow. In this work, slug and churn flow regimes are combined as intermittent flow regime. For this reason, no analysis will be carried for the transition between slug and churn flow.

Figure 4.8(a) shows good agreement for liquid holdup results for tubing and annulus in the bubbly flow region. In the annular flow region (observed by Usui and Sato (1989), the liquid holdup is consistently higher for flow in annulus than flow in tubing (even after considering the uncertainty related to the liquid holdup measurement technique and flow development). This difference is believed to be caused by the larger wetted perimeter in the annulus, which can cause an increase of the water volume in the liquid film.

(a) $u_{sl} = 2.16$ ft/sec

(b) $u_{sl} = 3.28$ ft/sec
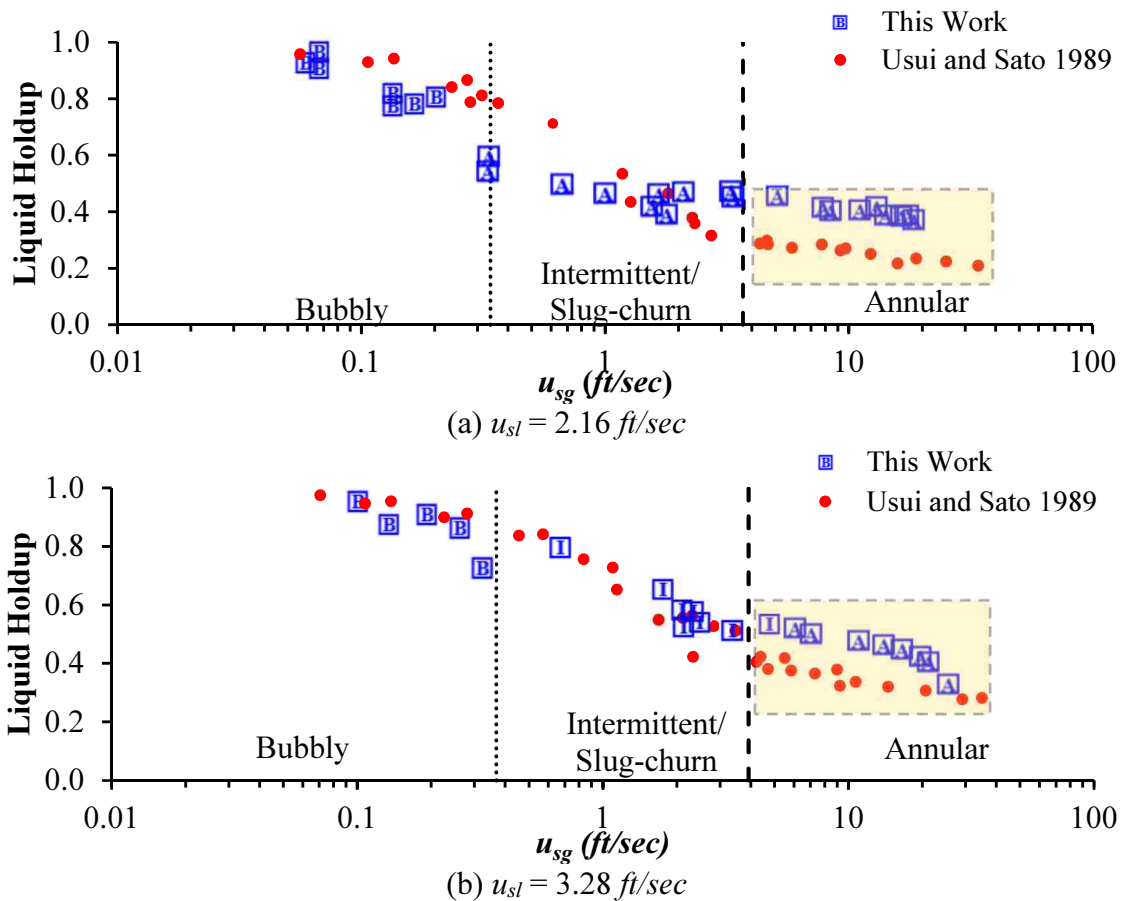
Figure 4.8. Comparison of liquid holdup for annulus (this work) and tubing [Usui and Sato (1989)] with same hydraulic diameter. The flow regime transition observed by Usui and Sato (1989) are represented by dotted vertical lines. The flow regime observed this work is presented in the bullets using "A" for annular flow, "I" for intermittent flow and "B" for bubbly flow.

The results presented in Figure 4.8(a) show that, for lower liquid velocities, there is a difference in the flow regime observation for annulus and pipes with similar hydraulic diameter. Usui and Sato (1989) observed the presence of intermittent flow regime for flow in pipes for gas superficial velocities between 0.33 and 3.28 *ft/sec*, while this work observed the presence of annular flow for the same range of superficial gas velocities. This difference in flow regime between flow in pipes and annulus can also be noticed in the liquid holdup results. While the liquid holdup results for flow in annulus present a linear trend with the same slope for velocities ranging from 0.33 to 16.4 *ft/sec*, the results from Usui and Sato (1989), for flow in pipes, show an change in the slope as the transition from annular to slug/churn flow occurs.

Figure 4.8(b) shows that for higher liquid velocities, similar flow regimes are observed for flow in pipes and annulus. It also shows that the flow regime transition for both pipe geometries present good agreement. Nevertheless, the liquid holdup for flow in pipes is slightly lower than for annulus, similar to what was observed in Figure 4.8(a).

The study of Caetano *et al.* (1992) shows that the friction factor for fully concentric annulus configurations can be substantially higher than in pipes of same hydraulic diameter, which can consequently affect the liquid holdup. As shown in Figure 4.8, the experimental liquid holdup results indicate that downward two-phase flow in pipes and annulus have similar behaviors for the bubbly flow regime, where the friction effects are generally not dominant in the total pressure gradient. However, for the annular flow regime, the liquid holdup is higher for the flow in annulus, and it is possibly caused by the larger effects of friction as a consequence of the larger wetted perimeter in annulus configurations.

4.3.3   *Pressure Gradient*

Figure 4.9 presents the experimental results for the total pressure gradient at three different axial locations in the vertical test section: top (39 L/D_H from injection), middle (101 L/D_H from

injection) and bottom (163 L/D_H from injection). Figure 4.9 also presents the flow regime for the different test runs included in this figure. These results are used to assess the axial flow development. The cases presented in the Figure 4.9 are for superficial liquid velocities between 3.06 to 3.39 *ft/sec*, which include the cases with higher axial variance of pressure gradient.
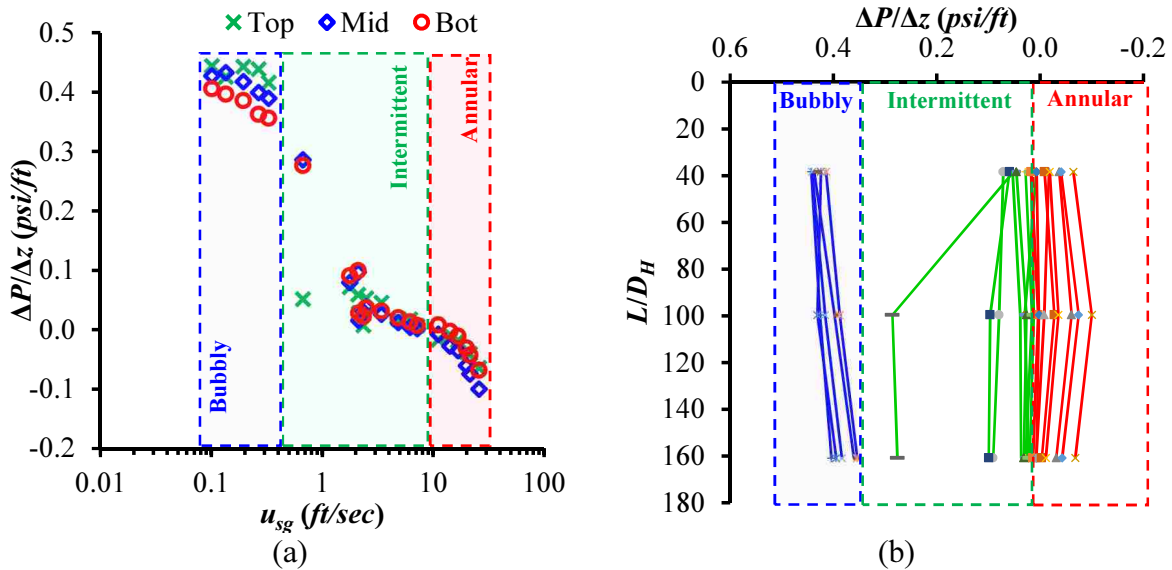

Figure 4.9. Pressure gradient for top, middle and bottom interval in the test section as a function of (a) gas superficial velocity and (b) and pipe length (L/D_H). For this case u_{sl} = 3.06 to 3.39 *ft/sec*.

The results presented in Figure 4.9 show that, for bubbly and annular flow regimes, the variation in the pressure gradients in all three axial locations is within the measurement uncertainty, which is approximately 10%. Therefore, these results indicate that the flow is fully developed for annular and bubbly flow regimes in all three axial locations. For the intermittent flow regime, there are cases where the pressure gradient in the top section of the annulus is much lower than in the other two sections, for instance, for u_{sg} = 0.66 *ft/sec* (see Figure 4.9a). These results indicate that the flow is not fully developed at the top of the test section, but show fully developed flow for the between the middle and bottom section. For this reason, in the analysis of the pressure gradient, the pressure gradient is calculated using only the middle and bottom section of the vertical annulus.

(a) u_{sl} = 1.49 to 1.69 ft/sec

(b) u_{sl} = 1.98 to 2.34 ft/sec

(c) u_{sl} = 2.61 to 2.90 ft/sec

(d) u_{sl} = 3.06 to 3.39 ft/sec

(e) u_{sl} = 4.17 to 4.53 ft/sec
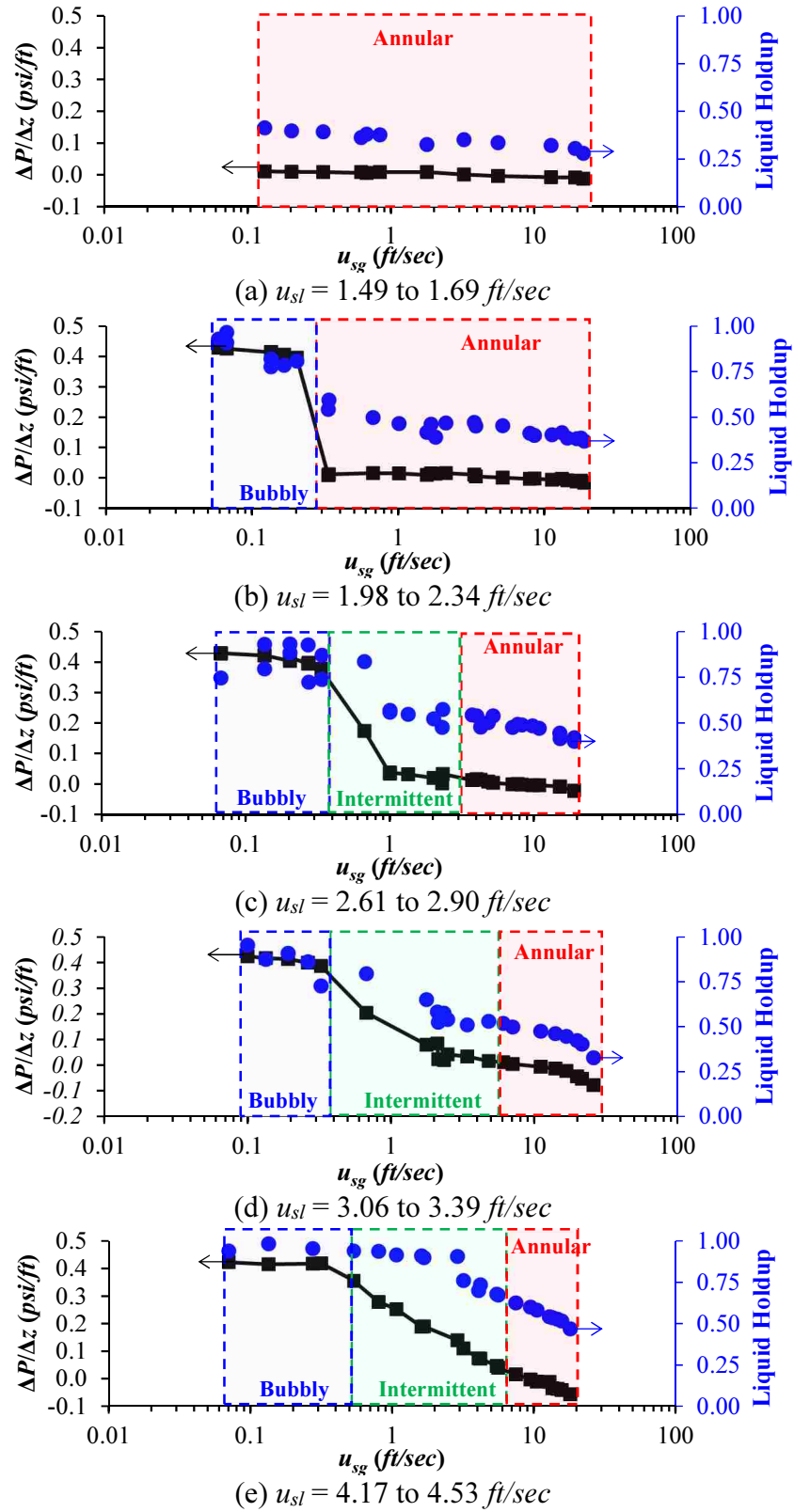
Figure 4.10. Pressure gradient as a function of gas superficial velocity for five liquid superficial velocities.

Figure 4.10(a) presents experimental pressure gradient results for low superficial liquid velocities. The results show that the pressure gradient does not present significant variation with the increase of the superficial gas velocity, for superficial liquid velocities between 1.49 and 1.69 *ft/sec*. This behavior is obtained because only annular flow regime is observed for this range of superficial liquid and gas velocities. For annular flow, the liquid holdup goes to its lower values and, consequently, the hydrostatic pressure gradient goes to values closer to zero. It is also expected to have higher values for the friction pressure gradient due to the high liquid and gas velocities in the annular flow region.

Figure 4.10(b) shows the pressure gradient for larger superficial liquid velocities where bubbly flow is observed for low gas superficial velocities (0.06 to 0.23 *ft/sec*). In the bubbly flow region, the pressure gradient presents values around 0.42 *psi/ft*, which is a value close to the hydrostatic pressure gradient for fresh water (0.43 *psi/ft*). This similarity with the fresh water gradient is explained by the high liquid holdup and low friction and acceleration effects for bubbly flow regime. The transition between bubbly and annular flow occurs for gas velocities approximately to 0.23 *ft/sec*, which is the same gas velocity the pressure gradient presents a sudden decrease.

Figure 4.10(c) and (d) show the pressure gradient for intermediate liquid velocities (2.61 to 3.39 *ft/sec*), which presents a similar behavior to the results in Figure 4.10(b). However, the intermittent flow regime is now observed between bubbly and annular flow regimes. For the intermittent flow regime, the pressure gradient presents a sharp decrease at the transition between bubbly and intermittent flow. However, this sharp decrease in pressure gradient for intermittent flow is only observed until the gas velocity reaches intermediate gas velocities (approximately 1.15 *ft/sec*). This shift in the pressure gradient curve for intermediate gas velocities for the

intermittent flow regime is a possible indication of transition between flow regimes, possibly a transition between slug and churn flow as observed by Usui and Sato (1989). However, from the visual observations of flow regimes obtained in this study, this transition was not possible to be observed. This is possibly due to the difficulties created by the concentric tubing, which partially blocks the observations and adds additional reflection of the light needed during the high-speed video recordings. For superficial gas velocities larger than 1.3 *ft/sec*, the pressure gradient for intermittent flow is approximately as low as in annular flow regime.

Figure 4.10(e) presents pressure gradient results for the highest liquid velocities tested in this study (4.17 to 4.53 *ft/sec*). Differently from the results for lower liquid velocities, the pressure gradient shows a monotonic decrease for superficial gas velocities higher than 0.66 *ft/sec*, which approximately coincides with the transition between bubbly to intermittent flow regime.

4.4   Conclusions

To the knowledge of the author, this study presents the first experimental characterization of vertical downward two-phase flow in annulus, generating unique experimental data for flow regimes, liquid holdup and pressure gradient. The following conclusions can be drawn from this study from the analysis of the experimental data:

- Three flow regimes were observed in downward two-phase flow in annulus: annular, intermittent and bubbly flow. Bubbly and annular flow regimes occur for superficial liquid and gas velocities similar to the ones observed by other authors for flow in pipes. However, there are evident differences for the intermittent flow regime, which is observed for flow in pipes for lower superficial liquid velocities than in annulus. This difference may represent substantial errors if one uses flow regime transition models developed for downward flow in pipes to predict flow regimes in annulus configurations.

- The liquid holdup results for downward flow in annulus for bubbly and intermittent flow regime are in reasonable agreement with results in the literature for downward two-phase flow in pipes, with the same hydraulic diameter. It is an indication that the use of numerical models developed for tubing in annulus for these flow conditions has potential to provide good liquid holdup prediction. However, for the annular flow regime, the liquid holdup measurements are consistently higher (around 35%) for flow in annulus than for flow in pipes with the same hydraulic diameter. This difference is likely related to the larger wetted perimeter than in pipes, and to the different velocity profile for annulus configurations. The wetted perimeter and velocity profiles are more likely to have a greater effect on the friction component of the total pressure gradient, which is generally dominant in annular flow regime.

- The pressure gradient results show that, for the bubbly flow regime, the pressure gradient is similar to the pressure gradient of fresh water, and it does not seems to be affected by the liquid superficial velocity. During the intermittent flow region, the superficial liquid velocity has a higher influence in the pressure gradient, and during the intermittent flow the pressure gradient varies from values close to the bubbly pressure gradient to values close to the annular pressure gradient.

5   Transient Simulation of Liquid-Assisted Gas-Lift Unloading

This chapter describes the use of a commercial transient multiphase flow simulator to model Liquid-Assisted Gas-Lift unloading operations. The proposed model is used to perform sensitivity analysis on the controlling parameters behind the LAGL unloading operation. These sensitivity analyses are essential to develop an optimized procedure for an efficient use of the LAGL technique during well unloading.

This model is validated with experimental data from a field-scale test well, as presented in Chapter 2. From the simulation results and experimental data, it is possible to demonstrate how the use of a gas-liquid flow injection can significantly decrease the injection pressure for unloading operations. Different combinations of gas-liquid injection rates are numerically tested to evaluate the effect of these parameters in the injection pressure during the full unloading operation.

5.1   Simulating the Liquid-Assisted Gas-Lift Unloading

The commercial transient multiphase flow simulator OLGA® (OLGA, 2015) is used in this study. The model built in this simulator is based in the configuration of the field-scale test well at PERTT Lab (see Figure 2.1). The flow model built in the simulator is a three-fluid model, which considers separate continuity equations for each phase. This simulator solves seven conservation equations (three for mass, three for momentum and one for energy) and one equation of state for pressure (OLGA, 2015). The simulation model built for this study is divided in three sections, as shown in the schematic diagram in Figure 5.1:

- Section 1: represents the casing/tubing annular flow line. 2,728 *ft* long vertical section is composed by 4.9 *inch* ID casing (outer pipe) and tubing (inner pipe) with 2.88 *inch* OD.

This section is used to simulate downward two-phase flow in annulus. The material used for the pipe walls in the simulator was steel and the pipe roughness is 16.4×10^{-5} *ft*. For flow calculation purposes the simulator considers the hydraulic diameter (D_H) of the annulus. D_H can be calculated using Equation 4.3 (OLGA, 2015).

- Section 2: represents the vertical tubing flow line, with a 2,728 *ft* long vertical section 2.44 *inch* ID steel pipe (roughness is 16.4×10^{-5} *ft*). This section is used to simulate upward two-phase flow in the tubing.

- Section 3: represents the gas-lift valve. A reverse flow check valve and an orifice valve that connects Sections 1 and 2 compose this section, and it simulates an orifice GLV located at the bottom of the well. The configuration for the valve model used in the simulator is presented in Table 5.1. The Hydrovalve™ uses a choke model to determine pressure drop through the valve and it can be applied for gas, liquid and gas/liquid mixtures. The option for no thermal phase is selected in the valve, and it means that the model considers that, when flowing through the valve, gas will have an isentropic expansion while the liquid is isothermal. The latter two assumptions are often acceptable for flow through restrictions (Ashford & Pierce, 1975; Sachdeva *et al.*, 1986). The orifice diameter selected in the model is 0.69 *inch*. No slip condition is considered in the valve. *Frozen* is the equilibrium model for no mass transfer between phases, which is expect in the model as the fluid are natural gas and water and no significant mass transfer are expected between these two fluids for the conditions simulated.

Table 5.1. Valve specification in OLGA®.

Model	Geometry	Equilibrium model	Thermal Phase	Slip model
Hrydrovalve™	Orifice	Frozen	No	No slip

The fluids (water and natural gas) are injected at the top of the Section 1, while this fluid mixture flows downward. At the bottom of the wellbore, the injected fluids flows through the Section 3, and enters Section 2 to flows upward through the production tubing.

(a) Test well   (b) Simulation model
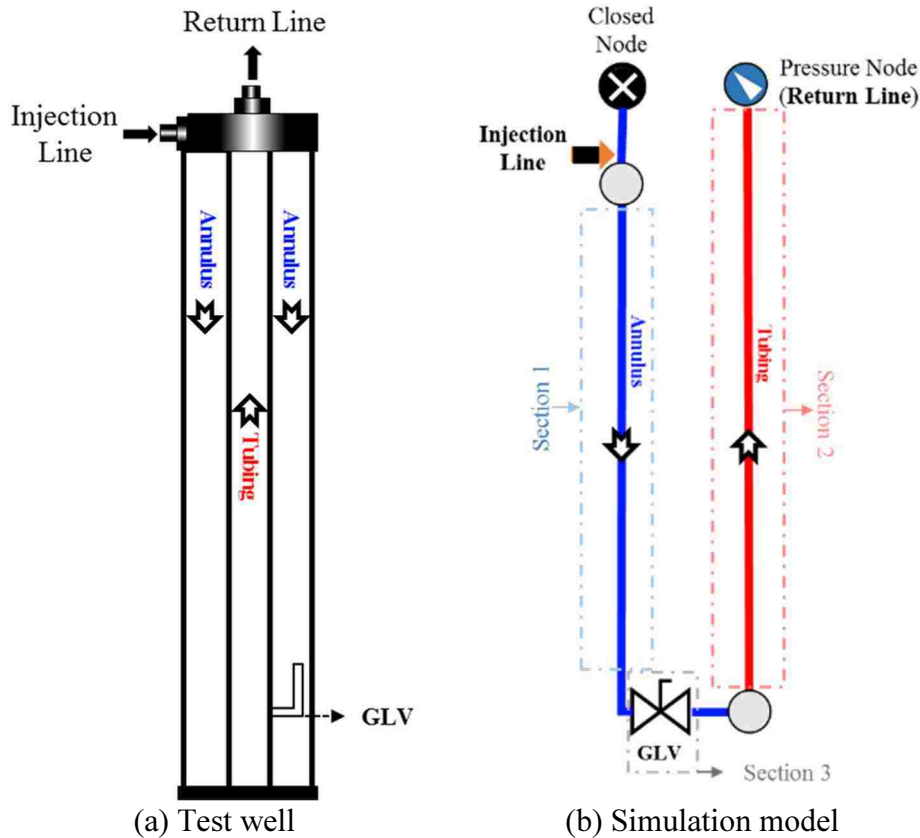
Figure 5.1. Schematic diagram of the (a) reference test well and (b) simulation model.

Boundary conditions: The input variables for this model are the following: wellhead tubing pressure (p_{wh}), injection liquid flow rate (q_L) and injection gas flow rate (q_G) with time.

Initial conditions: 80 ^oF for inlet and outlet fluid temperatures, 1 psi for injection pressure, 0 psi for outlet fluid pressure, for inlet void fraction and 0 for outlet void fraction. Both inlet and outlet watercut (water-liquid fraction) are 1.

Fluid model: The simulation uses compositional fluid model and this work considers that the natural gas is composed only by methane. Based on this assumption, the compositional model considers fluid properties of water and methane.

5.2   Simulation Procedure

Initially, the experimental results for the tests using the field-scale test well are used to validate the model that is built in the transient multiphase flow simulator. For the validation process, simulations are performed trying the replicate the conditions for each of the 15 experimental cases presented in Chapter 2. The wellhead tubing pressure, water and gas flow rates (at standard conditions) inputted in the model are obtained from each experimental case and the main output from simulations is the injection pressure.

The first set of simulations is performed with single-phase water flow. The single-phase water simulations are used to calibrate the discharge coefficient (C_D) of the GLV, since this discharge coefficient needs to be experimentally characterized for each valve if not given by the manufacture. Once the C_D is obtained, the simulations for the LAGL experiment are performed.

5.3   Characterization Results of C_D for GLVs

5.3.1   Single-Phase Liquid Flow

The experimental characterization of the C_D for the GLV is performed comparing experimental results presented in Figure 2.2 and simulation results performed with the same boundaries conditions (p_{wh}, q_L, q_G) of the experiments. The C_D value obtained from the experimental data for single-phase water flow is 0.29.

Once C_D is obtained, the main result from the simulation is the pressure drop through the GLV. Figure 5.2 shows the experimental data and simulation results for the pressure drop through the GLV for the different water flow rates injected in the well. It is important to notice that the C_D obtained is exclusive for the GLV used in this work.

As shown in Figure 5.2, the pressure drop increases with the water flow rates. These results are in accordance with other studies in the literature (Surbey *et al.*, 1989). Figure 5.3 shows a comparison of experimental data versus simulation results for pressure drop through the GLV after

C_D calibration. These results show that simulation has an agreement within 5% of the experimental
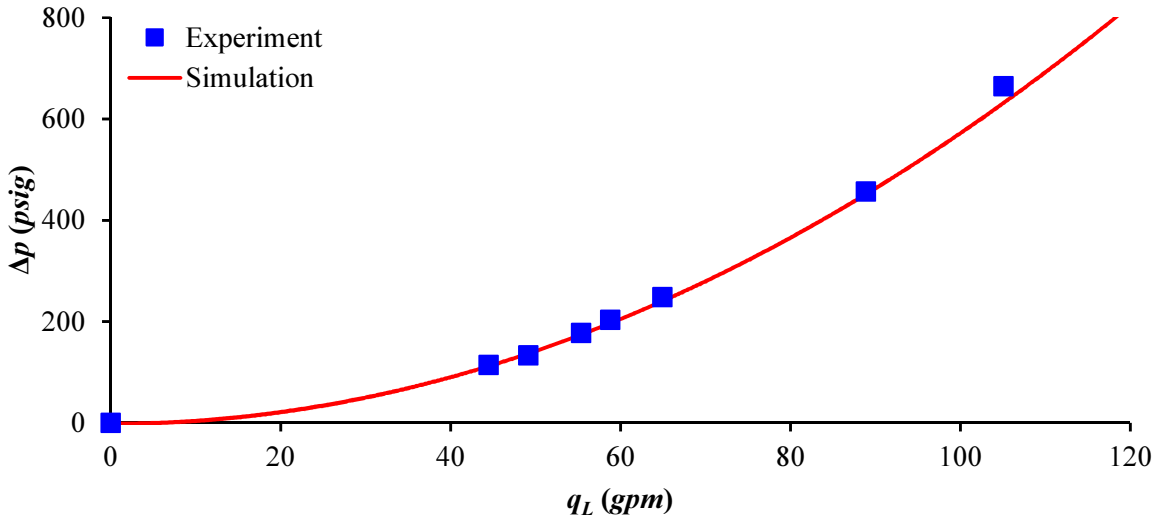
data.

Figure 5.2. Differential pressure as a function of water flow rate through the GLV.
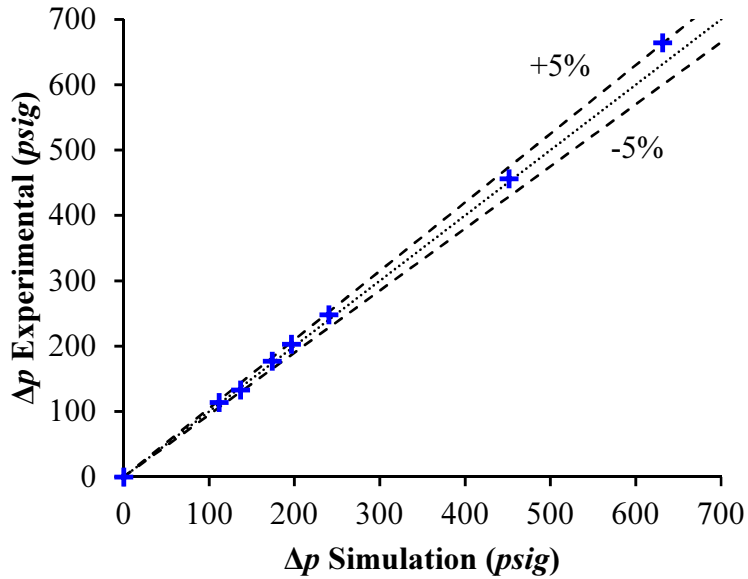
Figure 5.3. Comparison between experimental data and simulation results for pressure drop through the GLV after the calibration of the C_D coefficient.

5.3.2 *Two-phase gas-liquid flow*

During the LAGL simulations, the C_D inputted in the model was 0.29 for single-phase water

conditions and 0.67 for two-phase flow conditions. The experimental characterization of the C_D

for two-phase flow conditions is described in Chapter 3. A high-pressure two-phase flow loop was

built exclusively to test this valve for two-phase conditions, as discussed in Chapter 3.

5.4 Model Validation for LAGL Unloading

In order to validate the model for the LAGL unloading technique, the simulation results are

compared with experiments using the test well shown in Chapter 2. Fifteen simulation cases are

performed to validate the model for LAGL. Each of the simulation cases has the objective of

numerically replicate what is performed in the well tests for the proof of concept of the LAGL

presented in Chapter 2 (see Table 2.1).

Table 5.2 shows a summary of the comparison between experimental and simulation results

for all 15 cases evaluated in Chapter 2. $P_{inj,max}$ error represents the perceptual difference for each

case between the maximum injection pressure obtained in experiments and simulations. The

average error (Avg. Error) represents an average of the absolute difference (in %) between the

experimental and numerical injection pressure during the entire flow process for each case.

Table 5.2. Differences between experiment and simulation results.

Case #	q_G (actual gpm)	q_L (gpm)	$P_{inj,max}$ Error (%)	Avg. Error (%)
1		20	5	9
2		30	6	4
3	5	40	31	11
4		50	11	9
5		60	13	8
6		20	9	33
7		40	7	7
8	10	45	13	6
9		50	11	6
10		55	9	5
11		20	3	17
12		30	8	5
13	20	40	2	10
14		50	10	12
15		70	15	14

The average error for most of the cases is lower than 15%. Errors higher than 15% are only observed for cases 6 (33%) and 11 (17%). The average errors are at acceptable levels and can be related to the modeling of downward two-phase flow in vertical annulus, as it was previously discussed in Chapter 4. The behavior of two-phase upward flow in small-diameter pipes (up to 4 *inch* ID) has been extensively studied in the literature, and it is expected the simulations errors to be lower than in the downward two-phase flow in the annulus and GLV.

Figure 5.4 shows the simulation and experimental results for the injection pressure as a function of time for six combinations of gas and water flow rates, while using the LAGL technique. From the comparison between simulation and experimental results is possible to conclude that the simulation model captures the same trend observed in the experiments with reasonable accuracy for all cases. However, in some cases, the injection pressure is overestimated or underestimated. It is believed that this error is related to the modeling of the downward two-phase flow in the vertical annulus, as discussed in Chapter 1.

Figure 5.5 presents the experimental data and simulation results for the maximum injection pressure as a function of the water injection flow rate for all cases. This figure presents results for three gas injection flow rates: 5, 10 and 20 *agpm*. As can be seen in this figure, experimental and simulation results for all pressure injection curves have similar shapes, which show similar trends. For the three gas rates that are evaluated in this study, the water injection rate that provides the minimum injection pressure (optimum interval) is between the water flow rates of 40 and 53 *gpm*.
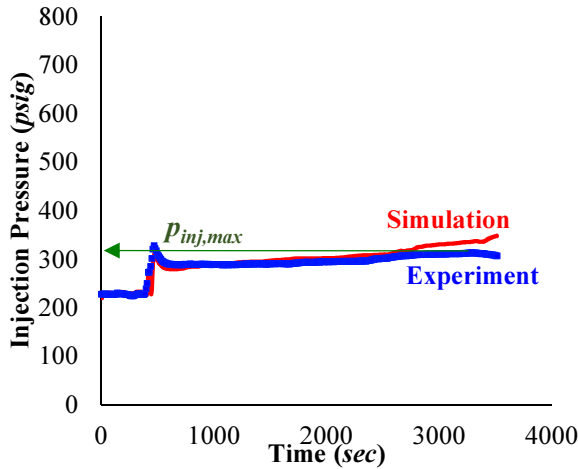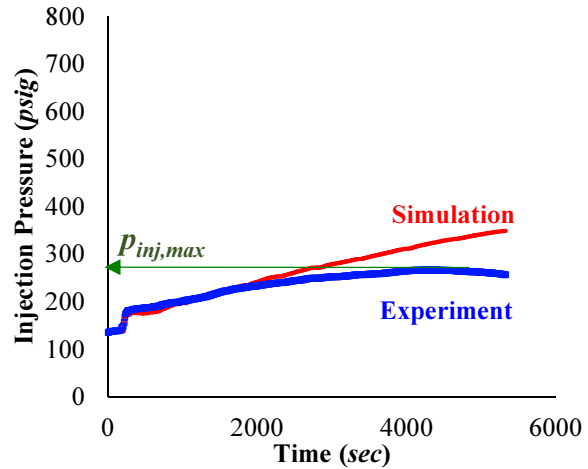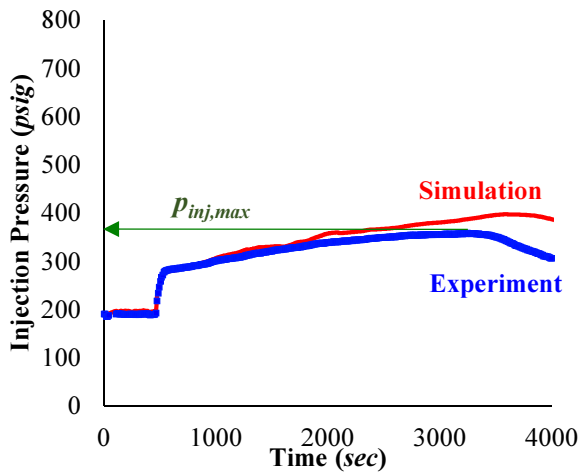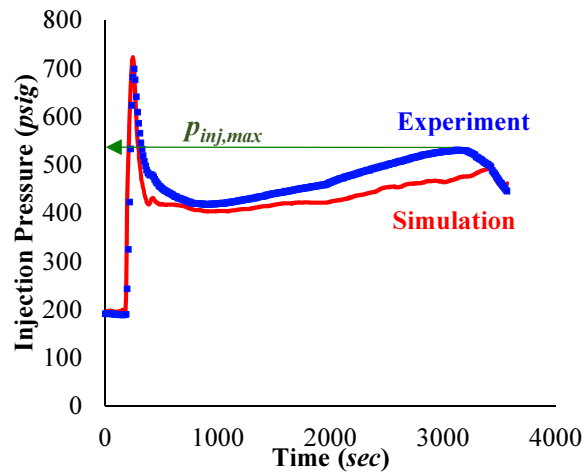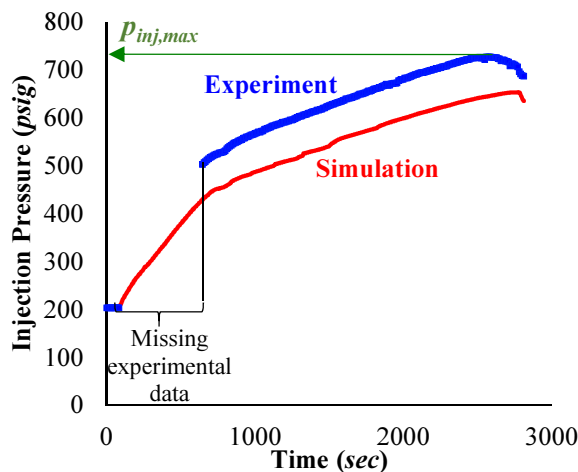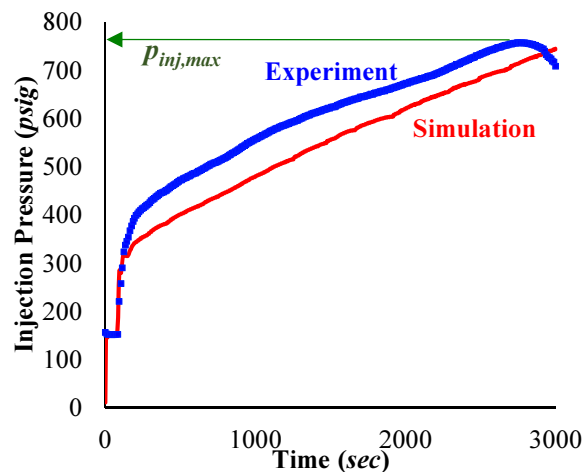
Figure 5.4. Injection Pressure as a function of time for water and gas injection rates at line (actual) condition. These figures show simulation and experimental results for six combinations of gas and water flow rates while using the concept of LAGL.
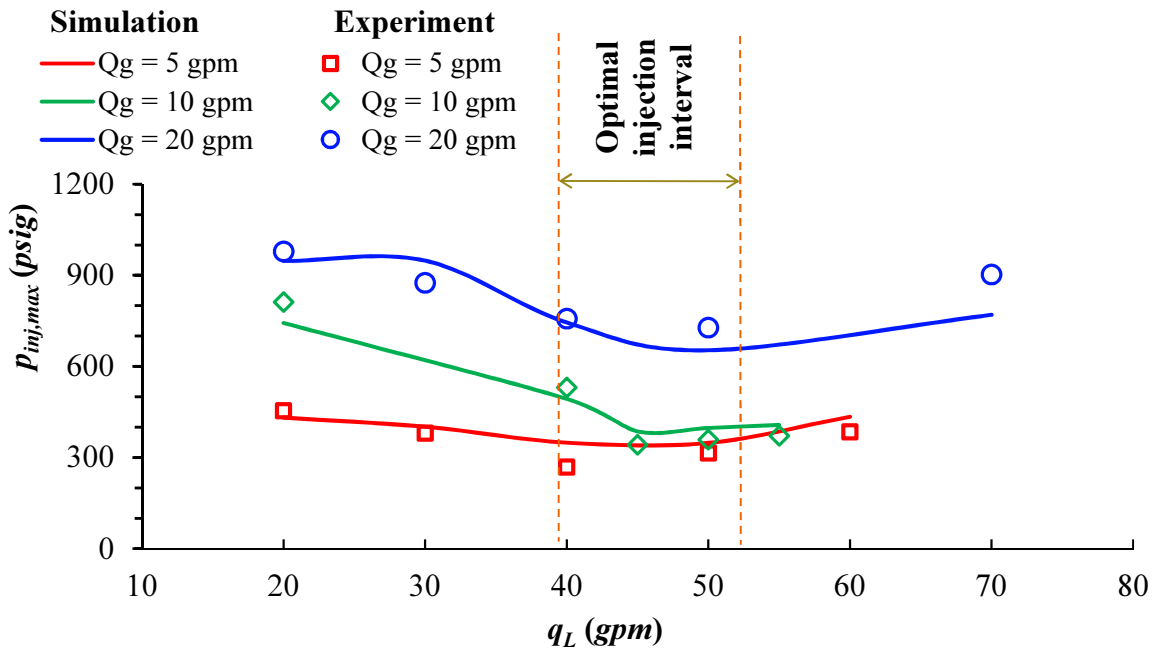
94

Figure 5.5. Comparison between experimental data and simulation results for maximum injection pressure as a function of water flow rate for different gas injection rates.

Figure 5.3 shows the gas and liquid superficial velocities, and void fractions in the casing annulus for all sixteen tests obtained from the OLGA® simulation results. The void fractions are below 30% for the points close to the optimal injection pressure (for a constant water flow rate). These results are in accordance with the 0.65 void fraction lower limit necessary to avoid annular flow regime (falling liquid film) in two-phase downward flows, as presented by Barnea *et al.* (1982a), Bhagwat and Ghajar (2012) and Almabrok *et al.* (2016). The latter authors observed experimentally that void fractions lower than 0.65 cannot be achieved for annular flow regime in downward two-phase flow in pipes. High void fractions mean larger injection pressures, as a consequence of lower mixture fluid density in the annulus (see Equation 1.1).

The increase in the maximum injection pressure due to lower fluid mixture densities in the annulus can also be seen in Figure 5.5, as the gas rate is increased. At a constant water flow rate,

the maximum injection pressure increases with the gas flow rate. This behavior is a consequence of the change in the hydrostatic pressure effects, which is dominant at low water flow rates.

Table 5.3. Gas and liquid superficial velocities, and void fraction and flow regimes at the injection location obtained from the simulation results for the different well tests.

Case	q_G	q_L	u_{sg}	u_{sl}	α	$p_{inj,max}$	Flow regime in the Casing Annulus
	(agpm)	(gpm)	(ft/s)	(ft/s)	(%)	(psi)	Well depth: 10ft
1		20	0.520	2.079	21	432	Annular
2		30	0.520	3.119	10	401	Slug
3	5	40	0.520	4.159	12	349	Slug
4		50	0.520	5.199	10	348	Slug
5		60	0.520	6.238	9	390	Bubbly
6		20	1.040	2.079	32	743	Annular
7		40	1.040	4.159	23	493	Slug
8	10	45	1.040	4.679	18	386	Slug
9		50	1.040	5.199	15	398	Slug
10		55	1.040	5.718	14	407	Slug
11		20	2.079	2.079	54	947	Annular
12		30	2.079	3.119	46	948	Annular
13	20	40	2.079	4.159	34	745	Slug
14		50	2.079	5.199	32	653	Slug
15		70	2.079	7.278	27	770	Slug

In Figure 5.6 the flow regime results for the simulations using OLGA® (presented in Table 5.3) are comapred to the flow regime map developed using experimental results presented in Chapter 1. As can be oserved in Figure 5.6, for similar gas and liquid superficial velocities, there are few discrepancies between some of the flow regime predictions obtained in the transient simulations and the flow regimes observed experimentally in this study (see Figure 4.5). These discrepancies in flow regimes may be one of the reasons for the errors obtained in OLGA® simulations. The misprediction of flow regime could result in the use of wrong models/parameters for predictions of pressure gradient and liquid holdup.
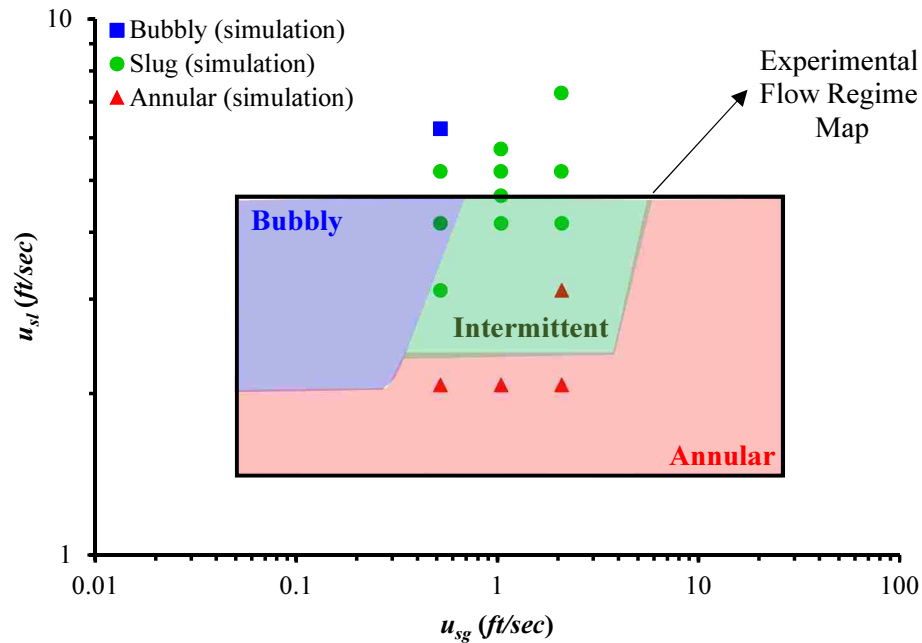
Figure 5.6. Comparison of the flow regimes obtained in OLGA® simulations (presented in Table 5.3) and the experimentally developed map for downward two-phase flow as presented in Figure 4.5).

5.5   Using Simulation Model to Select GLV for LAGL Application

The results presented in Figure 5.5 indicate that an increase in the orifice size could potentially reduce the maximum injection pressure for large water flow rates. As the simulation model was developed and validated with acceptable accuracy when compared to the well test data, this model is used to analyze the impact of larger orifice sizes on the maximum injection pressure during LAGL unloading operations. Three different orifice sizes (0.69, 1 and 2 *inch*) are evaluated, and the results are presented in Figure 5.7. The author acknowledges the fact that a 2 *inch* port size for GLVs is not viable in conventional gas-lift operations. However, this port size is simulated to evaluate how large port sizes would affect the LAGL operation. These results can be used to design new configurations for GLVs for LAGL applications.
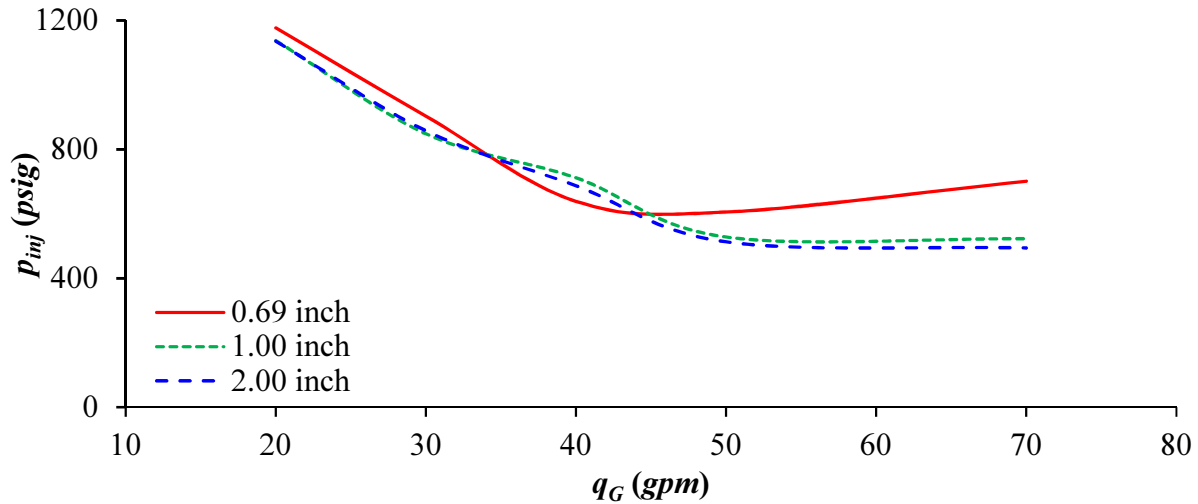
Figure 5.7. Maximum injection pressure as a function of water flow rate for gas flow rate of q_g = 20 *gpm*, and for three different orifice sizes: 0.69, 1 and 2 *inch*.

As can be seen from Figure 5.7, the maximum injection pressure is not affected for the large GLV orifice sizes for low water flow rates. These results can be explained by the predominance of hydrostatic effects for low water rates. As the water flow rate increases and the friction effects become more relevant, larger orifice sizes (1 and 2 *inch*) result in lower injection pressures. The injection pressure for the orifice sizes of 1 and 2 *inch* are approximately 20% lower than the injection pressure for the orifice size of 0.69 *inch*.

It is important to mention also that, although orifice sizes more than 1 *inch* do not promote lower injection pressures, the use of large orifice valves can alleviate erosion effects. Gas-liquid flow through small orifices create high velocities through the GLV and check valve. Large orifices will promote lower velocities, and thus, reduce erosion effects.

5.6   Simulation Results for Complete Unloading Operation

Section 5.4 previously presented the validation of a simulation model for LAGL unloading technique for both single-phase liquid and two-phase fluid (gas-liquid injection during unloading). This section now presents the validated model to simulate the complete unloading process. The simulations so far only showed the injection pressure for the gas-liquid mixture to reach the GLV

in the bottom of the well, but now simulation results showed the behavior of the injection pressure during the complete LAGL unloading process. The complete unloading operation requires the simultaneous reduction of liquid injection while the gas injection is raised to the final flow rates of gas, which provides the optimum oil production rate.

This work presents three simulation cases for the complete unloading simulations. At the beginning of the simulation, the well is full with liquid and four unloading stages are applied to remove the liquid from the well. The first simulation stage corresponds to the start of two-phase flow injection at the wellhead and the transport of injection fluids to the bottom of the well. During this stage, gas and liquid flow rates injected at the wellhead are constant.

The performance of this initial stage depends on the application of an optimum gas and liquid injection. The definition of the optimum flow rates requires the performance of experimental or simulation work similar to the one presented in Figure 5.5. This study takes in consideration the simulation results presented in Figure 5.5 to determine the initial flow rates applied to each of the three case studies. Table 5.4 shows the gas and water flow rates used in *Stage 1* for each case.

Table 5.4. Initial conditions for each complete unloading simulation case.

Complete Simulation Unloading Case	Initial q_G (agpm)	Initial q_L (gpm)
I	5	40
II	10	50
III	20	50

Stage 1 ends when injected fluids (gas and liquid) reach the bottom of the well and enters the tubing. At the beginning of *Stage 2* a small flow rate of gas is flowing in the tubing, water flow rate is kept constant and the gas flow rate is slowly increased, up to a point where the injection pressure reaches around 750 *psi* (considered the maximum available pressure for this example). When the injection pressure reaches a value between close to 750 *psi*, the gas flow rate is kept constant and stage 2 finishes. During Stage 3 the gas flow rate is kept constant and the water flow

rate is decreased. The reduction in the water flow rate is performed in small steps and the total volume of water in the well is closely monitored. As soon as the total liquid volume in the well reaches a level lower than the total tubing volume ($88\ ft^3$) the water injection is shut. At this point Stage 4 starts and single-phase gas is injected in the annulus. The single-phase injection is maintained up to the where the well is unloaded. Once the well is unloaded, the fluid injection stops and the simulations ends.

Annulus   Tubing

GLV   GLV   GLV   GLV   GLV

(a) Initial condition   (b) End of stage 1   (c) End of stage 2   (d) End of stage 3   (e) End of stage 4
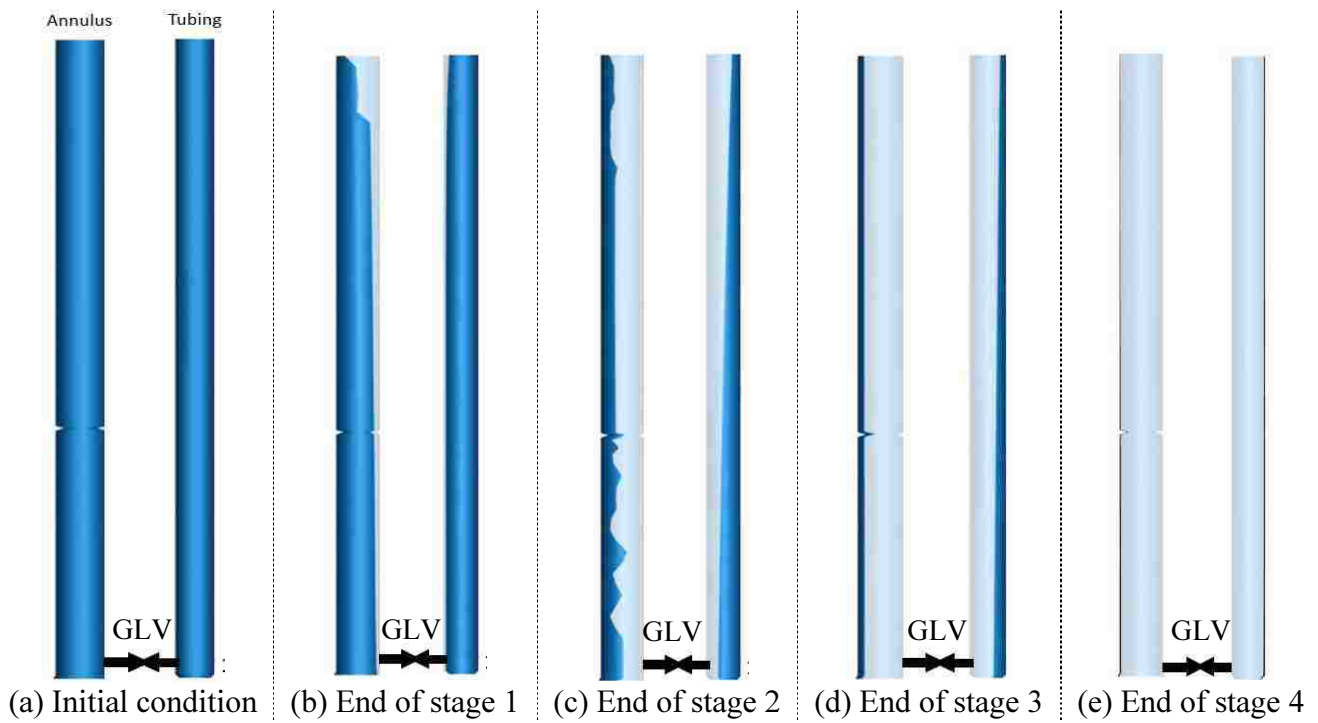
Figure 5.8. Gas/Liquid faction profile in the annulus and tubing at different simulation time.

Figure 5.8 shows an example of gas/liquid fraction profile in the well at the beginning of the process and at the end of the four unloading stages (different simulation times) for one case of complete unloading simulation. In Figure 5.8 the dark blue represents the liquid phase fraction and the light blue represents the gas phase fraction. The fractions are presented for the entire depth of the well for both the annulus (left-hand-side of each figure) and tubing (right-hand-side of each figure). Annulus and tubing are connected through a GLV that is also represented in each figure. A summary of the simulation methodology for each stage is presented:

Initial condition: At the beginning of the simulation, the well is full with liquid that has to be unloaded, and single-phase liquid is injected in the annulus. (Figure 5.8a).

Stage 1: To initiate the LAGL an optimized constant gas flow rate starts to be injected in the casing. Figure 5.8b it represents the moment that injected fluids reaches the bottom of the well and enters the tubing.

Stage 2: Once the gas reaches the bottom of the well, the gas flow rates are increased with the objective of decreasing the liquid holdup in the well. Figure 5.8(c) represents the gas/liquid fraction profile in the well at the end of this process. As can be seen in the figure, the gas fraction is now higher than at the beginning, but the liquid phase is still present in the well.

Stage 3: To reduce the liquid fraction, the liquid flow rate injected in the well is reduced in small steps. At the end of Stage 3 (Figure 5.8d), the total liquid volume in the system is smaller the total volume of the tubing.

Stage 4: At this point, the water injection is closed and single-phase gas is injected in the well. At the end of the simulation (Figure 5.8e), the well is completely unloaded. The results for three complete unloading simulations will be presented in the next section of this work.

This four stages simulation procedure is used in the three complete unloading simulation cases that are evaluated in this study and the results are presented in the next section.

5.6.1   Unloading Simulation Results

This section presents the results for the three cases of complete unloading simulations. Figure 5.9 shows the simulation results for the complete unloading case I. Figure 5.9a shows the evolution of the injection pressure with time, Figure 5.9b presents the water and gas flow rate versus time, and Figure 5.9c presents the water volume in the annulus, tubing, and total water volume in both tubing and annulus. Similar figures are created for the complete unloading cases II and III, presented in Figure 5.10 and Figure 5.11.

For the complete unloading case I, the experimental Case 3 (presented in Chapter 2) was used to initiate the simulation. The simulation result presented in Figure 5.9 has four important unloading stages, and each stage is highlighted in this figure. Prior to the initiation of stage 1 (times between 0 to 140 sec), the well is full with liquid and single-phase liquid is injected in the annulus. The beginning of LAGL unloading process (stage 1) occurs at time = 140 sec, when gas and liquid starts to be injected at a constant actual flow rate. This flow rate is kept constant between times 140 to 10,000 sec. At the end of stage 1, gas is already flowing upward in the annulus. Figure 5.9a shows that during the unloading stage 1 the injection pressure increases as the gas-liquid mixture (with lower density than the liquid previously in the annulus) reach a higher depth in the casing. When the injected gas-liquid mixture reaches the bottom of the well, and start flowing upward in the tubing, the injection pressure begging to decrease.

During stage 2 of the unloading process, the gas flow rate is increased with the objective of reducing the liquid fraction in the tubing. Therefore, the injection pressure rises in stage 2 as a consequence of increasing the gas flow rate to remove a higher amount of liquid out the tubing. The increase in the injection pressure is caused by a reduction in the density of the injected fluid and increase of the fluid flow friction in the annulus, GLV, and tubing. Once the injection pressure reaches around 650 psi, the elevation in the injection pressure is ceased, which indicates the end of the stage 3.
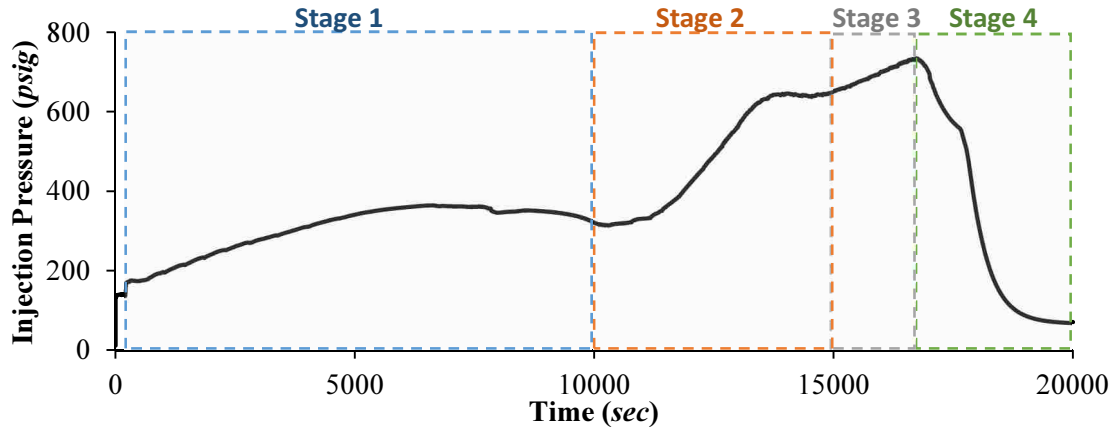
(a) Injection pressure
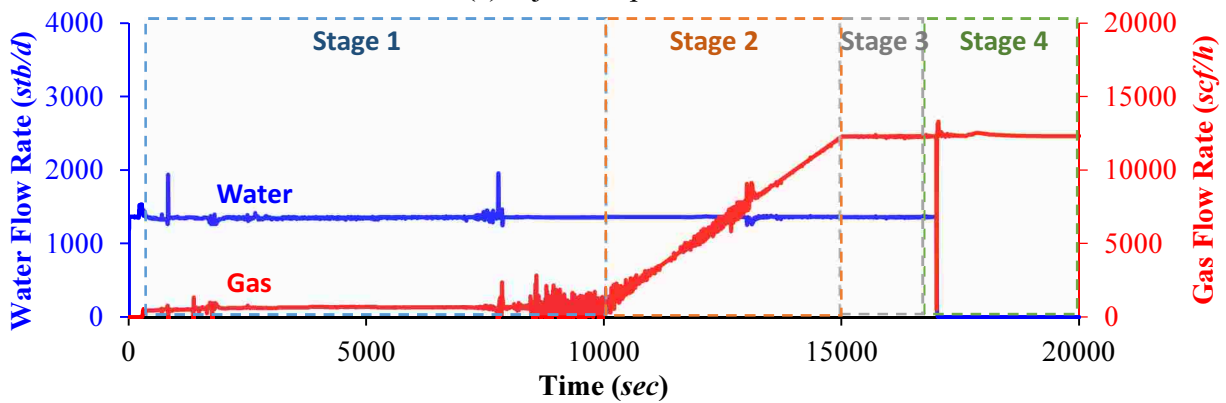
(b) Water and gas flow rates
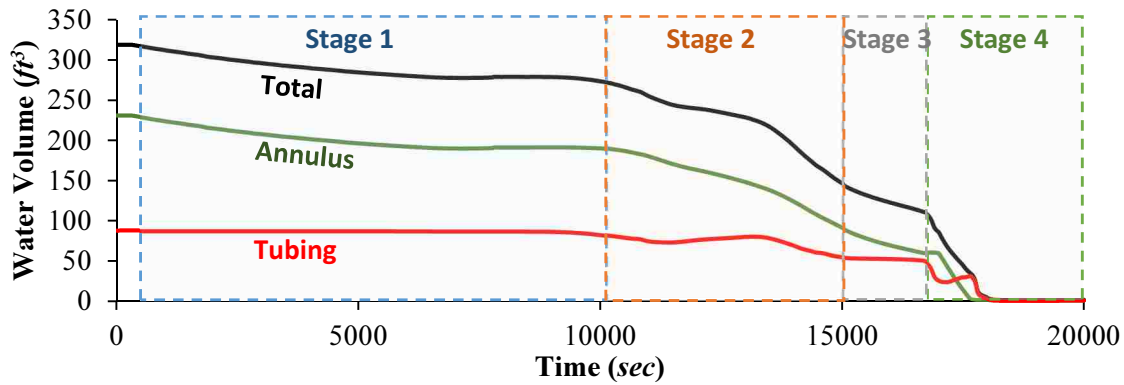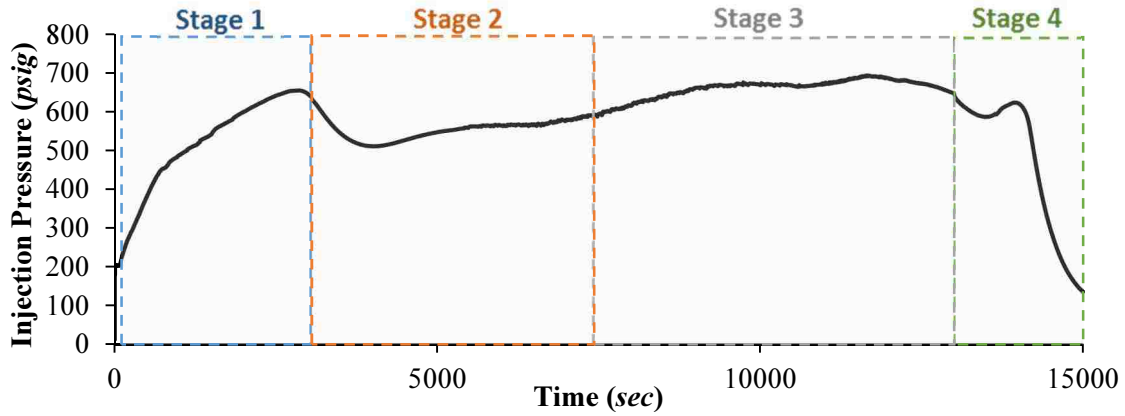

(c) Water volume in the annulus, tubing and total water volume
Figure 5.9. Complete unloading simulation (Case I).

As Figure 5.9c shows, at the end of stage 2, more than 50% of the liquid volume initially in the well has been unloaded. The objective of stage 3 is to reduce the water volume in the well to a level close to the total volume of the tubing. To achieve the objective in stage 3, the liquid flow rate is reduced and the water volume in the well is closely monitored. It is recommended to reduce

the water flow rate in small steps to avoid abrupt change in the density of the injection mixture and, consequently, abrupt increase in the injection pressure. As soon as the total water volume in the system is smaller than to total tubing volume, stage 3 ends.

At this point, the water volume in the system is considerably low and stage 4 is initiated to finalize the well unloading. At the beginning of stage 4, the water injection is interrupted, and single-phase gas is injected in the well for a period of time long enough to remove all the remaining volume of water from the well. At the end of stage 4, the well if unloaded and, as can be noticed in Figure 5.9ac, the total water volume in the system is zero.

At the end of the complete unloading case I, it is observed that the maximum injection pressure was 733 *psi*. This value can be adjusted according to the gas pressure available in the design of LAGL. It is important to remember that, for the simulation presented in this work, it is established that the available pressure on site is 750 *psi*. The 733 *psi* obtained in the simulation of complete unloading case I is around 44% lower than the gas injection pressure required to perform the gas-lift well unloading with single-point injection.

Two other complete unloading cases (II and III) are performed next following the same simulation procedure. The simulation results for cases II and III are presented in Figure 5.10 and Figure 5.11. The results for Cases II and III have the same characteristics of the result obtained in Case I.

The main result obtained in Figure 5.10 is the maximum injection pressure to unload the well. The maximum injection pressure for the Complete Unloading Simulation II was 634 *psi*, which is around 51% lower than the pressure required to unload the well applying single-point conventional gas-lift.
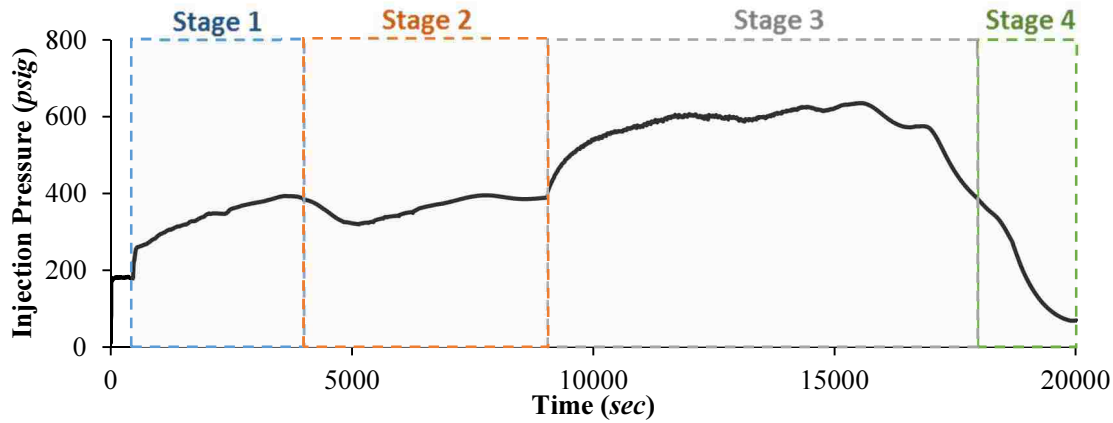
(a) Injection pressure
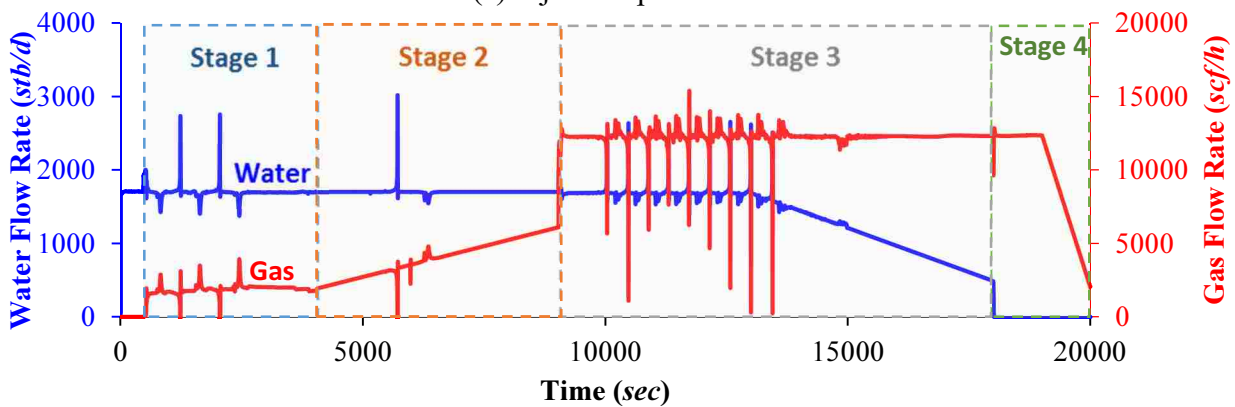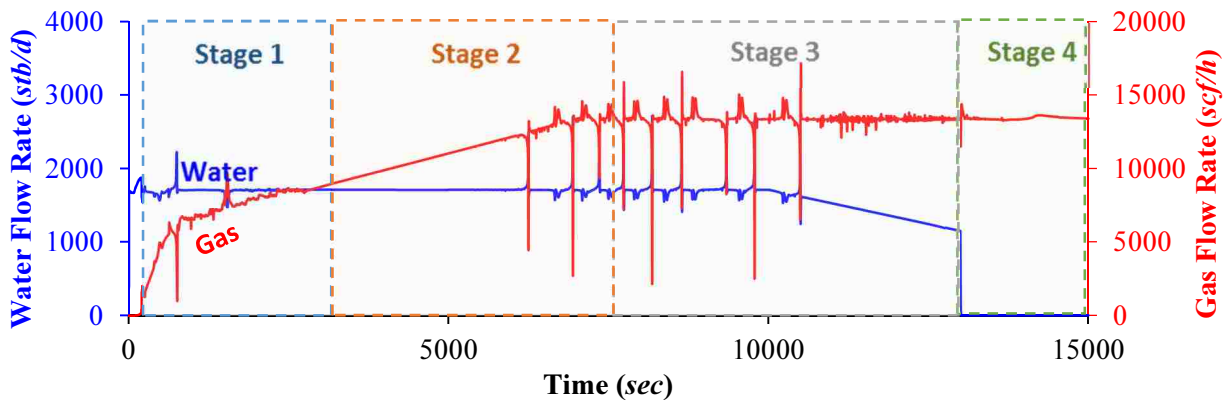

(b) Water and gas flow rates
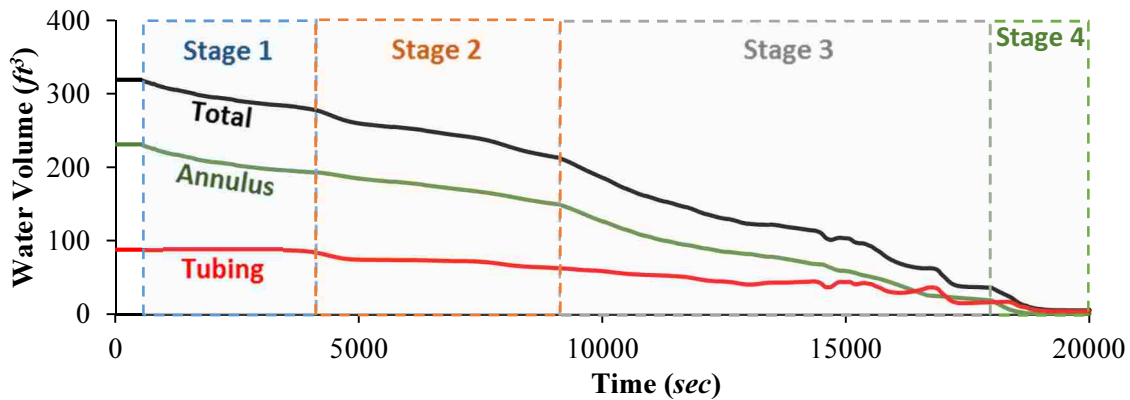
(c) Water volume in the annulus, tubing and total water volume
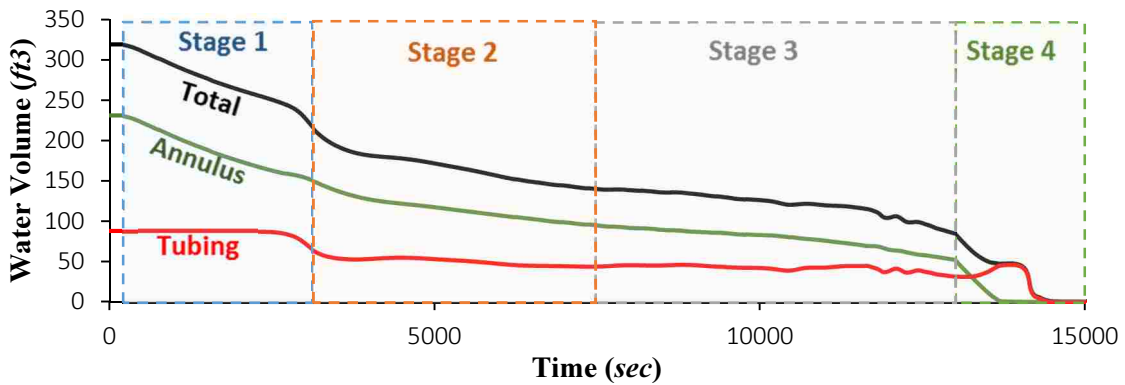Figure 5.10. Complete unloading simulation (Case II).

The same data analyses used for Complete Unloading Simulation I and II can be used for Case II, which simulation data results are presented in Figure 5.11. The maximum injection pressure to unload the well in Case III was around 693 *psi*, and it represents 56% reduction in the required injection pressure when compared to single-point gas-lift.

(a) Injection pressure

(b) Water and gas flow rates

(c) Water volume in the annulus, tubing and total water volume
Figure 5.11. Complete unloading simulation (Case III).

The complete unloading simulations results showed that the simulation procedure proposed in this work is able to successful unload the well evaluated in this work. Future work should consider to couple reservoir with different characteristics in the wellbore model. Coupling the reservoir in the simulation model will help to understand the effect of reservoir fluid in the LAGL.

5.7   Conclusions

The results for single-phase water shows that, once C_D is calibrated, the model is capable of simulating the field scale experiments with high accuracy. The difference between experimental and numerical results are smaller than 5%.

A model using the commercial software OLGA® was also built and validated with field scale experimental data. The average error for most of the cases is lower than 15%. Out of 15 cases, only two cases showed average error higher than 15%. These average errors are considered acceptable in this study, particularly if taking into account the lack of experimental and numerical studies in the literature about the characterization of downward two-phase flow in vertical annulus and errors related to two-phase flow through the office valve, as it is previously discussed in Chapter 3. The behavior of two-phase upward flow in small-diameter pipes (up to 4 *inch* ID) has been extensively studied in the literature, and it is expected the simulations errors to be negligible to this component of the LAGL system .

After the model validation, the model is used evaluate the effect of different components of the gas-lift system on the efficiency of the LAGL concept. From the simulation results, it is possible to conclude that the use of gas-lift valves with large orifice sizes (larger than 0.69 *inch*) reduces the maximum injection pressure by 18% for larger water flow rates. For low water rates, the effect of the orifices sizes is negligible.

The complete unloading simulation results indicated that the use of LAGL has potential to decrease the injection pressure requirement in more than 50% when compared to the conventional single-point gas injection.

6 A Basic Economic Analysis for LAGL Unloading

This chapter presents a basic economic evaluation of LAGL unloading. This economic evaluation compares the application of LAGL unloading, single-point gas-lift unloading and multipoint gas-lift unloading. The analysis takes into consideration the Capital Expenditure (CAPEX) and Operating Expenses (OPEX) for field deployment of all three techniques. Two case studies are presented, one for test well used in this work and one for an offshore field in India (selected due to the availability of information about CAPEX and OPEX for this particular field).

6.1 Capital Expenditure (CAPEX)

Capital expenditures is the sum of costs to purchase major physical goods or services that will be used for more than one year. For example, a company might have capital expenditures to increase its fixed assets or improve its fixed assets. Fixed assets are treated as noncurrent assets from an accounting standpoint, meaning they won't be consumed up in the first year (Investopedia, 2018).

In the case of gas-lift installations, this work consider as CAPEX the cost for acquisition of major equipment like gas compressors and liquid pumps. The cost for installation, instrumentation and flow lines are not considered because of their minor contribution in the cost difference among the unloading techniques in comparison with costs to acquire compressors and pumps.

6.1.1 CAPEX – Gas Compressor

To calculate the acquisition cost for the gas compressor it is first necessary to calculate the horsepower (HP) required for the compressor. Equation 6.1 is used to calculate the theoretical horsepower requirement for an adiabatic compression cycle (Hodge, 1985). The acquisition price for gas compressors is estimated at US$750/HP for onshore applications and US$1,800/HP for offshore applications.

$$HP = \frac{\frac{144 N p_1 q_G k}{33000(k-1)}\left(\frac{p_2}{p_1}^{\frac{k-1}{Nk}} - 1\right)}{\varepsilon} \qquad\qquad 6.1$$

where N is the number of compression stages, k is the adiabatic expansion coefficient, p_1 is the absolute inlet atmospheric pressure (*psi*), p_2 is the absolute final pressure after compression (*psi*), q_G is the flow rate of compressed gas at atmospheric pressure (ft^3/min) and ε is the efficiency.

6.1.2 CAPEX – Liquid Pump

Hydraulic horsepower required for the liquid pump used in the LAGL system is obtained using Equation 6.2 (Fox *et al.*, 2004). The market value for liquid pumps is estimated at US\$250/HP. The efficiency (ε) of the system (motor and pump) is assumed to be 0.85.

$$HP = \frac{\Delta p q_L \gamma_L}{1714\varepsilon} \qquad\qquad 6.2$$

where Δp is the pressure increase in the pump (*psi*) and q_L is the flow rate of liquid (*gpm*), γ_L is the liquid specific gravity.

6.2 Operating Expenses (OPEX)

Operating expenses are the total costs for running the system. For this work, it is the cost for running gas-lift unloading operations on a daily basis. Example of costs included in the OPEX are: energy consumption, system repair, rental equipment, utilities, and salaries. As operational expenses make up the bulk of a company's regular costs, management typically looks for ways to reduce operating expenses without causing a critical drop in quality or production output. In contrast to capital expenditures, operating expenses are fully tax-deductible in the year they are made (Investopedia, 2018).

For the economic evaluation that will be presented in this work, the OPEX is considered as the energy consumption for running the gas compressor and liquid pump during gas-lift unloading

operations, and also the cost related to well workovers that is generally necessary when multipoint gas lift unloading is applied, for instance, to replace malfunctioning gas-lift valves.

The electricity costs that included are in the OPEX calculation are based on US$0.1262/$kWh$. This cost value was published by the U.S. Energy Information Administration (EIA, 2018) for February 2018. The electricity expenses for an unloading operation are calculated using Equation 6.3.

$$Cost_{elec} = \frac{HP}{0.746} t \qquad\qquad 6.3$$

where t is the total time of unloading operations in *hours*.

The costs related to well workovers is discussed in each case study.

6.3   Case Studies

Two case studies are presented in this chapter. The first case study shows an economic analysis comparing the application of LAGL and single-point gas-lift unloading to a shallow vertical well. In this comparison both techniques will use the configuration of the LSU PERTT lab test well. For the second case study, an economic analysis compares the application of LAGL and multipoint gas-lift unloading in a field located in Western offshore of India. The selection of this field is based on the availability of the costs related to unloading operations for this field, described in the study of Kumar and Gupta (2003) for the period of 5 years (from 1994 to 1999).

6.3.1   Case Study 1 – LSU PERTT Lab

The geometry of the LSU PERTT Lab test well has been previously discussed in this work. This well has a vertical depth of approximately 2,800 *ft* and a gas-lift valve installed at the bottom of the well. This configuration allows for a comparison between single-point gas-lift unloading and the LAGL unloading method. For this case study, the well is initially full with water, and the unloading of the well is accomplished when all the water is completely removed from the wellbore.

According to the results for LAGL unloading presented in Chapter 5 (Figure 5.11), an injection pressure of 600 *psi* is required for the complete well unloading using the LAGL method. In addition to that, a liquid flow rate of 35 *gpm* and a gas injection rate of 0.15 *MMscfd* is also needed. The suction pressure for the compressor is assumed at 50 *psi*, as it is usual in the industry. Based on this information and using Equations 6.1 and 6.2, the horsepower requirements for both compressor and pump, and the CAPEX for the LAGL unloading is presented in Table 6.1.

Table 6.1. Horsepower, CAPEX and OPEX for LAGL and single point gas lift.

	LAGL	**Single-point gas-lift**	**Savings between Single point and LAGL**	**Savings (%)**
Compressor HP (1 well)	26	37	-	-
Pump HP (1 well)	10	-	-	-
CAPEX (1 well)	$22,439	$28,113	$5,674	20%
OPEX (1 *year*)	$593	$809	$216	27%
OPEX (15 *years*)	$8,902	$12,135	$3,233	27%
Total (15 *years*, 1 well)	$31,341	$40,248	$8,907	22%
Total (15 *years*, 200 wells)	$6.2MM	$8MM	$1.8MM	23%

Table 6.1 also presents the horsepower required for the compressor to perform the well unloading using the single-point gas-lift technology. It is important to remember that, for the case of single-point gas lift, the required injection pressure to initiate the well unloading is 1246 *psi*. The flow rate for the injected gas during the unloading is 0.15 *MMscfd*. Table 6.1 shows that the CAPEX for the LAGL unloading is around US$22,000 and for the single-point gas-lift unloading, the CAPEX is around US$28,000. It indicates cost savings of approximately 20% in the CAPEX when the LAGL technology is chosen to perform the unloading of the well.

For the OPEX calculation it is necessary to estimate how many times per year it would necessary to unload the well. According to information obtained from gas-lift operators, it is reasonable to perform in average five unloading operations per well in a year. Considering that the unloading operation is performed in 24 *hours*, the OPEX for LAGL and single point gas-lift are also presented in Table 6.1.

The results for OPEX presented in Table 6.1 show that, the use of LAGL would result in savings on the order of 27% when compared to single-point gas-lift. In a period of 15 years, this saving would be around US$3,200 per well. Considering the application of CAPEX and OPEX for a period of 15 years, using LAGL would result in savings on the order of US$ 9,000 per well. The US$ 9,000 per well may seems low at a first, however, in a field with 200 gas-lifted assisted wells, the saving would be in the order of US$1,8MM.

6.3.2   Case Study 2 – Mumbai High Field

The Mumbai High Field is located in western offshore of India. Kumar and Gupta (2003) presented a comparative evaluation of single and multipoint gas-lift system for the Mumbai High offshore field. To access the well servicing cost in multipoint gas-lit, Kumar and Gupta (2003) presented a detailed economic evaluation for a five years period (from 1994 to 1999). In this economic evaluation the authors presented the costs related to every minor (wire-line job) and major (work over job) well service for replacement of faulty GLVs in the five years period.

For the period of 1994-95, more than 100 wells were operating with multipoint gas-lift systems. By the end of the study (1998-99), 381 wells were operational. According to the authors, between four and six gas-lift mandrels were used in each well, and an injection pressure from 1,000 to 1,350 *psi* is necessary to perform the well unloading. A gas flow rate of 0.15 *MMscfd* is required during the unloading operations. Based on this information for multipoint gas-lift unloading and using Equations 6.1 to 6.3, the horsepower requirements for the gas compressor, and its CAPEX are calculated, and presented in Table 6.2.

Table 6.2 also presents results for the application LAGL unloading. The gas flow rate for the LAGL is 0.15 *MMscfd*, and the liquid flow rate for LAGL is 25 *gpm*. The optimum injection pressure and liquid flow rate for the LAGL were obtained using an optimization routine in an Excel® spreadsheet. The optimization routine uses a steady-state two-phase flow model developed

by Beggs and Brill (1973) for two-phase flow in the tubing and annulus, the model developed by Sachdeva *et al.* (1986) for two-phase flow through gas-lift valve. The results presented in Table 6.2 shows that the LAGL presents CAPEX 11% lower than for multipoint injection.

Table 6.2. Horsepower and CAPEX per well for multipoint gas-lift and LAGL.

	LAGL	Multipoint gas-lift	Savings between Multipoint and LAGL	Savings (%)
Compressor HP (1 well)	29	37	-	-
Pump HP (1 well)	12	-	-	-
CAPEX (1 well)	$58,396	$65,735	$7,339	11%
OPEX (1 *year*)	$652	$21,515	$20,863	97%
OPEX (15 *years*)	$9,790	$322,737	$312,947	97%
Total (15 *years*, 1 well)	$68,187	$388,472	$320,285	82%
Total (15 *years*, 200 wells)	$26MM	$148MM	$122MM	82%

For the OPEX calculation it is considered that five unloading operations are performed per well every year, and each unloading operation lasts, on average, 24 *hours*. For multipoint gas-lift, the service cost to replace faulty GLVs is added in the OPEX. The study presented by Kumar and Gupta (2003) showed that the average service cost for a well operating with multipoint gas-lift in the Mumbai High field is US$20,727/year (value updated for the inflation rate of India from 2003 to 2017). Based on this information and using Equation 6.3, the OPEX for the two techniques evaluated are presented in Table 6.2.The OPEX results presented in Table 6.2 show that the LAGL can allow savings on OPEX of approximately 97%, when compared to multipoint gas-lift. This difference is a consequence of the well servicing cost in the OPEX for the multipoint injection, which is not needed when using the LAGL technique. The servicing costs are not relevant for LAGL because its system has only a single operating GLV at the bottom of the well, and the well servicing cost is related to replacement of faulty unloading GLVs.

Considering the CAPEX and OPEX for a period of 15 years, the use of LAGL would result in savings in the order of US$320,000 when compared to multipoint gas-lift. Considering the 381

wells that were operational in the High Mumbai field, the savings when using LAGL would be in the order of US$122MM when compared to multipoint injection.

It is important to mention that some important factors are not considered in this economic analysis. Some of these costs that are not considered are: flow lines, instrumentation (pressure and temperature transmitter, flow meters), control system, separation system and servicing surface equipment. These costs are relevant in both multipoint gas-lift and LAGL systems, and it is believed that it inclusion of such costs would not result in major changes in the initial economic analysis.

7 Conclusions and Future Work

7.1 Conclusions

- This work proposes a new technique, named Liquid Assisted Gas-Lift (LAGL), to perform well unloading. The LAGL unloading is based on the concept of injecting a fluid (two-phase fluid) with higher density in the annulus to reduce the maximum injection pressure required to perform gas-lift unloading. The proposed technique was validated in a field-scale test well (approximately 2800 ft deep), and it was able to reduce the maximum injection pressure in more than 75% when compared to single-point gas-lift unloading.

- For a complete understanding of LAGL system, two-phase flow though GLVs was experimentally and numerically investigated. The analysis of two-phase flow through GLVs showed that some mechanistic models existent in the literature were able to predict experimental results for both critical and sub-critical flow behavior with high accuracy (average errors lower than 10%). However, the discharge coefficient has to be experimentally tuned for each model every time a new GLV is used.

- Experimental investigation of two-phase downward flow through annulus was also carried out in this work. Three flow regimes were observed in downward two-phase flow in annulus: annular, intermittent and bubbly flow. Bubbly and annular flow regimes occur for superficial liquid and gas velocities similar to the ones observed by other authors for downward flow in circular pipes. However, there is evident differences for the intermittent flow regime, which is observed for flow in circular pipes for lower superficial liquid velocities than in annulus. This difference may create substantial errors if one uses flow regime transition models developed for downward flow in pipes to predict flow regimes in annulus configurations.

- The transient simulation model developed using a commercial flow simulator was validated with field-scale experiments and presented errors lower than 15% for 13 of the 15 study cases. The simulation model is shown to be a powerful tool to perform system analysis and optimization of LAGL. The simulation model can also be used to define application procedures for future field trials using LAGL.

- In some cases, as presented in Chapter 2, multipoint gas-lift unloading can present better economics, in terms of energy consumption, than LAGL unloading. However, the use of LAGL is an alternative to perform well unloading not only based on economic aspects, but also is cases where multipoint unloading is not indicated due to technical restrictions.

- The case studies presented in the economic analysis showed that the use of LAGL unloading would reduce capital and operational expenses when compared to both single and multipoint gas-lift unloading. For the case study comparing LAGL to single-point gas-lift, it was shown that the LAGL would result in savings in the order of 25%. For the multipoint injection, the saving are approximately 80% when using the LAGL technique.

7.2 Suggestions for Future Work

- Field trials of LAGL unloading are recommended to demonstrate the applicability of the technique. It is initially recommended to perform the field trial in an on-shore vertical well that is operated using conventional single-phase gas-lift.

- Perform further experimental investigations of downward two-phase flow in annulus for different geometries (hydraulic diameter, and inner/outer diameter ratio) and configurations (inclined annulus and eccentric pipe). It is also recommended to develop numerical model to predict flow regime transitions, liquid holdup and pressure gradient for the different flow regimes.

- Evaluate the applicability of Computational Fluid Dynamics (CFD) models for the characterization of two-phase flow in orifice GLVs. The use of CFD would be a beneficial alternative to determine the discharge flow coefficient for GLVs and it would also be a useful tool for the design of new GLVs to be applied in LAGL.

- Evaluate the applicability of LAGL in horizontal wells. To perform this evaluation further experimental work in two-phase flow in horizontal annulus is suggested to validate the use of commercial flow simulators.

- Development of a simplified transient flow model that could be applied in LAGL unloading process. This model would be an alternative to the use of commercial flow simulators, which are not available for many industry operators and are not flexible. For example, it is not possible to implement the flow regime map developed in this work in OLGA®, but it would be possible to implement in an open-source simplified transient flow simulator for LAGL.

- The addition of surfactant and/or friction reducers in the injection fluid (gas-liquid mixture) may increase the efficiency of LAGL. It is recommended to evaluate the effect of addition of surfactant in the LAGL application.

References

Achong, I. (1961). Revised Bean Performance Formula for Lake Maracaibo Wells. Retrieved from

Al-Attar, H. (2010). New Correlations for Critical and Subcritical Two-Phase Flow Through Surface Chokes in High-Rate Oil Wells. doi:10.2118/120788-PA

Almabrok, A. A., Aliyu, A. M., Lao, L., & Yeung, H. (2016). Gas/liquid flow behaviours in a downward section of large diameter vertical serpentine pipes. International Journal of Multiphase Flow, 78, 25-43. doi:http://dx.doi.org/10.1016/j.ijmultiphaseflow.2015.09.012

Ashford, F. E. (1974). An Evaluation of Critical Multiphase Flow Performance Through Wellhead Chokes. doi:10.2118/4541-PA

Ashford, F. E., & Pierce, P. E. (1975). Determining Multiphase Pressure Drops and Flow Capacities in Down-Hole Safety Valves. doi:10.2118/5161-PA

Barnea, D., Shoham, O., & Taitel, Y. (1982a). Flow pattern transition for downward inclined two phase flow; horizontal to vertical. Chemical Engineering Science, 37(5), 735-740. doi:http://dx.doi.org/10.1016/0009-2509(82)85033-1

Barnea, D., Shoham, O., & Taitel, Y. (1982b). Flow pattern transition for vertical downward two phase flow. Chemical Engineering Science, 37(5), 741-744. doi:http://dx.doi.org/10.1016/0009-2509(82)85034-3

Baxendell, P. B. (1957). Bean Performance-Lake Wells. Retrieved from

Beggs, D. H., & Brill, J. P. (1973). A Study of Two-Phase Flow in Inclined Pipes. doi:10.2118/4007-PA

Bhagwat, S. M., & Ghajar, A. J. (2012). Similarities and differences in the flow patterns and void fraction in vertical upward and downward two phase flow. Experimental Thermal and Fluid Science, 39, 213-227. doi:http://dx.doi.org/10.1016/j.expthermflusci.2012.01.026

Brill, J. P., & Beggs, H. D. (1991). Two-phase Flow in Pipes: Univ.

Brill, J. P., & Mukherjee, H. K. (1999). Multiphase Flow in Wells: Henry L. Doherty Memorial Fund of AIME, Society of Petroleum Engineers.

Caetano, E. F., Shoham, O., & Brill, J. P. (1992). Upward Vertical Two-Phase Flow Through an Annulus—Part I: Single-Phase Friction Factor, Taylor Bubble Rise Velocity, and Flow Pattern Prediction. Journal of Energy Resources Technology, 114(1), 1-13. doi:10.1115/1.2905917

Candido, S. F. (1989). Offshore Production Systems in Deep Waters: Artificial Lift Methods and Flow Lines Design. (Master), Campinas State University (UNICAMP), Campinas, Brazil. (vtls000035394)

Capucci, E. C., & Serra, K. V. (1991). Transient Aspects of Unloading Oil Wells Through Gas-Lift Valves.

Chisholm, D. (1983). Two-phase flow in pipelines and heat exchangers: London ; New York : G. Godwin in association with Institution of Chemical Engineers, 1983.

Coutinho, R. P., Williams, W., Waltrich, P., Mehdizadeh, P., & Scott, S. (2017). A model for liquid-assisted gas-lift unloading. Paper presented at the 18th International Conference on Multiphase Production Technology, Cannes, France.

Coutinho, R. P., Williams, W. C., Waltrich, P. J., Mehdizadeh, P., Scott, S., Xu, J., & Mabry, W. (2018). The Case for Liquid-Assisted Gas-Lift Unloading. Submitted to SPE Journal Of Production and Operations, 33(1). doi:https://doi.org/10.2118/187943-PA

Decker, K. L. (1993). Gas-Lift Valve Performance Testing.

Decker, K. L. (2007). IPO Gas Lift Design Using Valve Performance.

Economides, M. J. (2013). Petroleum production systems. [electronic resource]: Upper Saddle River, NJ : Prentice Hall, c2013. 2nd ed.

EIA, U. E. I. A. (2018, 4/26/2018). Eletricity. Retrieved from https://www.eia.gov/electricity/

Elmer, D., Elmer, W., & Harms, L. (2017). High Pressure Gas-Lift: Is Industry Missing a Potentially Huge Application to Horizontal Wells? Paper presented at the SPE Annual Technical Conference and Exhibition, San Antonio, Texas, USA.

Faustinelli, J. G., & Doty, D. R. (2001). Dynamic Flow Performance Modeling of a Gas-Lift Valve.

Fortunati, F. (1972). Two-Phase Flow through Wellhead Chokes.

Fox, R. W., McDonald, A. T., & Pritchard, P. J. (2004). Introduction to fluid mechanics: New York : Wiley, c2004. 6th ed.

Gilbert, W. E. (1954). Flowing and Gas-lift well Performance.

Green, D. W., & Perry, R. H. (2007). Perry's Chemical Engineers' Handbook (8th Edition). Blacklick, USA, UNITED STATES: McGraw-Hill Professional Publishing.

Guzov, A. J., & Medviediev, V. F. (1962). Critical flow of two phase fluid through wellhead chokes. Oil Economy - Moscow, 11.

Halim, A. H., & Samad, J. A. A. (2016). Gaslift Compressor Initial Start-Up Outside of the Design Envelope.

Hall, J. W., & Decker, K. L. (1995). Gas-Lift Unloading and Operating Simulation as Applied to Mandrel Spacing and Valve Design.

Hasan, A. R. (1995). Void Fraction in Bubbly and Slug Flow in Downward Two-Phase Flow in Vertical and Inclined Wellbores. SPE Production & Facilities, 10(03), 5. doi:10.2118/26522-PA

Hepguler, G., Schmidt, Z., Blais, R. N., & Doty, D. R. (1993). Dynamic Model of Gas-Lift Valve Performance. doi:10.2118/21637-PA

Hernandez, A., Gonzalez, L., & Gonzalez, P. (2002). Experimental Research on Downward Two-Phase Flow. Paper presented at the SPE Annual Technical Conference and Exhibition, San Antonio, Texas.

Hodge, B. K. (1985). Analysis and design of energy systems: Englewood Cliffs, N.J. : Prentice-Hall, c1985.

Investopedia. (2018). What Is The Difference Between CAPEX And OPEX? Retrieved from https://www.investopedia.com/ask/answers/020915/what-difference-between-capex-and-opex.asp

Kumar, A., & Gupta, V. P. (2003). Comparative Evaluation of Single vs. Multi-Mandrel Gas Lift System for an India Offshore Field. Paper presented at the SPE Asia Pacific Oil and Gas Conference and Exhibition, Jakarta, Indonesia.

Laing, C. M. (1989). Gas-Lift Design and Production Optimization Offshore Trinidad. doi:10.2118/15428-PA

Laing, C. M. (1991). Gas-Lift Design and Performance Analysis in the North West Hutton Field. doi:10.2118/19280-PA

Neely, A. B., Montgomery, J. W., & Vogel, J. V. (1974). A Field Test and Analytical Study of Intermittent Gas Lift. doi:10.2118/4538-PA

OLGA. (2015). OLGA Dynamic Multiphase Flow Simulator: Schlumberger.

PIPESIM. (2015). PIPESIM Steady-State Multiphase Flow Simulator: Schlumberger.

Pittman, R. W. (1982). Gas Lift Design and Performance. Paper presented at the International Petroleum Exhibition and Technical Symposium, Beijin, China.

Ros, N. C. J. (1959). Theoretical Approach to the Study of Critical Gas-Liquid Flow Through Beans. Retrieved from Internal Report:

Sachdeva, R., Schmidt, Z., Brill, J. P., & Blais, R. M. (1986). Two-Phase Flow Through Chokes.

Selmer-Olsen, S., Holm, H., Haugen, K., Nilsen, P. J., & Sandberg, R. (1995). Subsea Chokes as Multiphase Flowmeters. Paper presented at the International Confonference on Multiphase Production, Cannes, France.

Steele, R. D. (1976). Application and Economics of Artificial Lift in the Judy Creek Field, Alberta.

Surbey, D. W., Kelkar, B. G., & Brill, J. P. (1989). Study of Multiphase Critical Flow Through Wellhead Chokes. SPE Production Engineering, 4(02), 5. doi:10.2118/15140-PA

Taitel, Y., Bornea, D., & Dukler, A. E. (1980). Modelling flow pattern transitions for steady upward gas-liquid flow in vertical tubes. AIChE Journal, 26(3), 345-354. doi:10.1002/aic.690260304

Takács, G. (2005). Gas Lift Manual. Tulsa, Oklahoma: PennWell.

Tang, Y., Schmidt, Z., Blais, R. N., & Doty, D. R. (1999). Transient Dynamic Characteristics of the Gas-Lift Unloading Process. SPE Journal, 4(03), 13. doi:10.2118/57659-PA

Tangren, R. F., Dodge, C. H., & Seifert, H. S. (1949). Compressibility Effects in Two-Phase Flow. Journal of Applied Physics, 20(7), 637-645. doi:10.1063/1.1698449

Turner, R. G., Hubbard, M. G., & Dukler, A. E. (1969). Analysis and Prediction of Minimum Flow Rate for the Continuous Removal of Liquids from Gas Wells. Journal of Petroleum Technology, 21(11), 1,475 - 471,482. doi:10.2118/2198-PA

Usui, K. (1989). Vertically Downward Two-Phase Flow, (II). Journal of Nuclear Science and Technology, 26(11), 1013-1022. doi:10.1080/18811248.1989.9734422

Usui, K., & Sato, K. (1989). Vertically Downward Two-Phase Flow, (I). Journal of Nuclear Science and Technology, 26(7), 670-680. doi:10.1080/18811248.1989.9734366

Winkler, H. W., & Camp, G. F. (1987). Dynamic Performance Testing of Single-Element Unbalanced Gas-Lift Valves. doi:10.2118/14348-PA

Xu, Z., Richard, B. M., & Kritzler, J. H. (2013). Smart Gas Lift Valves Enhance Operation Efficiency of Offshore Wells. Paper presented at the SPE Annual Technical Conference and Exhibition, New Orleans, Louisiana.

Appendix A: Pressure Data for Downward Two-Phase Flow Experiments

q_L	q_G	PT1 Aver.	PT1 Std. Dev.	PT2 Aver.	PT2 Std. Dev.	PT3 Aver.	PT3 Std. Dev.	PT4 Aver.	PT4 Std. Dev.	Flow Regime
ft3/s	ft3/s	psi	-	psi	-	psi	-	psi	-	
0.07	0.01	-0.20	0.08	-0.10	0.06	-0.10	0.06	-0.03	0.08	Annular
0.06	0.01	-0.19	0.08	-0.09	0.05	-0.09	0.07	-0.03	0.07	Annular
0.07	0.01	-0.18	0.09	-0.11	0.06	-0.06	0.07	-0.02	0.09	Annular
0.07	0.03	-0.16	0.09	-0.12	0.05	-0.08	0.06	-0.01	0.06	Annular
0.07	0.03	-0.02	0.12	0.06	0.08	0.09	0.08	0.10	0.10	Annular
0.07	0.03	-0.15	0.09	-0.07	0.05	-0.05	0.07	0.00	0.09	Annular
0.08	0.04	-0.03	0.11	0.05	0.07	0.13	0.06	0.16	0.07	Annular
0.07	0.07	-0.16	0.09	-0.12	0.05	-0.08	0.06	-0.01	0.06	Annular
0.07	0.13	0.23	0.12	0.25	0.09	0.27	0.10	0.28	0.11	Annular
0.06	0.23	0.35	0.13	0.31	0.09	0.26	0.08	0.32	0.09	Annular
0.07	0.54	0.70	0.18	0.65	0.14	0.66	0.14	0.63	0.15	Annular
0.06	0.79	0.99	0.17	0.91	0.13	0.92	0.14	0.90	0.14	Annular
0.07	0.90	1.25	0.18	1.18	0.19	1.16	0.18	1.12	0.18	Annular
2.09	0.00	-6.48	0.10	-4.61	0.06	-1.98	0.06	-0.24	0.08	Bubbly
2.24	0.01	-6.27	0.10	-4.41	0.06	-1.88	0.07	-0.22	0.06	Bubbly
2.23	0.01	-6.16	0.08	-4.37	0.06	-1.86	0.06	-0.22	0.08	Bubbly
2.20	0.01	-5.99	0.09	-4.21	0.05	-1.78	0.07	-0.19	0.08	Bubbly
2.05	0.01	-0.27	0.13	-0.21	0.09	-0.09	0.09	-0.11	0.10	Annular
2.14	0.03	-0.36	0.14	-0.27	0.09	-0.13	0.10	-0.11	0.11	Annular
2.16	0.04	-0.30	0.13	-0.20	0.08	-0.04	0.08	-0.05	0.09	Annular
2.13	0.07	-0.26	0.11	-0.19	0.06	-0.04	0.07	-0.02	0.09	Annular
2.25	0.09	-0.23	0.10	-0.11	0.05	0.00	0.07	0.01	0.10	Annular
2.09	0.14	-0.05	0.12	0.04	0.05	0.09	0.07	0.03	0.08	Annular
2.33	0.21	0.06	0.14	0.07	0.06	0.10	0.06	0.09	0.08	Annular
2.15	0.33	0.13	0.12	0.11	0.07	0.15	0.06	0.10	0.08	Annular
2.21	0.46	0.22	0.12	0.15	0.08	0.22	0.08	0.16	0.10	Annular
2.16	0.59	0.33	0.15	0.30	0.07	0.29	0.08	0.23	0.09	Annular
2.23	0.68	0.45	0.13	0.40	0.08	0.41	0.09	0.30	0.09	Annular
2.20	0.77	0.56	0.13	0.47	0.10	0.46	0.10	0.35	0.13	Annular
2.66	0.00	-6.39	0.08	-4.51	0.05	-1.97	0.09	-0.16	0.07	Bubbly
2.61	0.01	-6.28	0.09	-4.34	0.06	-1.85	0.08	-0.14	0.09	Bubbly
2.68	0.01	-6.00	0.08	-4.17	0.11	-1.70	0.16	-0.09	0.13	Bubbly
2.73	0.01	-5.83	0.09	-4.05	0.09	-1.66	0.11	-0.06	0.11	Bubbly
2.76	0.01	-5.45	0.11	-3.74	0.06	-1.49	0.08	0.03	0.09	Bubbly
2.73	0.04	-0.23	0.13	-0.05	0.09	0.19	0.11	0.31	0.11	Intermittent
2.74	0.06	-0.11	0.13	0.10	0.08	0.29	0.10	0.39	0.11	Intermittent
2.80	0.08	0.28	0.15	0.41	0.10	0.54	0.11	0.61	0.12	Intermittent
2.73	0.10	0.80	0.18	0.80	0.12	0.85	0.13	0.88	0.13	Intermittent
2.79	0.18	0.43	0.15	0.52	0.10	0.62	0.11	0.66	0.10	Annular
2.75	0.20	0.55	0.14	0.60	0.10	0.67	0.11	0.69	0.13	Annular
2.71	0.30	0.84	0.18	0.84	0.11	0.89	0.13	0.86	0.14	Annular
2.84	0.34	1.06	0.19	1.02	0.14	1.06	0.14	1.07	0.15	Annular
2.70	0.45	1.18	0.20	1.12	0.11	1.16	0.10	1.16	0.13	Annular
2.68	0.63	1.83	0.17	1.79	0.16	1.78	0.15	1.74	0.14	Annular
2.63	0.79	2.54	0.23	2.43	0.24	2.31	0.22	2.25	0.20	Annular
2.84	0.00	-6.51	0.09	-4.64	0.05	-1.99	0.06	-0.22	0.10	Bubbly
2.70	0.01	-6.39	0.09	-4.46	0.05	-1.86	0.06	-0.20	0.10	Bubbly
2.72	0.01	-6.25	0.09	-4.33	0.05	-1.88	0.07	-0.18	0.08	Bubbly

2.69	0.01	-6.00	0.08	-4.18	0.05	-1.81	0.08	-0.19	0.08	Bubbly
2.79	0.01	-5.52	0.10	-3.73	0.04	-1.68	0.10	-0.16	0.07	Bubbly
2.81	0.01	-5.66	0.08	-3.89	0.05	-1.78	0.08	-0.17	0.10	Bubbly
2.90	0.03	-2.74	0.12	-2.61	0.08	-1.35	0.16	-0.12	0.11	Intermittent
2.72	0.04	-0.69	0.14	-0.51	0.09	-0.29	0.12	-0.10	0.12	Intermittent
2.76	0.10	-0.57	0.13	-0.41	0.08	-0.19	0.11	-0.05	0.10	Intermittent
2.82	0.16	-0.16	0.15	-0.05	0.06	0.05	0.09	0.06	0.09	Intermittent
2.75	0.17	-0.17	0.14	-0.07	0.06	0.01	0.07	0.08	0.08	Intermittent
2.80	0.22	0.07	0.13	0.04	0.06	0.03	0.06	0.14	0.09	Annular
2.74	0.32	0.13	0.16	0.14	0.06	0.14	0.08	0.15	0.09	Annular
2.69	0.41	0.24	0.14	0.20	0.07	0.17	0.07	0.20	0.09	Annular
2.79	0.63	0.45	0.18	0.41	0.08	0.36	0.08	0.35	0.09	Annular
2.69	0.79	0.79	0.16	0.66	0.10	0.46	0.10	0.46	0.10	Annular
0.14	0.00	-6.05	0.10	-4.10	0.11	-1.59	0.08	0.16	0.05	Bubbly
0.14	0.01	-6.00	0.10	-4.14	0.11	-1.60	0.08	0.12	0.05	Bubbly
0.13	0.01	-6.00	0.08	-4.06	0.09	-1.61	0.08	0.06	0.06	Bubbly
0.13	0.01	-5.70	0.11	-3.78	0.11	-1.43	0.08	0.14	0.05	Bubbly
0.13	0.01	-5.46	0.09	-3.64	0.09	-1.35	0.09	0.19	0.06	Bubbly
0.13	0.03	-2.76	0.32	-2.54	0.28	-0.86	0.14	0.34	0.09	Intermittent
0.14	0.07	-0.55	0.30	-0.23	0.25	0.23	0.30	0.63	0.12	Intermittent
0.14	0.10	0.61	0.15	0.64	0.11	0.82	0.11	0.92	0.11	Intermittent
0.13	0.09	0.65	0.19	0.78	0.15	0.87	0.13	0.99	0.12	Intermittent
0.14	0.09	-0.77	0.24	-0.51	0.24	0.06	0.27	0.49	0.14	Intermittent
0.13	0.10	0.06	0.16	0.29	0.12	0.52	0.11	0.68	0.10	Intermittent
0.14	0.14	0.31	0.17	0.51	0.12	0.66	0.12	0.80	0.12	Intermittent
0.13	0.20	0.78	0.17	0.86	0.13	0.93	0.11	1.02	0.10	Intermittent
0.13	0.25	1.00	0.19	1.08	0.16	1.10	0.15	1.16	0.15	Annular
0.13	0.29	1.17	0.20	1.20	0.13	1.21	0.13	1.24	0.13	Annular
0.14	0.46	1.86	0.23	1.79	0.17	1.74	0.15	1.77	0.16	Annular
0.13	0.58	2.34	0.22	2.30	0.15	2.14	0.19	2.13	0.23	Annular
0.14	0.69	3.23	0.27	3.15	0.21	2.94	0.23	2.89	0.25	Annular
0.13	0.81	3.92	0.34	3.76	0.27	3.40	0.34	3.26	0.45	Annular
0.13	0.88	4.54	0.37	4.37	0.34	3.93	0.43	3.74	0.57	Annular
0.13	1.06	6.35	0.48	6.07	0.47	5.48	0.55	5.19	0.76	Annular
0.18	0.02	-4.37	0.17	-2.61	0.14	-0.62	0.10	0.80	0.06	Bubbly
0.17	0.03	-3.30	0.14	-2.30	0.17	-0.31	0.14	0.86	0.10	Intermittent
0.17	0.04	-2.73	0.19	-1.61	0.19	-0.01	0.21	0.99	0.12	Intermittent
0.18	0.07	-1.65	0.27	-0.74	0.26	0.44	0.25	1.14	0.14	Intermittent
0.18	0.07	-1.63	0.25	-0.70	0.21	0.48	0.23	1.17	0.14	Intermittent
0.18	0.12	-0.80	0.23	-0.09	0.20	0.69	0.21	1.24	0.16	Intermittent
0.18	0.13	-0.23	0.23	0.34	0.23	0.95	0.22	1.37	0.16	Intermittent
0.18	0.17	0.53	0.22	1.03	0.13	1.38	0.18	1.60	0.16	Intermittent
0.18	0.23	0.93	0.21	1.22	0.14	1.37	0.17	1.58	0.16	Intermittent

0.18	0.17	0.38	0.27	0.86	0.18	1.24	0.17	1.44	0.15	Intermittent
0.18	0.23	1.24	0.22	1.48	0.13	1.72	0.15	1.84	0.14	Annular
0.18	0.31	2.14	0.27	2.24	0.15	2.33	0.13	2.38	0.14	Annular
0.18	0.39	2.71	0.26	2.66	0.22	2.71	0.20	2.69	0.22	Annular
0.18	0.44	2.88	0.30	2.83	0.22	2.79	0.23	2.74	0.27	Annular
0.17	0.53	3.08	0.26	3.13	0.20	2.99	0.23	2.91	0.29	Annular
0.18	0.56	3.74	0.30	3.67	0.23	3.38	0.26	3.22	0.38	Annular
0.18	0.60	4.21	0.34	4.15	0.25	3.88	0.30	3.68	0.43	Annular
0.18	0.65	4.51	0.33	4.45	0.28	4.07	0.36	3.89	0.49	Annular
0.17	0.74	5.10	0.35	5.00	0.27	4.51	0.37	4.24	0.51	Annular

Appendix B: Permissions to Publish Previously Published Works

The following is a license agreement to publish the article "The Case for Liquid-Assisted Gas

Lift Unloading" in this dissertation. The content of this article presented in Chapters 2.

126

prohibited without permission.If for any reason, the copyright on the paper is missing or unclear, please follow Example 1 above, using SPE as the default copyright holder. SPE administers copyright for OTC, IPTC and other joint events on behalf of all parties in those events.

8. SPE makes no representations or warranties with respect to the licensed material and adopts on its own behalf the limitations and disclaimers established by CCC on its behalf in its Billing and Payment terms and conditions for this licensing transaction.

9. You hereby indemnify and agree to hold harmless SPE and CCC, and their respective officers, directors, employees and agents, from and against any and all claims arising out of your use of the licensed material other than as specifically authorized pursuant to this license.

10. This license is personal to you, but may be assigned or transferred by you to a business associate (or to your employer) if you give prompt written notice of the assignment or transfer to SPE. No such assignment or transfer shall relieve you of the obligation to pay the designated license fee on a timely basis (although payment by the identified assignee can fulfill your obligation).

11. This license may not be amended except in a writing signed by both parties (or, in the case of SPE, by CCC on SPE's behalf).

12. SPE hereby objects to any terms contained in any purchase order, acknowledgment, check endorsement or other writing prepared by you, which terms are inconsistent with these terms and conditions or CCC's Billing and Payment terms and conditions. These terms and conditions, together with CCC's Billing and Payment terms and conditions (which are incorporated herein), comprise the entire agreement between you and SPE (and CCC) concerning this licensing transaction. In the event of any conflict between your obligations established by these terms and conditions and those established by CCC's Billing and Payment terms and conditions, these terms and conditions shall control.

13. This Agreement shall be governed and interpreted by the laws of the State of Texas, United States of America. Regardless of the place of performance or otherwise, the Agreement, and all schedules, amendments, modifications, alterations, or supplements thereto, will be governed by the laws of the State of Texas, United States of America. If any provisions of the Agreement are unenforceable under applicable law, the remaining provisions shall continue in full force and effect.

Other Terms and Conditions:

v1.1

The following is a license agreement to publish the article "Experimental investigation of vertical downward two-phase flow in annulus" in this dissertation. The content of this article presented in Chapters 4.

MPT 2018
11ᵗʰ North American Conference on
Multiphase Production Technology

Authors details and Consent to publish

Paper number: *39*
Paper title: *Experimental Investigation of Vertical Downward Two-Phase Flow in Annulus*

Please provide details of corresponding author

| Title: Dr   Name: Paulo Waltrich | |
| Organisation: Louisiana State University | |

Please provide details of all co-authors

| Title: Name: Renato P Coutinho | |
| Organisation: Louisiana State University | |

Consent to publish

So that works published by BHR Group can be protected by copyright against unauthorised use, it is necessary that consent to publish be obtained from contributors. This form is for the purpose of giving such consent. Please complete and return it to the Conference Organiser.

I consent for BHR Group to publish the above paper

Name: RENATO PEIXOT COUTINHO ....Date: 5/8/2018

BHR accept your typed name and email as receipt of consent

Terms and Conditions

In consideration for publication of the contribution named above, the undersigned hereby assigns to BHR Group the copyright in the said contribution, whereby BHR Group shall have the right to publish the contribution and/or translation of it throughout the world during the full term of copyright, including renewals and/or extensions, and all subsidiary rights. The undersigned shall, however, retain the right to republish his/her contribution in any scholarly journal consisting solely of his/her own writings, subject only to notifying BHR Group of his/her intention to do so and to his/her ensuring that the publication by BHR Group is properly credited and that the copyright notices repeated verbatim. The undersigned may also self-archive the final version of their paper on their

Organiser Contact Information:

Ally Lynes
Events Manager
Email: ...@bhrgroup.co.uk
Phone: +44 (0) 1234 750 422
Website: www.bhrgroup.com/events

BHR Group
The Fluid Engineering Centre
Cranfield, Bedfordshire
MK43 0AJ
United Kingdom

BHR Group

BHR Group - a trading name of VirtualPiE Limited
A company registered in England No 843 0598

www.bhrgroup.com/events

The following is a license agreement to publish the article "A model for liquid-assisted gas-lift unloading" in this dissertation. The content of this article presented in Chapters 5.

MPT 2017
15th International Conference on
Multiphase Production Technology

Authors details and Consent to publish

Paper number: 49
Paper title: Modelling of the Liquid-Assisted Gas-Lift Unloading

Please provide details of all co-authors

Title: Graduate Research Assistant Name: Renato P. Coutinho Organisation: Louisiana State University	
Title: Professional in Residence Name: Wesley Williams Organisation: Louisiana State University	
Title: Consultant Name: Parviz Mehdizadeh Organisation: Production Technology Inc	
Title: Director of Technology Name: Stuart L Scott Organisation: Petroleum ETC	
Title: Assistant Professor Name: Paulo J. Waltrich Organisation: Louisiana State University	

Consent to publish

So that works published by BHR Group can be protected by copyright against unauthorised use, it is necessary that consent to publish be obtained from contributors. This form is for the purpose of giving such consent. Please complete and return it to the Conference Organiser.

In consideration for publication of the contribution named above, the undersigned hereby assigns to BHR Group the copyright in the said contribution, whereby BHR Group shall have the right to publish the contribution and/or translation of it throughout the world during the full term of copyright, including renewals and/or extensions, and all subsidiary rights. The undersigned shall, however, retain the right to republish his/her contribution in any scholarly journal consisting solely of his/her own writings, subject only to notifying BHR Group of his/her intention to do so and to his/her ensuring that the publication by BHR Group is properly credited and that the copyright notices repeated verbatim.

Organiser Contact Information

Ally Lyons
Events Manager
Email: confs2@bhrgroup.co.uk
Phone: +44 (0) 1234 750 422
Website: www.bhrgroup.com/events

BHR Group
The Fluid Engineering Centre
Cranfield, Bedfordshire
MK43 0AJ
United Kingdom

BHR Group

BHR Group - a trading name of VirtualPiE Limited
a company registered in England No 07285413

www.bhrgroup.com/events

Vita

Renato Peixoto Coutinho, a native of Fortaleza, Ceara, Brazil, received his Master's Degree in Transportation Engineering from Universidade Federal do Ceara (UFC) and his Bachelor's Degree in Chemical Engineering from the same University. Prior to enrolling at the Petroleum Engineering program at Louisiana State University, he has worked as Assistant Professor at the CENTEC in Brazil. He anticipates graduating with his Ph.D. degree in August 2018.